UNIVERSITY OF LATVIA

FACULTY OF PHYSICS, MATHEMATICS AND OPTOMETRY

MELDRA ĶEMERE

LUMINESCENCE AND ENERGY TRANSFER OF RARE EARTH IONS IN CO-DOPED OXYFLURIDE GLASSES AND GLASS-CERAMICS

SUMMARY OF DOCTORAL THESIS

For a Doctoral Degree in Physics and Astronomy
Subfield of Solid State Physics

Riga, 2023

UNIVERSITY OF LATVIA

FACULTY OF PHYSICS, MATHEMATICS AND OPTOMETRY

Meldra Ķemere

LUMINESCENCE AND ENERGY TRANSFER OF RARE EARTH IONS IN CO-DOPED OXYFLURIDE GLASSES AND GLASS-CERAMICS

SUMMARY OF DOCTORAL THESIS

For a Doctoral Degree in Physics and Astronomy
Subfield of Solid State Physics

Riga, 2023

The doctoral thesis was carried out at the Institute of Solid State Physics, University of Latvia from 2015 to 2023.

The thesis contains an introduction, 4 chapters, conclusions and a reference list.

Type of thesis: dissertation in Physics and Astronomy in the subfield of solid state physics.

Supervisor: *Dr. habil. phys*. **Uldis Rogulis**, leading researcher at the Institute of Solid State Physics, University of Latvia

Reviewers:

1) **Linards Skuja,** *Dr. habil. phys*., leading researcher, University of Latvia;
2) **Artūrs Medvids,** *Dr. habil. phys.,* professor, Riga Technical University;
3) **Vitali Nagirnoi,** *Dr. phys,* professor, University of Tartu, Estonia.

The thesis will be defended at the public session Doctoral Committee of Physics and Astronomy, University of Latvia, at 15:00 on September 8th, 2023, in the conference hall of the Institute of Solid State Physics, University of Latvia, Kengaraga Street 8, Riga.

The thesis and its summary are available at the Library of the University of Latvia, Kalpaka blvd. 4.

Chairman of the Doctoral Committee _____/ *Dr. habil. phys. Linards Skuja* /
(signature)

Secretary of the Doctoral Committee _____/ *Sintija Siliņa* /
(signature)

ABSTRACT

In this work the luminescence properties of Dy^{3+}/Eu^{3+} and Tb^{3+}/Eu^{3+} co-doped oxyfluoride glasses and glass ceramics are studied. Oxyfluoride glass ceramics containing CaF_2 or SrF_2 nanocrystallites with the size of 10-60 nm are investigated. Rare earth ions in oxyfluoride glass ceramics are located both in the amorphous glass matrix and in fluoride nanocrystals where they substitute Ca^{2+} or Sr^{2+} ions, and the luminescence and energy transfer of rare earth ions in both of these environment are studied. Although a large number of studies on rare earth ion activator pairs in glass can be found in the literature, there are few studies considering oxyfluoride glass ceramics, this work increases the knowledge in the field.

Glass samples were synthesized by the melt quenching method, and by a successive heating at a temperature of 650-750 °C glass ceramics were obtained. The samples were studied using differential thermal analysis, X-ray diffraction, optical spectroscopy, electron paramagnetic resonance methods.

Energy transfer from Dy^{3+} and Tb^{3+} ions to Eu^{3+} ions has been observed in the studied glasses and glass ceramics. In the CaF_2 and SrF_2 nanocrystals containing sample series with Dy^{3+} and Eu^{3+} ions, the most significant contribution to the luminescence signal comes from the rare earth ions in the glassy environment, and the energy transfer efficiency in glass and glass ceramics is similar. It is concluded that the luminescence quenching of Dy^{3+} ions occurs due to cross-relaxation processes, which become more pronounced in glass ceramics. In a series of samples containing SrF_2 nanocrystallites with Tb^{3+} and Eu^{3+} ions, effective incorporation of rare earth ions into SrF_2 nanocrystallites was observed, which leads to changes in luminescence spectra and color and an increase in energy transfer from Tb^{3+} to Eu^{3+} ions. In all series, Eu^{2+} ions in low concentrations were observed.

The incorporation of rare earth ions into fluoride crystallites and the subsequent changes in the luminescence spectra can be employed to adjust the color coordinates of luminescence for application in white light-emitting diodes and other optical devices.

Table of Contents

INTRODUCTION

1.1. Actuality and motivation of the work

Rare earth (RE) ion luminescence has been studied for several decades and is used in lighting devices, displays, sensors, solid state lasers, etc. One of the current research directions (actuality is proven by the high citation rate of author's publications) is materials doped with rare earth ions for use in white light emitting diodes (WLED). Such diodes most often consist of a phosphor material – yttrium aluminum garnet activated with cerium (Ce^{3+}) ions – and a LED chip for excitation, or from three different colored LED chips. Deterioration of the materials can negatively change the characteristics of the light emitted by the diode. Improvements in the spectral composition are also needed – the YAG:Ce phosphor does not emit in the red spectral region.

Oxyfluoride glass ceramics, on the other hand, are considered good materials for optical applications, including white light-emitting diodes, because it combines the good properties of oxide glasses and fluoride nanocrystallites – the chemical and thermal stability of the oxide matrix and the low phonon energy inherent to fluorides. In oxyfluoride glass ceramics, RE ions tend to be in the crystalline fluoride phase, and its low phonon energy allows reducing the probability of non-radiative transitions of RE ions and increasing the luminescence intensity. Aluminosilicate glass ceramics with CaF_2 and SrF_2 nanocrystallites are relatively easy to synthesize, moreover, the light refraction coefficients of these crystalline phases and the aluminosilicate matrix are similar, allowing to obtain materials with high transparency.

Rare earth ions Eu^{3+}, Tb^{3+} and Dy^{3+} are characterized by intense luminescence bands in the visible spectral range, and these ions are widely used in industry (will be discussed in the following chapters). The luminescence the energy transfer of RE ions depending on their concentration in glasses have been widely studied, but there are relatively few studies on energy transfer in oxyfluoride glass ceramics. The interaction of rare earth ions in oxyfluoride glass ceramics is affected by many factors: their concentration, distance between them, environment (glass matrix or nanocrystallites), phonon energy, sample crystallization properties and nanocrystallite size, etc. In addition, it should be taken into account that using different excitation wavelengths in co-doped samples it is possible to obtain luminescence of different colors in the materials. In summary, the luminescence spectra of co-doped glasses and glass-ceramics can differ.

When considering the development of RE ions co-doped oxyfluoride glass ceramics for applications in optical devices, it is necessary to understand how the concentration of RE ions and the heat treatment conditions of the glass ceramics affect their luminescence properties.

This thesis investigates the luminescence properties of oxyfluoride glasses and glass ceramics doped with rare earth ions to evaluate their potential in white light emitting diodes and other optical applications. In the research, the main emphasis is placed on the properties of the environment of rare earth ions and its influence on their luminescence.

1.2. Aim and tasks of work

The aim of the work is to investigate the luminescence properties and environment of rare earth ions in oxyfluoride glass and glass ceramics containing CaF_2 and SrF_2 nanocrystallites, and to analyze the influence of the environment on the energy transfer efficiency between rare earth ions.

The following tasks have been set to achieve the objective:

1. Production of oxyfluoride glass and glass ceramic samples;
2. Characterization of the samples by X-ray diffraction (XRD) and differential thermal analysis (DTA) methods;
3. Measurements of luminescence excitation and emission spectra of samples, and time-resolved luminescence measurements;
4. Measurements of luminescence decay kinetics and analysis of energy transfer between RE ions;
5. Electron paramagnetic resonance (EPR) measurements of Eu^{2+} ions and data analysis;
6. Analysis of the obtained results.

1.3. Scientific novelty of the work

Energy transfer between rare earth activators has been studied in oxyfluoride glass, but very few publications are found in the literature on energy transfer in oxyfluoride glass ceramics, where the energy transfer processes are also affected by the reduction of the distance between rare earth ions and the partial incorporation of rare earth ions into the crystalline environment (fluoride nanocrystallites) with lower phonon energy. Energy transfer between Tb^{3+} and Eu^{3+} ions in glass ceramics containing CaF_2, β-PbF_2, $NaYF_4$, $SrLaF_5$ nanocrystallites, and in glass ceramics containing SrF_2 nanocrystallites obtained with the sol-gel method has been previously studied in the literature as well as energy transfer from Eu^{2+} to Dy^{3+} ions in glass ceramics containing CaF_2 nanocrystallites. No studies can be found on the energy transfer between Dy^{3+} and Eu^{3+} ions in glass ceramics containing CaF_2 and SrF_2 nanocrystallites and Tb^{3+} and Eu^{3+} ions in SrF_2 containing glass ceramics obtained by heating the precursor amorphous glasses. The thesis contributes to the research of oxyfluoride glass ceramics doped with rare earth ions, which could be important in the development of these materials for optical applications.

Energy transfer in ion pairs Dy^{3+}/Eu^{3+} and Tb^{3+}/Eu^{3+} in oxyfluoride aluminosilicate glass ceramics containing CaF_2 or SrF_2 nanocrystallites was studied for the first time. In addition to the interaction of rare earth ions through energy transfer, their environment have also been studied using time-resolved and site-selective spectroscopy.

1.4. Author's contribution

Sample synthesis and all experimental measurements have been performed at the Institute of Solid State Physics, University of Latvia (ISSP UL). The author of the paper performed sample synthesis, as well as X-ray diffraction (XRD) measurements, luminescence excitation, emission, luminescence decay and time-resolved luminescence measurements, as well as data processing and interpretation, analysis of scientific literature. Electron paramagnetic resonance (EPR) measurements and analysis of the results were carried out by Andris Antuzevics. Differential thermal analysis (DTA) measurements were carried out in cooperation with colleagues Andris Antuzevics and Edgars Elsts.

The author of the paper is the first and corresponding author of two scientific publications and co-author of one scientific publication in cited journals on the subject of the doctoral thesis.

1.5. The structure of the thesis

Chapter 2 of the thesis "Theory and literature review" provides a review of theory and literature on photoluminescence mechanisms, oxyfluoride glasses and glass ceramics, luminescence of rare earth ions, crystalline structure of CaF_2 and SrF_2, luminescence of Dy^{3+}, Eu^{3+}, Tb^{3+} ions. Chapter 3 "Research methodology" provides an insight into the procedure of making samples and the methodology used in the research. The experimental results are summarized in 3 subdivisions of chapter 4.

4.1. Dy^{3+}/Eu^{3+} co-doped glasses and glass ceramics containing CaF_2 nanocrystallites

4.2. Dy^{3+}/Eu^{3+} co-doped glasses and glass ceramics containing SrF_2 nanocrystallites

4.3. Tb^{3+}/Eu^{3+} co-doped glasses and glass ceramics containing SrF_2 nanocrystallites

Although the studied series of samples have a similar composition, the aim of the thesis is not to conduct a direct comparative study between these series.

The final part summarizes conclusions, theses and author's publicity.

2. THEORY AND LITERATURE REVIEW

2.1. Mechanisms of luminescence in solids

2.1.1. Types and mechanisms of luminescence

Luminescence is radiation emitted by a body in addition to thermal radiation, which is significantly longer than the period of light oscillations [1]. During the process of luminescence, electrons from an excited state return to the ground state, simultaneously emitting a quantum of electromagnetic radiation (visible light, UV, IR) whose energy corresponds to the energy difference between the involved energy levels (excited level and ground state). For luminescence to be possible, the material must have a discrete spectrum of energy levels. Quantum energy (also – the energy difference between two energy levels) can be written using the Planck-Einstein equation.

Excitation of electrons from the ground state to a state with higher energy is possible using various sources of excitation – electromagnetic radiation quanta (called photoluminescence), X-rays (X-ray fluorescence), electrons (cathodluminescence), α, β, γ radiation (radioluminescence), etc. [2,3]. In this thesis the photoluminescence will be investigated.

In the case of photoluminescence, the excitation of the electron occurs when the substance absorbs energy in the form of electromagnetic radiation – a quantum of light (or UV, IR radiation). After absorbing a quantum, the electron returns to the ground state in the form of a radiative or non-radiative transition. The processes related to luminescence are shown in **Figure 2.1.** (this type of energy level diagram with processes shown is called a *Jablonski* or *Perina-Jablonski diagram*) [1,4].

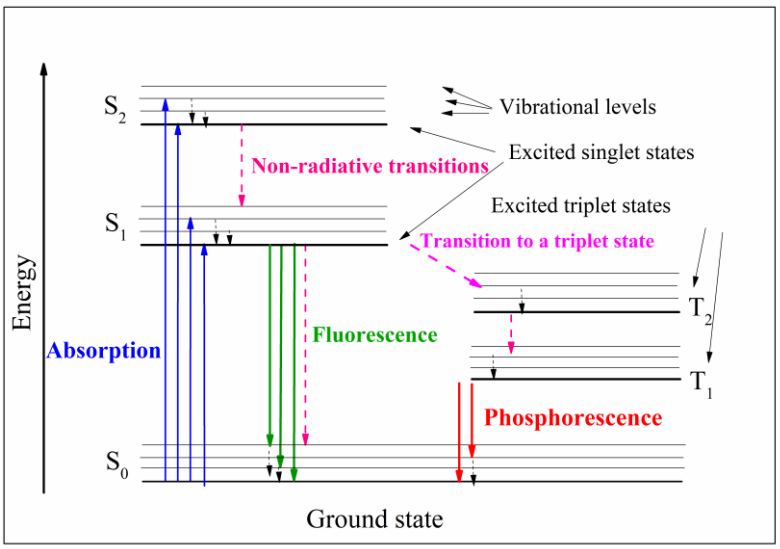

Figure 2.1. Schematic representation of luminescence-related processes in a solid state.

Absorption is a fast *radiation process* (i.e. a real photon is absorbed) that occurs on a time scale of 10^{-15} s [1,4]. Due to the interaction with phonons (vibrational relaxation) the excited electron gets to the lowest vibrational level of the excited state (levels are separated by energy $\hbar\omega$), in a time interval of 10^{-12} s. If the vibrational levels of two electronic levels overlap, the electron can return to a lower energy level in a non-radiative manner [1]. While, as a result of a radiative transition luminescence is observed, which can be divided according to its duration: the duration of *fluorescence* is 10^{-9} – 10^{-7} s, but *phosphorescence* – 10^{-4} – 10^{-1} s or longer.

Luminescence in a material in most cases occurs in places where its ideal structure is disrupted. One can distinguish between the luminescence of the substance itself and the luminescence of impurities. The intrinsic luminescence is caused by the intrinsic defects – ion vacancies, interstitial atoms, various agglomerates of defects. Impurity luminescence is most often introduced by adding activator ions at low concentrations to obtain desired material properties.

2.1.2. Luminescence decay and non-radiative transitions

The electron population in the excited state decreases due to both radiative and non-radiative transitions. The intensity of luminescence (radiation transitions) is proportional to the electron density in the excited state. The population change in the excited state depending on time is described by the formula (2.1) [1]:

$$\frac{dN}{dt} = -(k_R + k_{NR}) \cdot N(t) \tag{2.1}$$

where N – the number of electrons in an excited state, k_R – the probability of radiative transitions (rate of radiative transitions), k_{NR} – the probability of non-radiative transitions (rate of non-radiative transitions).
The number of electrons in the excited state decays exponentially, with a time constant τ, called the lifetime of the excited state (2.2) [1]:

$$\tau = \frac{1}{k_R + k_{NR}} \tag{2.2}$$

Luminescence intensity can also be reduced by *multiphonon relaxation* – a case when instead of emitting a photon, a number of phonons are emitted so that the sum of their energy is equal to the energy difference between the minimum of the excited state and the ground state [1, 2]. The larger number of phonons is required, the less likely the multiphonon relaxation process will occur. The luminescence intensity of RE ions can also be reduced by energy transfer processes between them, for example cross-relaxation, energy migration.

In experimental measurements, luminescence decay (the change in luminescence intensity proportional to the population of the excited level) can be described using a single exponent or a double exponent. But if the decay is affected by more than two physical processes, it is common to use the *effective lifetime*, which is obtained by integrating the area under the normalized luminescence decay curve and its product with time (2.3) [8]:

$$\tau_{ef} = \frac{\int I(t)tdt}{\int I(t)dt} \tag{2.3}$$

2.1.3. Energy transfer between activators

An excited luminescent center can return to its ground state radiatively or non-radiatively, but it can also transfer its energy to another luminescent center by exciting it. Such a process is called *energy transfer*. Energy transfer involves a luminescence center that gives energy and a luminescence center that receives energy. The first one is called a *sensitizer* or *donor*, the second one is called an *activator* or *acceptor* [3]. The terms *donor* and *acceptor* in this context refer to the energy transfer from an excited to an unexcited luminescent center, they do not refer to the transfer of charges like in semiconductors.

Energy transfer between activators in most cases is a non-radiative process, i.e. no real photon is emitted or absorbed. In order for energy transfer to happen between the luminescence centers: 1) the energy difference between the excited state and the ground state in both luminescence centers must be the same (i.e. the resonance condition must be fulfilled), 2) there must be an interaction between the two centers. Energy transfer processes were described by scientists Förster and Dexter, therefore the energy transfer process is often called *Förster-Dexter energy transfer* or *resonant energy transfer*.

Energy transfer between activators can occur due to the following types of interaction: 1) *multipole* (*Coulomb*) *interaction* – dipole-dipole, dipole-quadrupole, quadrupole-quadrupole interaction (the mechanism was described by Förster), or 2) exchange interaction (mechanism described by Dexter) [6,7].

In the case of multipole interaction, the electrons of the donor and acceptor ions do not change their belonging to the ions and do not come into contact in space – energy transfer occurs when the excited donor ion induces the dipole oscillation of the acceptor ion [6]. On the other hand, in the case of

exchange interaction, electron wave functions (charge distribution) overlap in space, and electron exchange takes place between donor and acceptor ions [6]. The probability of energy transfer is higher when the energy transfer has the nature of dipole-dipole or exchange interaction [3]. The energy transfer efficiency depends on the distance between the activators – in the case of multipole interaction as R^{-n} (n=6,8,10, respectively, in the case of electric dipole-dipole, dipole-quadrupole, quadrupole-quadrupole), while in the case of exchange interaction it is exponential [3]. The distance between the donor and acceptor ions, at which the energy transfer from the donor ion to the acceptor ion and the radiative transition of donor ion to the ground state are equally probable, is defined as the *critical distance* R_c [3, 8]. If the real distance between the donor and acceptor ions $R > R_c$, then the dominant process is the luminescence of the donor ions, if $R < R_c$ – energy transfer to the acceptor ion dominates.

In experimental luminescence measurements, the efficiency of energy transfer between ions is determined by analyzing the kinetics of donor luminescence decay in samples 1) without the presence of an acceptor and 2) with added acceptor ions (2.4) [9, 10]:

$$\eta_{EP} = \left(1 - \frac{\tau}{\tau_0}\right) \qquad (2.4)$$

where τ_0 – decay time of donor ions without added acceptor ion, τ – decay time of donor ions when acceptor ions are added to the sample.

2.2. Oxyfluoride glasses and glass ceramics

2.2.1. Glasses

Glass is defined as an amorphous solid material, the structure of which does not have long-range order, and which has a characteristic glass transformation temperature region [11, 12]. Only a material, that possesses both of the mentioned properties can be called glass – an amorphous material without the characteristic properties of glass transformation cannot be considered glass. The classic method of synthesizing a glass is *the melt quenching method*, where a molten mass of raw materials is rapidly cooled, obtaining a solid glass.

Glass transformation properties can be presented using the enthalpy (or volume) dependence on temperature. Let us consider a material, which is initially in a liquid state at a temperature higher than the melting point T_m. By lowering the temperature of the liquid, the structure of the material adapts to the temperature at each existing moment of time (i.e. takes a thermodynamic equilibrium state). When the temperature drops below the melting point, the substance can form a crystalline structure with short- and long-range order. If the crystallization of the material does not occur, a *supercooled liquid* is obtained [11]. As the temperature continue to decrease, the viscosity of the material increases until it reaches such a high value that the atoms are no longer able to rearrange themselves to adapt to the equilibrium structure of the liquid [11]. The enthalpy value deviates from the expected equilibrium value and forms a curved line, until the moment when, due to the high viscosity, the structure is completely "frozen", and it no longer changes depending on the temperature – then a glass is obtained [11].

In practice, glass transformation parameters are usually described using *the glass transition temperature* T_g, which is obtained from experimental differential thermal analysis curves or thermal analysis curves. T_g depends both on the synthesis conditions of the specific glass and on the analysis conditions, so it cannot be generalized to a class of materials [11, 13].

Depending on the glass-forming chemical elements, glasses can be divided into several groups: oxide, halide, chalcogenide, metallic glasses. Oxide glasses are the most widely used. Oxide glass components, depending on the nature of their chemical bonds with oxygen ions, are divided into the followings groups: network formers, intermediates, conditional glass formers, modifiers [11, 12]. Bonds of glass formers and oxygen have about 50% ionic nature, conditional formers – mostly ionic nature, modifiers – only ionic. Glass formers together with oxides are able to form single-component glasses, conditional glass formers are able to partially replace glass formers, and modifiers are able to influence the structure of glasses, instead of independently forming single-component glasses [11].

In this PhD thesis, oxyfluoride aluminosilicate glasses were studied, in which the glass formers are SiO_2 and Al_2O_3, but CaO, Na_2O, ZnF_2, CaF_2, SrF_2 are added as modifiers.

2.2.2. Oxyfluoride glass ceramics

Glass-ceramic materials are most often produced by *heat treatment method* (i.e., isothermally annealing) of previously synthesized precursor glasses, and as a result nano- or micro-sized particles with a crystalline structure (i.e. nanocrystallites) are formed in the glass matrix [13, 14]. Schematically, the glass ceramic structure is shown in **Figure 2.2.** Formation of crystallites occurs in two steps: 1) formation of crystallization centers (nucleation), 2) growth of crystallites [11, 13]. Crystallization centers can be homogeneous (formed spontaneously in the liquid) or heterogeneous (formed on the surface of some defects, for example, on the walls of the crucible) [11].

Most often in technology, multicomponent glasses are used, in which crystallization of several different phases is possible, which do form in a certain order [13]. In oxyfluoride glass ceramics, the fluoride crystalline phase is almost always the first to crystallize [13]. In addition to the above-mentioned crystallization processes, many glasses are characterized by liquid-liquid phase separation (LLPS) – areas with different composition, different proportions of glass components can form in supercooled liquids [11, 13, 15]. These areas may be droplet-like, possessing an enhanced nanocrystallite formation. There is evidence that the formation of fluoride nanocrystallites in oxyfluoride glass ceramics primarily occurs directly through liquid phase separation [13-15].

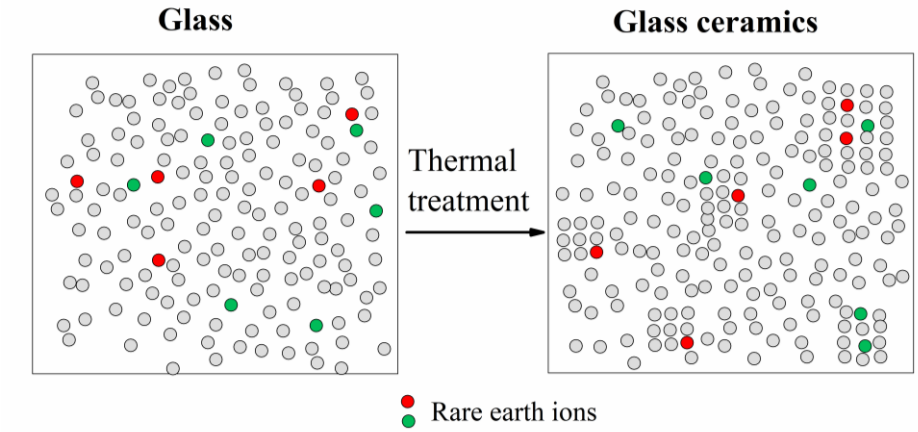

Figure 2.2. Schematic representation of glass and glass ceramics, the different environment of rare earth ions.

It should be mentioned that during melting and heat treatment of oxyfluoride glasses, some portion of fluorides is released into the air, and in glass ceramics the lack of fluorine atoms in the outer layer of the samples is observed [13, 14]. Reactions with water vapor, as well as exchange reactions, lead to fluorine loss [13].

Oxyfluoride glass ceramics is a nanocomposite material consisting of an oxide glass matrix and fluoride nanocrystallites formed in the matrix. These materials combine the good properties of oxides and fluorides – the stability of the oxide matrix and the low phonon energy of fluorides [13, 14].

Fluoride crystals have low phonon energy [13, 14, 16]. This property, important for optical applications, also applies to fluoride nanocrystallites in oxyfluoride glass ceramics. Although the desired size of crystallites to ensure the transparency of glass ceramics is small (around 10-30 nm), their structure is crystalline and provides an environment with low phonon energy for the activators introduced into it [13, 14]. Low phonon energy allows reducing the probability of non-radiative transitions and increasing the luminescence quantum yield, as well as increasing the luminescence decay time of the activators. RE ions tend to enter nanocrystallites instead of remaining in the oxide glass phase, however, the concentration of RE ions in fluoride nanocrystallites is affected by its composition and production conditions [13, 14, 16]. To preserve transparency, the difference in the refractive index of the crystalline glass phase should not exceed 0.3 [13].

Optically homogeneous glass ceramics can be obtained if their crystalline phase (its structure) is isotropic. This rule is fulfilled for crystals with cubic, hexagonal and tetragonal symmetry [13].

Therefore, fluorite-type difluorides MF_2 (M = Ca, Sr, Ba, Cd, Pb) or solid solutions $M_{1-x}R_xF_{2+x}$ (R – rare earth ions) or LaF_3, $NaYF_4$, $LiYF_4$ type nanocrystallites are often chosen for crystallites [13, 14].

Oxyfluoride glass ceramics doped with rare earth ions have been most widely studied for use in white light sources, diodes and to improve the efficiency of solar cells [13, 16].

In white light emitting diodes (WLEDs), which are used in light indicators, background lighting, car lights, lighting, oxyfluoride glass ceramics could offer longevity, stability, constant characteristics of the emitted light spectrum, and fluoride nanocrystals are able to improve the efficiency of luminescence [13].

By covering solar panels with transparent, luminescent oxyfluoride glass ceramics, it would be possible to convert UV and IR radiation coming from the sun into visible light and near infrared radiation (800-1000 nm), increasing the efficiency of silicon solar cells [13, 16, 17]. The potential applications of oxyfluoride glass ceramics in the active environment of lasers (including optical fiber lasers), especially in the IR spectral region, as well as in scintillators, temperature sensors, etc., are also mentioned [16].

In the PhD thesis, glass ceramics were obtained by isothermally annealing the precursor glasses synthesized by the classic melt quenching method.

In this thesis, series of oxyfluoride aluminosilicate glass and glass ceramic samples containing CaF_2 or SrF_2 nanocrystallites were made.

2.2.3. Luminescence of rare earth ions in the crystalline phase of CaF_2 and SrF_2

CaF_2 and SrF_2 crystals have a fluorite structure, they are isotropic crystals with central symmetry [18, 19], spatial symmetry group Fm3m [20]. The structure consists of CaF_8 or SrF_8 polyhedra, with a Ca^{2+} or Sr^{2+} ion in the center, surrounded by 8 fluorine ions F^-, while the F^- ion is in tetrahedral symmetry (surrounded by 4 Ca^{2+}/Sr^{2+} ions). The fluorite structure of CaF_2 is shown in **Figure 2.3.** (the VESTA program was used for modeling).

CaF_2 is an insulator with a band gap of 7.615 eV [18]. In [19] the following band gap energies were calculated: 7.45 eV (CaF_2), 7.12 eV (SrF_2) [19]. In the CaF_2 crystal, the phonon wave number is around 322.5 cm^{-1} [18], in SrF_2 around 280 cm^{-1} [21, 22]. CaF_2 and SrF_2 are perspective crystals for applications in optics and infrared lasers, because they have a very wide optical transmittance (0.13-11 μm), including in the vacuum ultraviolet range [18, 21].

The M^{2+} (M = Ca, Sr) ion position occupied by RE ions has cubic symmetry according to the crystal structure, since the M^{2+} ion is surrounded by 8 fluorine ions equidistant from M^{2+}. However, when a trivalent RE ion replaces a divalent cation (here, Ca^{2+} or Sr^{2+}) in the fluorite structure, charge compensation is required due to different valence [18, 23, 24]. If charge compensation occurs in the close vicinity of the activator (here: Dy^{3+}, Eu^{3+}, Tb^{3+}), then the symmetry of the initial cubic field is deformed, which, in turn, leads to changes in the luminescence properties of the RE ion [18, 23-35].

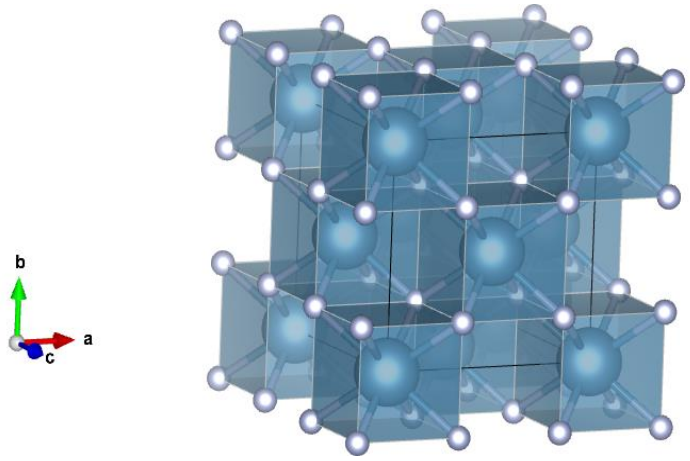

Figure 2.3. Crystal structure of CaF_2.

The number and proportion of different centers in each combination of crystalline material and activator is different, because the formation of centers is also influenced by differences in ionic radii [18, 23, 26]. The three most common RE^{3+} centers in MF_2 crystals (including crystallites) are: 1) cubic; 2) tetragonal; 3) trigonal.

Cubic RE^{3+} centers (O_h centers) in MF_2 crystals are formed when the charge compensation occurs at a sufficiently large distance from the RE^{3+} ion and does not affect its local environment [23, 25, 27-30]. Tetragonal RE^{3+} centers (C_{4v} centers) are formed when the charge compensator (F^- ion) occupies the closest interstitial position in the [100] direction. The F^- ion occupies the center of the adjacent empty cube (8 fluorine ions at the vertices of the cube), where there is no M^{2+} ion [23, 25, 29, 31, 32]. Trigonal RE^{3+} centers (C_{3v}) centers are formed when the charge compensator (F^- ion) occupies positions of the closest interstitials in the [111] direction [23, 25, 29, 31]. The literature also mentions RE^{3+}-O^{2-} trigonal centers when O^{2-} replaces the nearest F^- ion [33] and Eu-O dimer centers with two replacing O^{2-} ions [34].

The formation of RE clusters in crystallites can lead to concentration quenching of the luminescence of RE^{3+} ions and cross-relaxation processes between RE ions [18]. To avoid the formation of RE ion clusters, one of the optically inactive RE ions (Lu^{3+}, Gd^{3+}, Y^{3+}) can be added to the material as a second activator – these ions inhibit the formation of optically active RE ion clusters [18].

Eu^{2+} ion luminescence can also be observed in oxyfluoride glass ceramics containing CaF_2 and SrF_2 nanocrystallites [35-39]. The reduction of Eu^{3+} ions to Eu^{2+} takes place both when synthesizing glasses in a reducing atmosphere (H_2, CO), and when synthesizing them in air, as well as when irradiating the glass with femtosecond laser, γ, β rays [40]. The reduction is explained by the charge compensation model or the optical basicity model [35, 41]. The charge compensation model is more often used considering single crystals, while the optical basicity model is more often used for glassy materials.

2.3. Photoluminescence of rare earth ions

2.3.1. Rare earth ions and their applications

Rare earth elements include 17 group III elements: 15 lanthanides (^{57}La – ^{71}Lu), as well as scandium (^{21}Sc) and yttrium (^{39}Y), due to similar chemical properties. In nature, rare earth elements are most often found in the trivalent form.

The electronic configuration of lanthanide atoms (except lanthanum, cerium, gadolinium, lutetium) can be written in the form $[Xe]4f^n6s^2$ (for trivalent ions – $[Xe]4f^{n-1}$), where [Xe] is the electronic configuration of xenon atoms ($1s^22s^22p^63s^23p^63d^{10}4s^24p^64d^{10}5s^25p^6$ (n = 1-14)) [42-44].

The luminescence of RE ions (Eu^{3+}, Dy^{3+}, Tb^{3+}) studied in the work is widely used in the following applications a) Eu^{3+}: in fluorescent lamps [45], for temperature detection [46, 47], electroluminescent equipment [48], anti-counterfeiting elements [45], b) Dy^{3+}: military, in the telecommunications [49-51], phosphorescent paints [38], lasers [18], c) Tb^{3+}: in electroluminescent devices [43, 49, 52], lamps, trichromatic phosphors [43,52].

2.3.2. Energy levels of rare-earth ions in solid-state materials

For rare earth ions, the number of electrons in the 4f shell is from 0 to 14 – their 4f shell is not completely filled. The electrons in the unfilled 4f shell are well screened by the electrons of the filled 5s and 5p shells, as a result, electronic transitions in the 4f shell are little dependent on the surrounding electric and magnetic fields [45, 53]. The 4f shell has 7 orbitals that electrons can occupy.

In the solid materials, the degeneracy of the 4f shell levels of the activator ion is also affected by the interaction of the ion with its surroundings. The following types of physical interaction are distinguished, summarized in **Table 2.1**. [45].

Table 2.1. Interactions in a solid.

Interaction	Explanation
Coulomb interaction	Electrostatic interaction between electrons of the shell (here: 4f shell)
Spin-orbital interaction	The interaction between the magnetic moment of the electron spin and the magnetic field created by the electron's motion around the nucleus
Crystal field effect / perturbation	Interaction between 4f electrons and ligand electrons
Zeeman effect	Splitting of energy levels under the influence of an external magnetic field

As a result of the Coulomb interaction, in the $4f^6$ configuration (in the 4f shell) *terms* are formed, separated by the energy difference about $2 \cdot 10^4$ cm^{-1}. As a result of the spin-orbital interaction, terms split into energy levels with an energy difference of 10^3 cm^{-1}. Under the influence of the crystal field, the energy levels can split into *2J+1* components, resulting in *crystal field levels* or *Stark sublevels* [45] with an energy difference of 10^2 cm^{-1}. The number of components (Stark sublevels) and their distance on the energy scale depends on the crystalline environment of the activator, more precisely, on the symmetry class of the material (eg, cubic, hexagonal, etc.) [45]. All point groups of the same symmetry class have the same number of splitting. The symmetry of the crystal field also affects the properties of allowed and forbidden transitions. As a result of perturbations of the crystal field, some transitions which are forbidden in spherical symmetry, become partially allowed in case of lower symmetry [45]. Under the influence of a magnetic field, due to the Zeeman effect, splitting of sublevels with an energy difference of a few cm^{-1} is possible. The resulting energy levels are called *Zeeman sublevels* [45, 53].

Two types of electronic transitions are possible for RE ions.

In the case of *electric dipole* (*ED, or induced electric dipole) transitions*, the RE ion interacts with the electric field vector through the electric dipole, the occurrence of which is associated with linear charge movement. According to Laporte's selection rule, f-f transitions of the electric dipole of RE ions in the 4f shell should be forbidden because their parity is the same [42, 54]. However, the crystal field effect and the partial mixing of the electron wave functions of the 4f shell with higher configuration electron wave functions soften this prohibition and f-f transitions in solids are observed, but their intensity depends on the symmetry of the crystal field (they are significantly weaker in positions with inversion symmetry). For induced f-f electric dipole transition to be allowed, the following selection rules must be fulfilled: $|\Delta S|=0$; $|\Delta L| \leq 6$; $|\Delta J| \leq 6$ and $|\Delta J|=2,4,6$ if $J=0$ or $J'=0$ [45].

In *magnetic dipole (MD) transitions*, the rare-earth ion interacts with the magnetic field component of the light through the magnetic dipole. For magnetic dipole transitions, the trajectory of the charge during the transition is curved, it can be viewed as a rotation of the charge during the transition [45]. MD transitions are characterized by even parity [45]. In order for the transition of the magnetic dipole to be allowed, the following selection rules must be fulfilled: $\Delta S=0$; $\Delta L=0$; $\Delta J=0, \pm 1$, but the $0 \leftrightarrow 0$ transition is forbidden [45, 54]. According to Laporte's selection rule, MD f-f transitions are allowed, but their intensity is about 2 orders of magnitude weaker than the induced ED transitions [54].

2.3.3. Luminescence properties of Eu^{3+} ions

The luminescence of Eu^{3+} ions in the visible spectral range is associated with transitions in the 4f shell (f-f transitions). Eu^{3+} ion has 6 electrons in its 4f shell, its electronic configuration is $[Xe]4f^6$ [42, 45]. According to Hund's laws, the ground state of Eu^{3+} ions is $^7F_0$ [45, 53]. The level scheme of Eu^{3+} ions is shown in **Figure 2.4.a.**

The most intense luminescence bands are observed due to transitions from the excited state $^5D_0$ to ^7F_J (J=0-6) states. The $^5D_0 \rightarrow {}^7F_1$ transition is an MD transition, the other transitions to ^7F_J levels are ED transitions [45]. The luminescence intensity of Eu^{3+} is most intense in the orange-red spectral range.

The most intense luminescence is commonly observed due the transitions $^5D_0 \rightarrow {}^7F_1$ and $^5D_0 \rightarrow {}^7F_2$.

The intensity of $^5D_0 \rightarrow {}^7F_1$ as an MD transition (in the 585-600 nm spectral region) is relatively little dependent on the crystalline environment. In environments with a centrosymmetric crystal structure, the $^5D_0 \rightarrow {}^7F_1$ transition dominates in the luminescence spectrum [41, 45]. If the splitting of $^7F_1$ into more than 3 components is observed, it indicates the presence of Eu^{3+} ions in several non-equivalent crystalline positions [45]. On the other hand, the transition $^5D_0 \rightarrow {}^7F_2$ (610-630 nm) is called a hypersensitive transition – its intensity is strongly dependent on the crystalline environment [45]. Hypersensitive transitions obey selection rules: $|\Delta S|=0$; $|\Delta L| \leq 2$; $|\Delta J| \leq 2$ [45]. Because of its hypersensitivity, this transition is often used to study how symmetrical the Eu^{3+} position is. High intensity of the $^5D_0 \rightarrow {}^7F_2$ emission band is associated with low site symmetry [41, 45].

In addition, transitions from levels higher than $^5D_0$ are also observed in the solids: $^5D_1$, $^5D_2$, $^5D_3$. The luminescence bands associated with these levels often overlap with the $^5D_0 \rightarrow {}^7F_J$ bands in the spectrum. Eu^{3+} ions are widely used as a spectroscopic probe because the ground state $^7F_0$ and the excited level $^5D_0$ are non-degenerate, the emission bands are well separated and they split into a relatively small number of components in the crystal field.

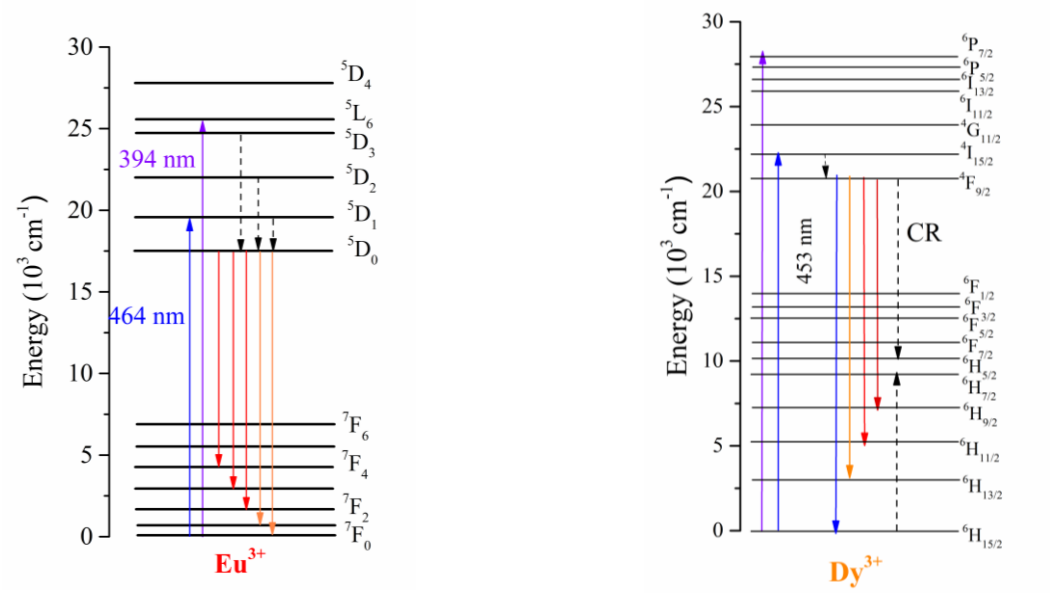

Figure 2.4.(a-b). a) Eu^{3+} ion energy level diagram, b) Dy^{3+} ion energy level diagram.

Absorption to excited Eu^{3+} levels occurs both from the ground state $^7F_0$ and also from $^7F_1$ and in rare case – $^7F_2$. At room temperature, the occupancy of the $^7F_0$ level is about 65%, $^7F_1$ – 35%, and $^7F_2$ ≤1% [45]. A characteristic feature of Eu^{3+} is a broad absorption band in the UV spectral region – the so-called *charge-transfer band* (CT band). It is caused by transferring an electron from one or more adjacent atoms (in oxyfluoride glass – oxygen ions O^{2-}) to the Eu^{3+} ion, which is formally reduced to the Eu^{2+} ion. This absorption is allowed by the selection rules, so the Eu^{3+} charge transfer bands are very intense compared to f-f transitions, which are forbidden.

2.3.4. Luminescence properties of Dy^{3+} ions

Dy^{3+} ions belong to the group of ions characterized by intense luminescence in the visible spectral range. The ground state from which electrons are excited is $^6H_{15/2}$, Dy^{3+} ion has 9 electrons in its 4f shell, its electronic configuration is $[Xe]4f^9$ [42, 53].

Dy^{3+} luminescence bands in the visible spectral range are associated with transitions from the excited state $^4F_{9/2}$ to ^6H term levels – $^6H_{9/2}$, $^6H_{11/2}$, $^6H_{13/2}$ and $^6H_{15/2}$ [51, 55-58]. The characteristic energy levels and transitions of Eu^{3+} ions are shown in **Figure 2.4b**. The most intense transition in most materials is $^4F_{9/2} \rightarrow {}^6H_{13/2}$ (ED transition) and is located in the yellow spectral range (with a peak at 570-575 nm) [55, 57, 59].

A drawback of Dy^{3+} ions for applications is the cross-relaxation processes characteristic for Dy^{3+} ions, which take place even at a small concentration of Dy^{3+} ions, reducing the intensity of Dy^{3+}

luminescence and the quantum yield of Dy^{3+} [56, 57, 59]. Possible cross-relaxation paths are shown in **Figure 2.4b** [56, 57].

Dy^{3+} ions are characterized by absorption in the near-infrared range (5000-1400 cm^{-1}, transitions allowed by the spin-selection rule) and in the UV-visible spectral range (18,000-30,000 cm^{-1} or 290-500 nm, transitions forbidden by the spin-selection rule). The transition in the infrared region $^6H_{15/2} \rightarrow {}^6F_{11/2}$ (7800 cm^{-1} or 1282 nm) is hypersensitive [56, 60].

2.3.5. Luminescence properties of Tb^{3+} ions

Tb^{3+} ions are characterized by intense luminescence in the visible spectral range. The ground state from which electrons are excited is $^7F_6$ [53]. Tb^{3+} ion has 8 electrons in its 4f shell, its electronic configuration is $[Xe]4f^8$ [42, 52, 53].

Tb^{3+} ions are characterized by emission transitions in the blue-green-red range due to transitions $^5D_4 \rightarrow {}^7F_J$, as well as transitions $^5D_3 \rightarrow {}^7F_J$ in the UV-blue spectral range [52, 61, 62]. Luminescence and excitation transitions are shown in **Figure 2.5a.**

The most intense luminescence transitions in the visible spectral range are $^5D_4 \rightarrow {}^7F_J$ (J=3-6), the highest intensity is usually due to $^5D_4 \rightarrow {}^7F_5$, which is in the 540-560 nm range [45, 52, 61-63].

The luminescence intensity of transitions $^5D_3 \rightarrow {}^7F_J$ is strongly influenced by concentration quenching associated with cross-relaxation processes between the following energy levels: $^5D_3 \rightarrow {}^5D_4$ and $^7F_6 \rightarrow {}^7F_{0,1}$ (see **Figure 2.5.a.,** [6, 52]). Cross-relaxation processes occur already at low Tb^{3+} concentrations, leading to luminescence transitions mainly from the $^5D_4$ level [52].

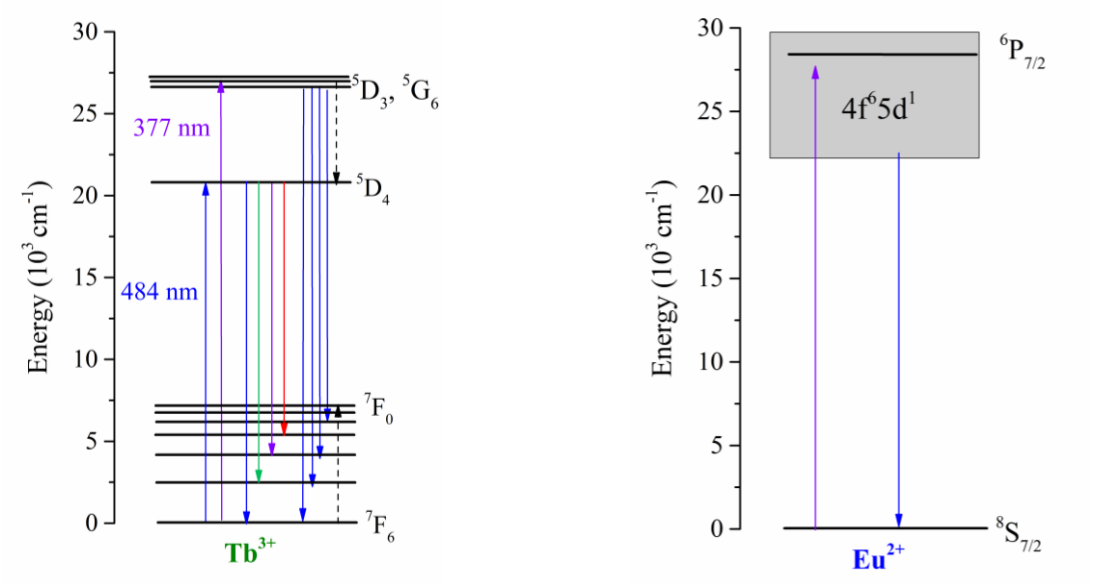

Figure 2.5.(a-b). a) Energy level diagram of Tb^{3+} ions, b) Energy level diagram of Eu^{2+} ions.

The luminescence of Tb^{3+} ions can be excited by UV radiation (300 – 380 nm), where absorption occurs from the ground state $^7F_6$ to a large number of nearby excited levels.

2.3.6. Luminescence properties of Eu^{2+} ions

The divalent europium ion (Eu^{2+}) has a different electron configuration compared to the trivalent RE ions described above. The electronic configuration of the Eu^{2+} ion is $[Xe]4f^7$ [43].

The ground state of the $4f^7$ configuration is $^8S_{7/2}$ [7]. Emission transition $4f^65d^1 \rightarrow 4f^7$, characteristic of Eu^{2+} ions [7, 43] occurs between different configurations – such transitions are allowed [61]. Unlike the 4f configuration (shell), the 5d shell is not shielded from external fields, so the energy of the $4f^65d^1$ configuration levels is strongly affected by the surrounding crystalline field, and the

luminescence of Eu^{2+} ions can be observed in different spectral ranges depending on its environment [41].

The energy level scheme of Eu^{2+} is shown in **Figure 2.5.b.** Broad Eu^{2+} excitation and luminescence bands are commonly observed [38-41, 61]. The broad luminescence band (i.e. transition) characteristic of Eu^{2+} ions is denoted by $4f^65d^1 \rightarrow {}^8S_{7/2}$, or 5d-4f for short [61]. The next highest level of the $4f^7$ configuration ($^6P_{7/2}$) is located relatively far from the ground state ($^8S_{7/2}$) – around 30,000 cm^{-1} [7], so transitions between these levels are rarely observed.

Absorption of Eu^{2+} ions occurs when the electron is excited from the ground state $^8S_{7/2}$ to $4f^65d^1$. However, in some publications, several components (for example, t_{2g} and e_g) are distinguished in the absorption bands, which are formed as a result of the crystal field splitting [40].

2.3.7. Literature review on luminescence and energy transfer of Eu^{3+}, Dy^{3+}, Tb^{3+} ions in oxyfluoride glass and glass ceramics

The luminescence properties of Eu^{3+} ions have been extensively studied in glass ceramics containing CaF_2 nanocrystallites obtained by heating the precursor glasses. They have been studied in oxyfluoride aluminosilicate glass and glass ceramics with matrix composition $SiO\text{-}Al_2O_3\text{-}CaO\text{-}CaF_2$ [30, 46, 59, 64, 65], $SiO_2\text{-}Al_2O_3\text{-}CaF_2$ [66, 67], $SiO\text{-}Al_2O_3\text{-}CaF_2\text{-}NaF$ [39] as the only activator, or co-doped with Tb^{3+}, Dy^{3+}, Sm^{3+} ions, have also been studied in other oxyfluoride materials.

When the Eu^{3+} ion enters the CaF_2 crystalline phase, i.e., replace Ca^{2+} ions in a centrosymmetric structure, its luminescence spectrum should change, as described above in *Chapter 2.3.3.*, – with a relative increase in the intensity of the MD transition $^5D_0 \rightarrow {}^7F_1$ in the range of 585 nm – 600 nm, but with a decrease in the intensity of the ED transition $^5D_0 \rightarrow {}^7F_2$ for intensity in the range 610 nm – 630 nm. However, the incorporation of Eu^{3+} ions into the CaF_2 phase occurs with different efficiencies in different studies. Time-integrated (steady-state) spectral measurements with one excitation wavelength, at room temperature, are not sufficient to estimate the environment of Eu^{3+} ions. As shown in [30], using site-selective-spectroscopy and performing measurements at low temperature, it is possible to identify Eu^{3+} luminescence signals in a cubic environment, as well as in other environments [30], while with a different excitation wavelength (464 nm) room temperature, there is no sign of Eu^{3+} ions in a crystalline environment in the luminescence spectrum. In the literature, there are few detailed studies on Eu^{3+} centers in CaF_2 nanocrystallites in glass ceramics.

Luminescence properties of Eu^{2+} ions in CaF_2-containing glass ceramics were also studied. It has been shown that Eu^{2+} luminescence in CaF_2 nanocrystallites is characterized by a broad luminescence band with a maximum around 425-430 nm and a half-width around 100 nm [36-40, 64, 67, 68].

The luminescence of Dy^{3+} ions was studied in aluminosilicate glass ceramics containing CaF_2 nanocrystallites with the composition $SiO_2\text{-}Al_2O_3\text{-}CaO\text{-}CaF_2$ [55, 59, 64, 68-71], as the only activator, or co-doped with Eu^{3+}, Eu^{2+}, Er^{3+}. In the studied oxyfluoride aluminosilicate glasses and glass ceramics, the Dy^{3+} emission transition in the yellow spectral range $^4F_{9/2} \rightarrow {}^6H_{13/2}$ is the most intense.

The luminescence of Tb^{3+} ions has been studied in oxyfluoride aluminosilicate glasses and glass ceramics [5, 46, 64, 72, 73], as well as in CaF_2 nanoparticles synthesized by the sol-gel method [74] and in sol-gel glass ceramics containing CaF_2 nanocrystallites [9]. [46] investigated the temperature dependence of the luminescence of Tb^{3+} ions, [72] – changes in the relative intensity of Tb^{3+} bands depending on temperature.

Luminescence of Eu^{3+}, Eu^{2+}, Dy^{3+}, Tb^{3+} ions in SrF_2-containing glass ceramics

Eu^{3+} ions have been studied in glass ceramics containing SrF_2 nanocrystallites with the composition $SiO_2\text{-}Al_2O_3\text{-}Na_2O\ SrF_2$ / $SiO_2\text{-}Al_2O_3\text{-}NaF\text{-}SrF_2$ [41], $SiO_2\text{-}Al_2O_3\text{-}NaF\text{-}SrF_2$ [39], $SiO_2\text{-}Al_2O_3\text{-}ZnF_2\text{-}SrF_2$ [75] and in other materials containing SrF_2 nanoparticles. When the Eu^{3+} ion replaces the Sr^{2+} ion in the centrosymmetric lattice of SrF_2, a change in the relative intensity of the luminescence bands is expected, as when entering CaF_2 nanocrystallites. [41, 66, 75] observed a change in the luminescence spectrum of Eu^{3+} (at room temperature) from glass to glass-ceramic, which indicates the effective incorporation of Eu^{3+} ions into SrF_2 nanocrystallites.

The luminescence of Eu^{2+} ions was studied in [41], where it was observed both in SrF_2 phase (maximum around 410 nm) and as a broad band in glass, which could be related to the sum of contributions from different Eu^{2+} environments (SrF_2 and glass). The luminescence of Eu^{2+} and its reduction from Eu^{3+} to Eu^{2+} have been studied in detail [39].

The luminescence of Dy^{3+} ions was studied in glass ceramics containing SrF_2 nanocrystallites with the composition SiO_2-Al_2O_3-CaO-CaF_2 [69], SiO_2-Al_2O_3-LiF-SrF_2 [76], telluride bismuth glasses [77], as well as in transparent SrF_2 ceramics with nanocrystallite size around 11-13 nm [78]. In transparent SrF_2 ceramics, the splitting of Dy^{3+} bands is well observed [78].

Tb^{3+} luminescence has been studied in SiO_2-Al_2O_3-LiF-SrF_2 glass ceramics [76], SiO_2-Al_2O_3-NaF-SrF_2 glass ceramics [79], SiO_2-Al_2O_3-ZnF_2-SrF_2 glass ceramics [80], as well as in other materials containing SrF_2 nanoparticles. The crystal-field splitting of Tb^{3+} bands in SrF_2 has been detected [74, 79, 81].

Energy transfer between Dy^{3+} and Eu^{3+} ions in oxyfluoride glass ceramics

There are fewer studies on energy transfer between Dy^{3+} and Eu^{3+} ions in oxyfluoride materials than on the other pair of ions (Tb^{3+}-Eu^{3+}) discussed in the thesis.

The reduction of the decay time of the donor ion Dy^{3+} by adding Eu^{3+} ions was examined in TeO_2 BaO-Bi_2O_3-SrF_2 oxyfluoride glass ceramics [80].

In BaF_2-containing glass with 0.5 mol% Dy^{3+} and 0.3 mol% Eu^{3+} ions, the energy transfer efficiency is 2.95% when excited at 350 nm, and monitoring the 482 nm (Dy^{3+}) emission [82]. Energy transfer between ions in glass ceramics containing CaF_2 nanocrystallites is discussed in the author's publication [59]. In glass ceramics containing CaF_2 nanocrystallites, energy transfer from Eu^{2+} to Dy^{3+} ions was also studied by excitation with 385 nm [68].

Energy transfer between Tb^{3+} and Eu^{3+} ions in oxyfluoride glass ceramics

Energy transfer between Tb^{3+} and Eu^{3+} ions has been extensively studied in various materials, including oxyfluoride glasses and glass ceramics. The luminescence and interaction of both activators have been studied in the following fluoride phases: CaF_2 ([46, 64], including those produced by the sol-gel method [9, 74]), SrF_2 (obtained by the sol-gel method [81]), as well as polycrystalline SrF_2 [83]), β-PbF_2 ([63], obtained by the sol-gel method [84]), cubic and hexagonal $NaYF_4$ [48], $SrLaF_5$ ([85]).

The efficiency of energy transfer strongly depends on the concentration of activators, the crystalline phase of the material, the size of nanocrystallites (nanoparticles) and other parameters.

Glass ceramics containing CaF_2 nanocrystals with a size of 7-15 nm, activated with 5 mol% Tb^{3+} and 1 mol% Eu^{3+} were obtained by heating calcium aluminosilicate glass at a temperature of 700 °C [46]. Exciting with 485 nm and monitoring the luminescence of Tb^{3+} ions at 541 nm, energy transfer efficiency was calculated to be 14%, while in the precursor glass it is lower – 8.7% [46]. In glass ceramics obtained by the sol-gel method with 1 mol% Tb and Eu, the energy transfer efficiency reaches 45.5 [9].

A comparative study of the luminescence of Tb^{3+} and Eu^{3+} ions in the cubic and hexagonal $NaYF_4$ phases is interesting, where it was concluded that the energy transfer between Tb^{3+} and Eu^{3+} ions occurs more efficiently in the cubic phase than in the hexagonal one [63]. For example, in glass ceramics containing a cubic $NaYF_4$ phase, the energy transfer efficiency from Tb^{3+} (5 mol%) to Eu^{3+} (5 mol%) is 25.6 %, and a hexagonal phase – 17.0 % [63].

3. RESEARCH METHODOLOGY

3.1. Sample synthesis and general characterization

3.1.1. Synthesis of glass samples

The glasses studied in the work were made at the Institute of Solid State Physics, University of Latvia, using the melt quenching method [11, 12]. Oxyfluoride glasses doped with rare earth activators in pairs (Eu^{3+}/Dy^{3+}; Eu^{3+}/Tb^{3+}) were synthesized. The procedure is shown schematically in **Figure 3.1.**

Commercially available high-purity (> 99.99%) ingredients in powder form were weighed and mixed in a porcelain pestle, then filled into aluminum oxide (corundum, Al_2O_3) crucibles. The total mass of raw materials was 8 g. The corundum crucibles were then covered with corundum lids to reduce the loss of fluorides during heating [13]. Covered corundum crucibles were placed in a Carbolite HTF 18/8 furnace and heated in air atmosphere from room temperature to 1450 ± 10 °C at a rate of ~30 °C/min and held at this temperature for 45 min, allowing the raw mass to melt. The molten mass was then rapidly poured into a stainless steel mold (see **Figure 3.1**, on the right), and pressed on top with another steel mold, rapidly cooling the mass. Immediately after pouring, a solid, transparent glass sample forms in the mold.

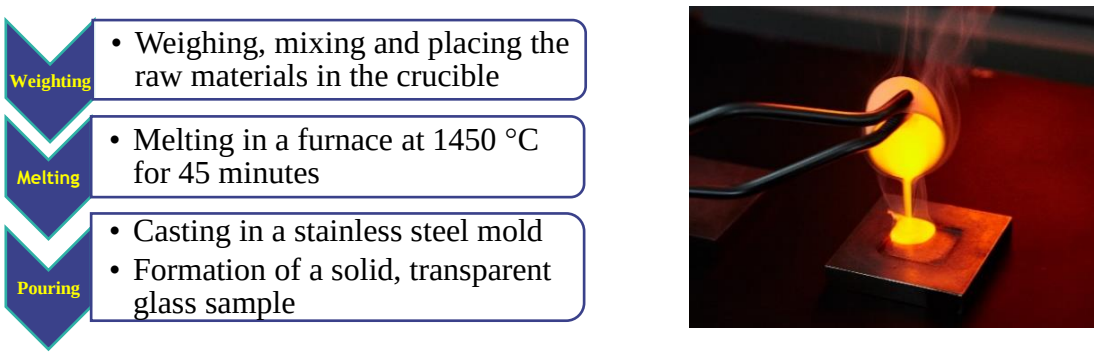

Figure 3.1. *on the left:* the process of glass synthesis, *on the right*: pouring the glass into the mold (photo author: Andris Fedotovs)

Three series of oxyfluoride glasses doped with one or two rare earth elements were synthesized. In each series of samples, the concentration of one activator (Dy^{3+} or Tb^{3+}) is fixed while the concentration of the other (Eu^{3+}) is varied to study the energy transfer efficiency in the samples.

1. **Series of samples. CaF_2-Dy^{3+}/Eu^{3+}.**

A series of oxyfluoride glasses with glass matrix composition SiO_2–CaF_2–Al_2O_3–CaO, activated with Dy^{3+} and Eu^{3+} ions. Initial glass composition: $45SiO_2$–$(27-(x+y))CaF_2$–$20Al_2O_3$–$8CaCO_3$-xDy_2O_3-yEu_2O_3, where x=0, 0.5, 1 mol% and y=0, 0.5, 1, 2 mol%. In this work, the samples are named by indicating the fluorides (here: CaF_2) and the concentration of rare earth ions, for example, Ca-Dy05 is a sample with 0.5 mol% Dy^{3+} ions, and Ca-Dy05Eu05 – with 0.5 mol% Dy^{3+} and 0.5 mol% Eu^{3+}.

2. **Series of samples. SrF_2-Dy^{3+}/Eu^{3+}**

A series of oxyfluoride glasses with the composition SiO_2–SrF_2–Al_2O_3–Na_2O, activated with Dy^{3+} and Eu^{3+} ions. Initial glass composition: $40SiO_2$–$(20-(x+y))SrF_2$–$25Al_2O_3$–$15Na_2CO_3$-xDy_2O_3-yEu_2O_3, where x=0, 0.5, 1 mol% and y=0, 0.5, 1, 2 mol%. Example: a sample with 0.5 mol% Dy^{3+} and 1.0 mol% Eu^{3+} ions will be called Sr-Dy05Eu1.

3. **Series of samples. SrF_2-Tb^{3+}/Eu^{3+}**

A series of oxyfluoride glasses with the composition SiO_2–SrF_2–Al_2O_3–Na_2O, activated with Dy^{3+} and Eu^{3+} ions. Initial glass composition: $40SiO_2$–$(20-(x+y))SrF_2$–$25Al_2O_3$–$15Na_2CO_3$-$xTbF_3$-$yEuF_3$, where

x=0, 0.5, 1 mol% and y=0, 0.5, 1 mol%. Example: a sample with 0.5 mol% Tb^{3+} and 1.0 mol% Eu^{3+} ions will be called Sr-Tb05Eu1.

3.1.2. Production of glass ceramic samples

Glass ceramics are obtained from the precursor glasses using heat treatment method. The original precursor glass samples that were described in *3.1.1. chapter*, were isothermally heated at 600–800 °C for 1 hour, placing the glasses in an already heated furnace. Additionally, some samples of the Sr-Dy^{3+}/Eu^{3+} series were heated for 4 hours. The names of the glass ceramic samples are formed by adding the processing temperature and, in the case of the Sr-Dy^{3+}/Eu^{3+} series, also the duration to the designation of the glass sample, for example, Ca-Dy05Eu1@680°C, Sr-Dy05@650°C-4h.

Heat treatment was performed in a narrow tunnel oven created under laboratory conditions, where the temperature was detected using a thermocouple. The temperature error is estimated to be ± 10 °C. The heat treatment temperature was selected based on the DTA (Differential Thermal Analysis) data.

Thermal treatment of glasses resulted in semi-transparent glass-ceramic samples containing nano-sized fluoride crystallites. Selected samples of glass and glass ceramics are shown in **Figure 3.2.**

Figure 3.2. The synthesized samples of glass and glass ceramics:
a) *Ca-Dy05Eu05 series (on the left):* glass, Ca-Dy05Eu05@680 °C, Ca-Dy05Eu05@750 °C;
b) *Sr-Dy05 series (middle)*: glass, Sr-Dy05@650 °C, Sr-Dy05@650-4h °C, Sr-Dy05@680 °C;
c) *Sr-Tb05Eu1 series (on the right):* glass, Sr-Tb05Eu1@650 °C, Sr-Tb05Eu1@680 °C.

3.1.3. Differential Thermal Analysis (DTA)

Differential thermal analysis (DTA) measurements allow determination of the characteristic glass temperatures: glass transition, crystallization and melting temperatures. DTA measurements were performed using a Shimadzu thermogravimetric analyzer (detector model DTG-60). A grinded powder of glass sample, and a reference sample (polycrystalline Al_2O_3 powder) were placed in the machine and heated from room temperature to 900 °C at a rate of 10 °C/min. During heating, the temperature of the sample is recorded and a DTA curve is taken, from which it is possible to determine the glass transition, crystallization and melting temperatures of the sample.

3.1.4. X-ray diffraction (XRD)

X-ray diffraction (XRD) analysis of glass and glass ceramic samples was performed using a Rigaku MiniFlex powder diffractometer with Cu anode, Cu Kα 0.154 nm radiation in 45 kV, 40 mA operating mode. (Additionally, the PANalytical X'Pert Pro powder diffractometer was used in the same operating mode for the samples investigated in the scientific publications.) XRD measurements were performed on grinded glass and glass ceramic sample powders.

In glass ceramics, diffraction peaks are observed in the diffractogram, which are caused by the crystalline phase of fluoride nanocrystallites. Crystallite sizes can be estimated using Scherrer's formula [5, 36]:

$$D = \frac{k\lambda}{\beta cos\theta} \tag{3.2}$$

D – crystallite diameter in vertical direction (hkl), k – form factor (here: k=0.9), λ – wavelength of X-ray radiation, β – half-width of the diffraction peak (in radians), θ – scattering angle (so-called Bragg angle) at which diffraction peak is observed (in radians).

Transmission electron microscopy (TEM) images taken for Sr-Eu1@670°C of the Sr-Tb^{3+}/Eu^{3+} sample series confirm the formation of SrF_2 nanocrystallites [41].

3.2. Photoluminescence measurements

3.2.1. Time-integrated luminescence excitation and emission measurements

The luminescence excitation and emission measurements of the samples were performed at room temperature.

Luminescence excitation and emission measurements were performed using an "Edinburgh Instruments FLS1000" luminescence spectrometer (model: FLS1000-DD-stm), equipped with a continuous wave (CW) 450 W xenon lamp (model: Xe2) and a cooled photoelectron multiplier (model: R928P) for luminescence detection. The photo of the equipment is shown in **Figure 3.3.a.**

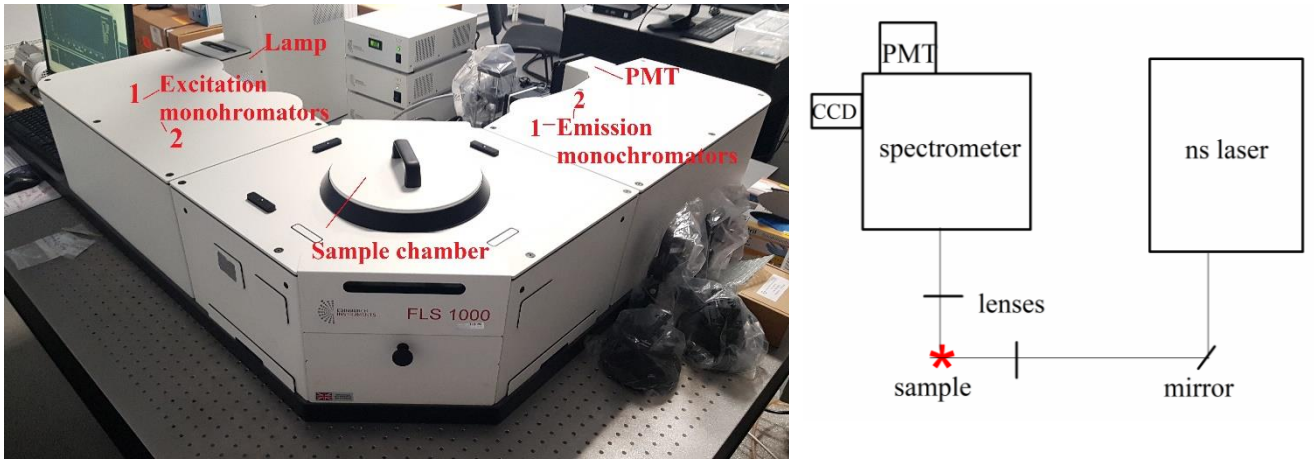

Figure 3.3.(a-b). a) "Edinburgh Instruments FLS1000" spectrometer with labeled components, b) the nanosecond laser system used in the measurements with a CCD camera for detection.

Excitation spectra were performed in the excitation range of 210-550 nm with a step of 0.5-2 nm, depending on the luminescence properties of the studied sample, emission spectra – in the range of ~270-800 nm. Each data point was measured by accumulating data for 0.5-1 s. The obtained spectra are automatically corrected regarding the sensitivity of the equipment (lamp, detector, diffraction grating) and power fluctuations of the excitation source.

Part of the measurements (with the equipment shown in **Figure 3.3a.**) were carried out for transparent glass and glass-ceramic samples, and a part – for grinded samples in powder form. Grinding of the samples was necessary in order to be able to correctly compare the intensity of the different samples. For comparative intensity measurements, grinded sample powders were placed in shallow stainless steel sample holders with an inner diameter of 9 mm. It should be noted that comparative measurements for powdered samples do not fully reflect the properties of glass and glass ceramics, because the powders are not transparent and the luminescence signal is detected only from their surface and not in the volume. For measurements in comparative intensity, the estimated error is ± 10% of the measured intensity. This error is caused by the position of the sample holder in the spectrometer and differences in sample loading in the sample holder.

3.2.2. Time-resolved luminescence measurements

Time-resolved luminescence measurements were performed using a nanosecond laser system consisting of a tunable solid-state pulse laser Expla (model NT342/3UV, pulse length around 4 ns, see **Figure 3.3b** – ns laser scheme) with a tunable wavelength (210 nm – 2300 nm range), Andor Technology

spectrometer (SR-303i-B) and CCD cameras (DH734-18F-A3). The light is directed using mirrors, lenses, if necessary, directing the luminescence signal from the sample to the spectrometer slit using an optical fiber. Luminescence spectra were recorded at different time intervals after the end of the laser pulses, thereby obtaining time-resolved luminescence spectra. The obtained luminescence spectra were not corrected regarding the spectral sensitivity, this would not provide important additional information within the scope of the work.

3.2.3. Luminescence quenching measurements

The luminescence decay kinetics were measured using a system comprising the aforementioned nanosecond laser system with additional devices. Measurements were made in two ways: 1) with a photoelectron multiplier (FED) and a Tektronix TDS 684A oscilloscope; 2) with Andor iStar CCD camera.

In the first case, the luminescence intensity is detected by the photoelectron multiplier (FED) (**Figure 3.3b**), and further, the oscilloscope analyzes the received signals, which are read and stored on the computer using the LabView interface. In the second case, the luminescence decay kinetics were obtained using time-resolved measurements similar to that described in *section 3.2.2.* This method is applied to measurements of the luminescence decay of Eu^{2+} ions. Luminescence spectra were measured in many time intervals, moving with a small time step – 50 ns –, respectively, in time intervals 30 ns – 80 ns, 80 ns – 130 ns, etc.

3.3. Electron paramagnetic resonance measurements

To analyze the environment of RE ions, electron paramagnetic resonance (EPR) spectra were measured for selected samples using two EPR spectrometers: Bruker ELEXSYS-II E500 CW-EPR and RE 13-06.

In the EPR method, the sample is placed in an external magnetic field (between magnets) and irradiated with microwave radiation at a frequency of 9.83 GHz (Bruker ELEXSYS-II E500) or 9.07 GHz (RE 13-06). A magnetic field induces Zeeman splitting of the energy levels of paramagnetic activators, while absorption of microwave radiation quanta induces transitions between Zeeman sublevels. The absorption of microwave radiation is measured depending on the value of the magnetic field. By modulating the magnetic field at a small amplitude, the first derivative of the absorption of microwave radiation is represented in the EPR spectrum. The obtained EPR signals are compared with the simulations performed within the framework of this work with the EasySpin program [86]. EPR analysis allows identification of cubic, tetragonal, etc. activator centers [87].

The EPR method can be used to study activators that are paramagnetic, i.e. they have an uncompensated spin in their outer electron shell. For this reason, it is difficult to study the trivalent RE ions (Eu^{3+}, Dy^{3+}, Tb^{3+}) examined in the work by the EPR method, so only the EPR spectra of Eu^{2+} ions were examined [86].

3.4. Color coordinates

The color of the emitted light (luminescence) of the samples can be characterized by color (or *photometrical*) coordinates. Based on the luminescence spectrum of the material and the spectral sensitivity of the human eye, the color coordinates show in what color the observer sees the color of the luminescence. Most often, the color of light is described using the CIE 1931 XYZ color space (CIE - International Commission on Illumination), which was created in 1931. The color is described. using two coordinates: x and y [59, 64, 88]. Color matching functions (related to the eye's spectral sensitivity) are used to find the so-called tristimulus values. In this work, CIE 1931 color coordinates were calculated using the ColorCalculator program offered by OSRAM SYLVANIA.

In the **Figure 3.4.** the luminescence of the glass samples of the activators studied in the work with different excitation wavelengths (ns laser excitation) is shown. The author of the photos is Andris Fedotovs.

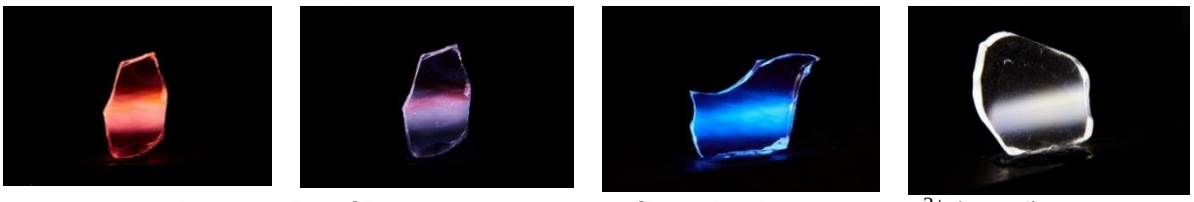

Figure 3.4. Photographs of luminescence in oxyfluoride glasses: a) Eu^{3+} ions (λ_{ex}=320 nm); b) Eu^{3+} and Eu^{2+} ions (λ_{ex}=350 nm); Eu^{2+} ions (λ_{ex}=350 nm); Tb^{3+} and Eu^{3+} ions (λ_{ex}=350 nm).

4. RESULTS

4.1. Dy^{3+}/Eu^{3+} activated glasses and glass ceramics containing CaF_2 nanocrystallites

4.1.1. Differential Thermal Analysis (DTA)

Differential thermal analysis (DTA) method was employed to find out at what temperature crystallization of the fluoride phase takes place in the studied glass samples. **Figure 4.1.a** shows the DTA curve of sample Ca-Dy05Eu1 and the characteristic phase transition temperatures are indicated.

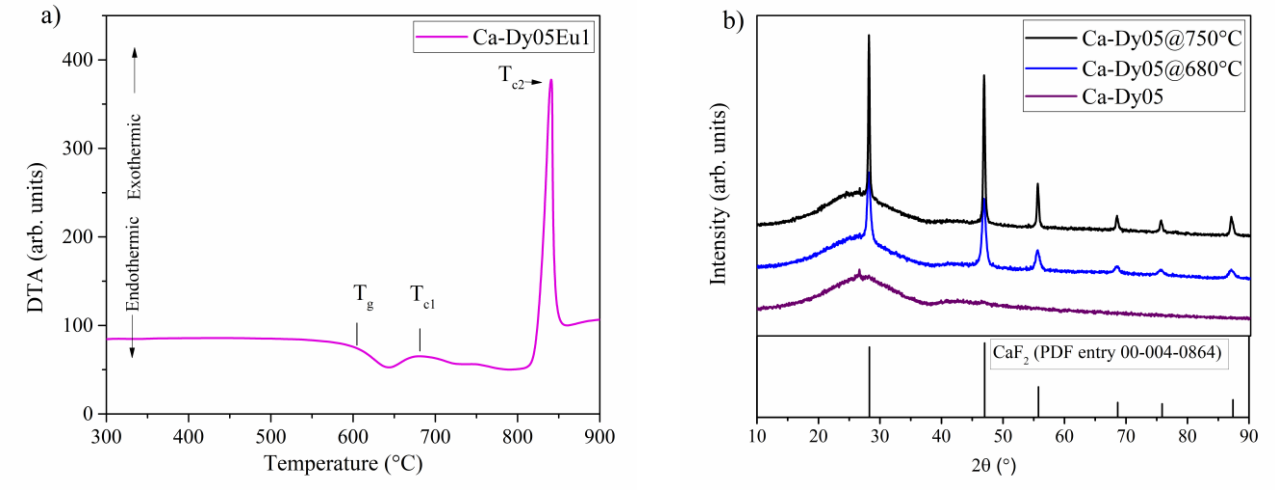

Figure 4.1(a-b). a) DTA curve and characteristic temperatures of sample Ca-Dy05Eu1, b) X-ray diffractograms of samples doped with Dy^{3+} ions (0.5 mol%) and diffraction peaks of CaF_2.

As can be seen in **Figure 4.1a**, the glass transition temperature (T_g) of the sample is around 604 °C, but two exothermic peaks are located around 680 °C and 840 °C (T_{c1} and T_{c2}). T_{c1} is associated with the formation of the crystalline phase of CaF_2 in the sample, while the intensive peak at T_{c2} is due to the crystallization of the aluminosilicate phase, which leads to the loss of transparency of the sample and is not desirable within the scope of this work.

Summary: Based on DTA data, temperatures of 680 °C and 750 °C were chosen for the production of glass ceramic samples containing CaF_2 nanocrystallites.

4.1.2. X-ray Diffraction (XRD)

X-ray diffraction (XRD) measurements were performed on glass and glass-ceramic samples in order to determine the crystalline structure of the prepared samples and to estimate the approximate sizes of the crystallites formed in the glass-ceramics. The diffractograms of the sample series Ca-Dy05 and the corresponding diffraction peaks of the crystalline phase of CaF_2 are shown in **Figure 4.1b**. XRD measurements were performed for all series of samples. X-ray diffractograms confirmed that all studied glass samples have an amorphous structure, while the diffraction peaks seen in the glass-ceramic samples correspond to the crystalline phase of CaF_2 (PDF entry 00-004-0864). The presence of aluminosilicate phases was not detected in the diffractograms.

Using Scherer's formula (expression (3.2) in *Chapter 3.1.4.* X-ray diffraction (XRD)), the dimensions of CaF_2 crystallites (diameter, nm, ± 2 nm) were calculated and summarized in **Table 4.1.**

Table 4.1. The calculated CaF_2 crystallite sizes (diameter, nm, ± 2 nm).

	680 °C	**750 °C**
Ca-Dy05	22	65
Ca-Dy05Eu05	15	50
Ca-Dy05Eu1	16	35
Ca-Dy05Eu2	10	29
Ca-Dy1	15	48

Summary: CaF_2 nanocrystallites with a diameter of 10-22 nm have formed in the samples heated at 680 °C, and 29-65 nm at 750 °C, it can be seen that in the samples heated at a higher temperature, CaF_2 nanocrystallites of a larger size have been formed.

4.1.3. Luminescence in glass

In order to find the wavelengths that can best excite the luminescence of Dy^{3+} and Eu^{3+} ions in glass samples, luminescence excitation spectra were measured. In the **Figure 4.2.** normalized excitation spectra of glass samples doped with Dy^{3+} ions are shown. The spectra were measured not at the peak of Dy^{3+} luminescence band (575 nm), but at 565 nm to avoid the influence of Eu^{3+} ion luminescence bands. The visible excitation transitions of Dy^{3+} ions and their corresponding excitation wavelengths are shown in **Table 4.2.**

Table 4.2. The excitation transitions of Dy^{3+} ions (from the $^6H_{15/2}$ ground state) [58, 59, 82, 89].

Position (nm)	**Electronic transition (from $^6H_{15/2}$)**
322	$^6P_{3/2}$, $^4D_{7/2}$
347	$^6P_{7/2}$
364	$^4P_{3/2}$, $^6P_{5/2}$
385	$^4I_{13/2}$
425	$^4G_{11/2}$
453	$^4I_{15/2}$
470	$^4F_{9/2}$

Dy^{3+} ions can be most intensively excited by UV excitation (347 nm – 350 nm, $^6H_{15/2}\rightarrow{}^6P_{7/2}$), and in the visible range with 453 nm ($^6H_{15/2}\rightarrow{}^4I_{15/2}$). 350 nm and 453 nm excitation wavelengths were selected for further studies.

From the **Figure 4.2.** it can be seen that the addition of Eu^{3+} ions affects the relative intensity of the excitation bands of Dy^{3+} ions. The inset shows the comparative intensity of Ca-Dy05 and Ca-Dy05Eu2 glass samples (i.e., measurements were made on powder samples) in the 340 nm – 400 nm range: the most pronounced change in excitation occurs for the 350 nm transition ($^6H_{15/2}\rightarrow{}^6P_{7/2}$), where upon addition of Eu^{3+} ions, the intensity of the Dy^{3+} ion excitation band decreases.

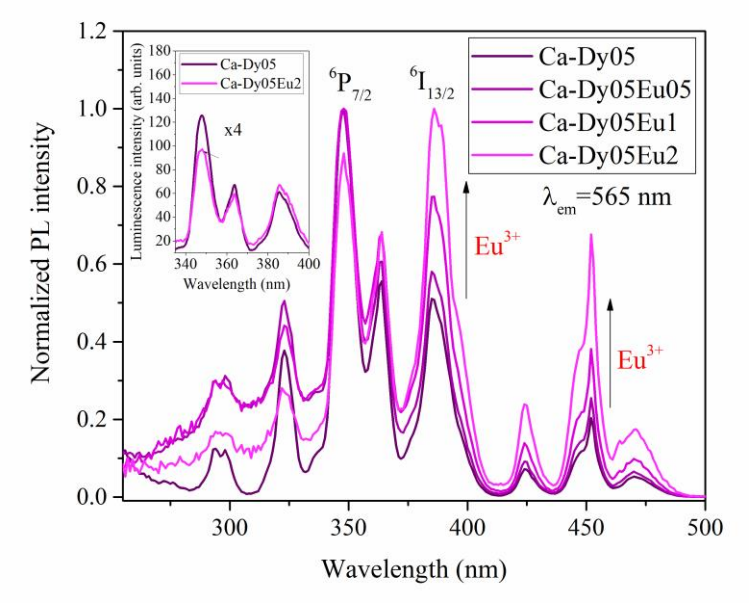

Figure 4.2. Normalized luminescence excitation spectra of Dy^{3+} ions in Dy^{3+} and Eu^{3+} co-doped glass samples with different Eu^{3+} concentrations (λ_{em}=565 nm).

Figure 4.2. In the range of 240 nm – 370 nm, a rise is visible in excitation spectra of Eu^{3+}-doped samples, which is related to the presence and excitation of Eu^{2+} ions in the samples. In the **Figure 4.3.** a comparison of the excitation spectra of Dy^{3+} and Eu^{2+} ions in normalized form is shown.

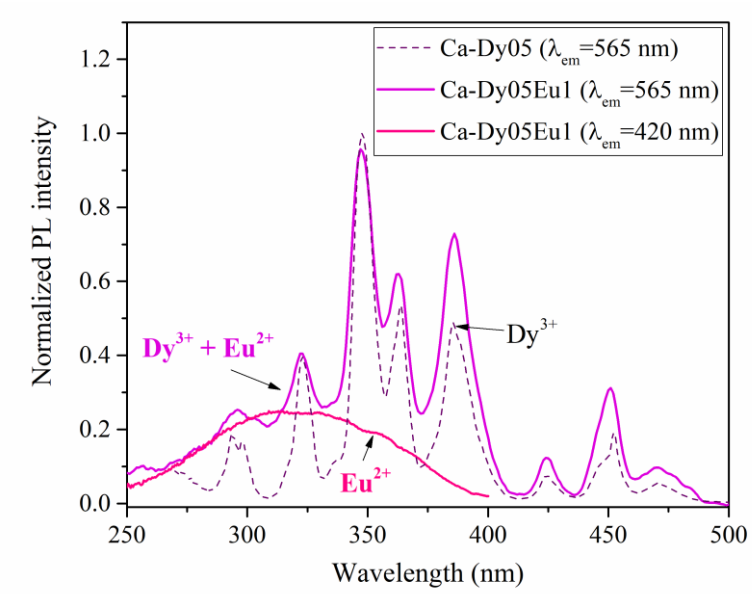

Figure 4.3. Comparison of excitation spectra of Dy^{3+} and Eu^{2+} ions.

Excitation spectra of Eu^{3+} ions and corresponding transitions are shown in **Table 4.3** and **Figure 4.4.** The most intense Eu^{3+} ion excitation bands are at 393 nm ($^7F_0 \rightarrow {}^5L_6$) and 464 nm ($^7F_0 \rightarrow {}^5D_2$).

In the **Figure 4.4.** it can be seen that in co-doped samples, excitation bands around 350 nm and 453 nm (marked with *) appear in the Eu^{3+} excitation spectrum, which are not observed in the sample doped only with Eu^{3+} ions – they correspond to the excitation peaks of Dy^{3+} ions (dashed line in the **Figure 4.4**.). The presence of Dy^{3+} ion excitation bands in the Eu^{3+} ion excitation spectrum indicates the energy transfer from Dy^{3+} to Eu^{3+} ions [57, 59].

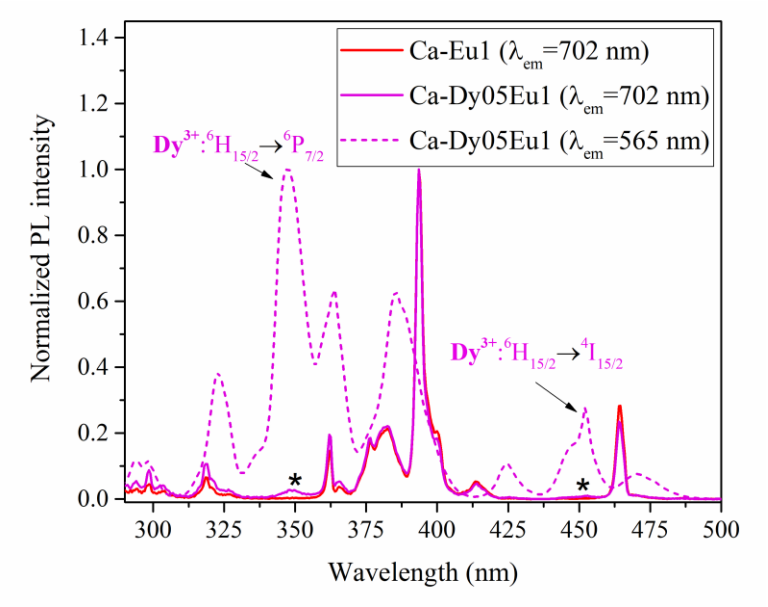

Figure 4.4. Normalized luminescence excitation spectra of Eu^{3+} ions in Eu^{3+}-doped and Dy^{3+}/Eu^{3+} co-doped glass samples (λ_{em}=702 nm).

Table 4.3. Excitation transitions of Eu^{3+} ions in glass samples [9, 45, 61, 63, 83].

Position (nm)	**Electronic transition (from ground state $^7F_0$)**
318	$^5H_6$
361	$^5D_4$
376	^5G_J , ^5L_J
393	$^5L_6$
414	$^5D_3$
464	$^5D_2$
525	$^5D_1$
533	(from $^7F_1$) $^5D_1$

In the **Figure 4.5.** luminescence spectra of glass samples with 453 nm excitation (exciting Dy^{3+} ions well) are shown in comparative intensity. For the measurements, the samples were grinded and filled in shallow samples holders, so that it was possible to compare the luminescence intensity of different samples. Measurement error – 10% of the intensity.

In all samples, the emission band of Dy^{3+} ions with a peak around 575 nm ($^4F_{9/2}\rightarrow {}^6H_{13/2}$) is the most intense. Dy^{3+} ion luminescence bands at 480 nm ($^4F_{9/2}\rightarrow {}^6H_{15/2}$) and 660 nm ($^4F_{9/2}\rightarrow {}^6H_{11/2}$) are also visible. Co-doped samples show luminescence of Eu^{3+} ions with a peak at 612 nm ($^5D_0\rightarrow {}^7F_2$). Its relative intensity to the emission bands of Dy^{3+} ions increases in proportion to the added concentration of Eu^{3+} ions. In the **Figure 4.5.** it can be seen that the highest luminescence intensity of Dy^{3+} ions is observed in the sample with 0.5 mol% Dy^{3+}. In the sample with 1 mol% Dy^{3+}, the luminescence intensity is about a third lower.

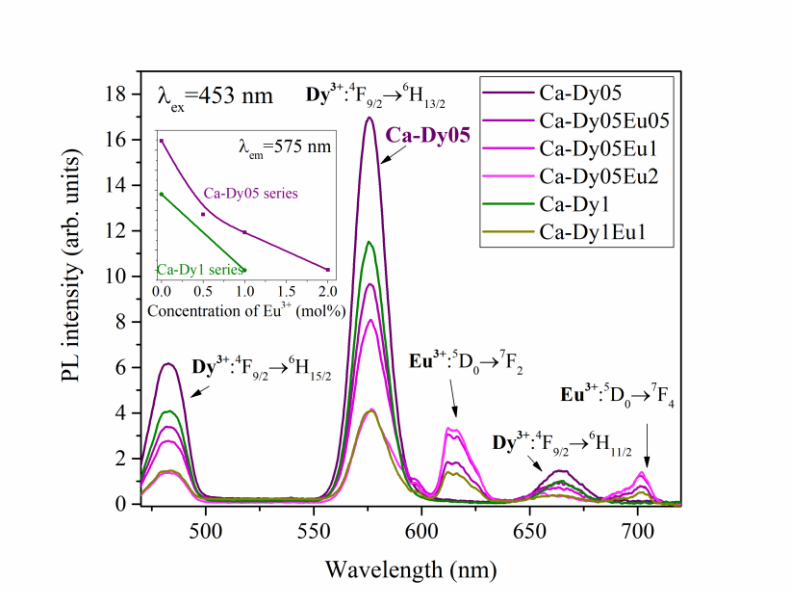

Figure 4.5. Luminescence spectra of glasses doped with Dy^{3+} and Eu^{3+} ions (λ_{ex}=453 nm). In the inset: the maximal luminescence intensity of Dy^{3+} ions (λ_{em}=575 nm) depending on the concentration of RE ions.

The decrease in luminescence intensity in samples with higher Dy^{3+} concentration could be explained by cross-relaxation from the $^4F_{9/2}$ level between nearby Dy^{3+} ions (see *Chapter 2.3.4. Luminescence properties of Dy^{3+} ions)* [56, 57, 59, 82, 89]. As a result of this process, part of the excited electrons return to the ground state not through a radiative transition, but by non-radiatively relaxation to a lower energy level. Also, a significant decrease in the luminescence intensity of Dy^{3+} ions is seen when Eu^{3+} ions are added to the samples. The decrease in the luminescence intensity of Dy^{3+} ions in co-doped samples is related to energy transfer from Dy^{3+} to Eu^{3+} ions, which will be discussed later [59, 82].

Figure 4.6.a. show normalized luminescence spectra of Eu^{3+} ions in sample Ca-Eu1 with 393 nm and 464 nm excitation, which effectively excite the luminescence of Eu^{3+} ions. Also, in co-doped glass samples with this excitation, the luminescence bands of Eu^{3+} ions dominate, but the characteristic bands of Dy^{3+} ions are not observed. The luminescence spectrum of Eu^{3+} ions in glass is dominated by the emission transition at 612 nm ($^5D_0 \rightarrow {}^7F_2$), which is an electric dipole (ED) transition and is a hypersensitive transition [41, 45]. The $^5D_0 \rightarrow {}^7F_2$ transition is dominant in materials without an inversion center, as expected in amorphous glass samples [41, 45, 75, 90, 91].

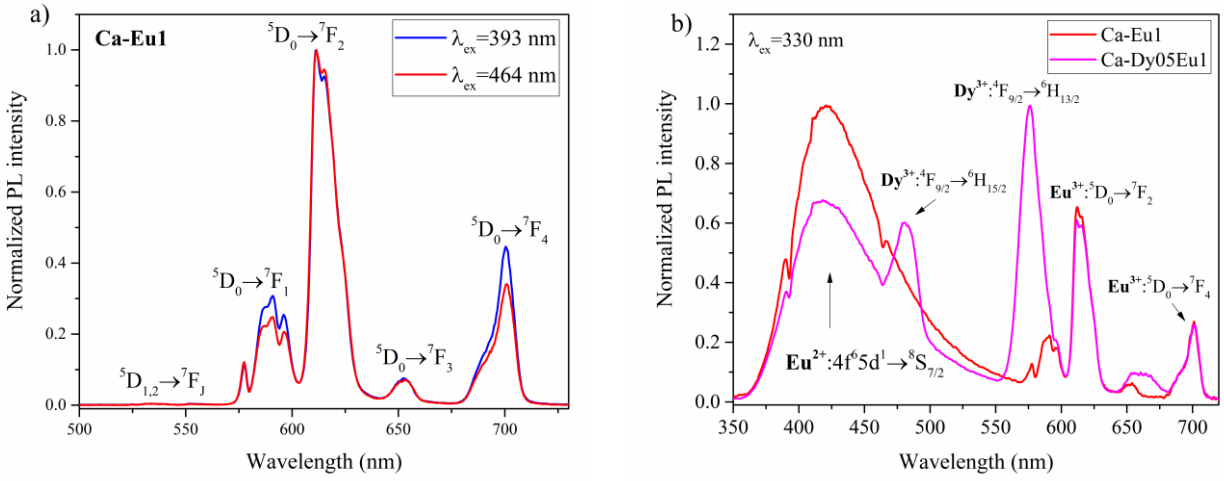

Figure 4.6.(a-b). a) normalized luminescence spectra of sample Ca-Eu1 with 393 nm and 464 nm excitation, b) luminescence of glass samples containing europium ions (λ_{ex} = 330 nm).

In the **Figure 4.6.b.** luminescence spectra of samples containing europium ions with 330 nm excitation are shown. A broad luminescence band in the blue-green spectral range (~350 nm – 580 nm) with a peak around 420 nm is observed, which corresponds to the luminescence transition of Eu^{2+} ions $4f^65d^1 \rightarrow {}^8S_{7/2}$ in oxyfluoride glass and partially overlaps with the luminescence bands of Dy^{3+} and Eu^{3+} ions [35, 36, 38, 41, 64]. 330 nm is the most effective excitation wavelength for Eu^{2+} ions in the studied oxyfluoride glasses, as can be seen from **Figure 4.3.**

Summary: In the investigated glass samples containing Dy^{3+}/Eu^{3+} ions, Dy^{3+} ions can be excited most effectively with ~350 nm and 453 nm, Eu^{3+} ions with 393 nm and 464 nm, and the excitation spectrum of Eu^{2+} ions with a maximum around 330 nm was observed. Excitation transitions of Dy^{3+} ions are observed in the excitation spectrum of Eu^{3+} ions, which indicates energy transfer from Dy^{3+} to Eu^{3+} ions.

In glasses, depending on the excitation wavelength, the most intense is the Dy^{3+} emission band at 575 nm ($^4F_{9/2} \rightarrow {}^6H_{13/2}$) or the Eu^{3+} ion emission band at 612 nm ($^5D_0 \rightarrow {}^7F_2$, ED transition), as expected in positions with amorphous environment without an inversion center.

The most intense luminescence of Dy^{3+} ions with 453 nm excitation is observed in the glass sample with 0.5 mol% Dy^{3+} ions, but it is lower in glass with 1 mol% Dy^{3+} and in Dy^{3+}/Eu^{3+} co-doped glass samples due to cross-relaxation processes between Dy^{3+} ions and the energy transfer from Dy^{3+} to Eu^{3+} ions. A luminescence band of Eu^{2+} ions ($4f^65d^1 \rightarrow {}^8S_{7/2}$) with a peak around 425 nm was observed in both Eu^{3+}-doped and Dy^{3+}/Eu^{3+} co-doped glasses, indicating a partial reduction of Eu^{3+} ions to Eu^{2+} ions during the preparation of a glass.

4.1.4. Luminescence in glass ceramics

In **Figure 4.7.(a-b).** normalized excitation spectra of a) Dy^{3+} ions and b) Eu^{3+} ions in glass-ceramic samples are shown. It can be seen that the relative ratio of excitation band intensities is slightly different in glass and glass ceramic samples.

In only Dy^{3+}-doped glass and glass ceramic samples, Dy^{3+} ions can be most effectively excited by 350 nm radiation (see **Figure 4.7a**). The inset shows that the intensity of the 350 nm excitation band in glass ceramics has decreased slightly more than the intensity of other excitation bands compared to glass. In co-doped samples, a relative decrease in the excitation intensity of Dy^{3+} ions in the UV spectral range (240 nm – 400 nm) was observed, compared to the glass sample.

Figure 4.7b shows Eu^{3+} excitation spectra in co-doped Ca-Dy05Eu1 sample series. The relative ratio of the excitation peaks at 394 nm ($^7F_0 \rightarrow {}^5L_6$) and 464 nm ($^7F_0 \rightarrow {}^5D_2$) changes slightly from glass to glass-ceramic samples – the intensity of the excitation band at 464 nm increased relatively in the glass-ceramic samples. In the spectral range 230 nm – 300 nm, a broad excitation band is observed, which is related to the Eu-O charge transfer in the samples [45].

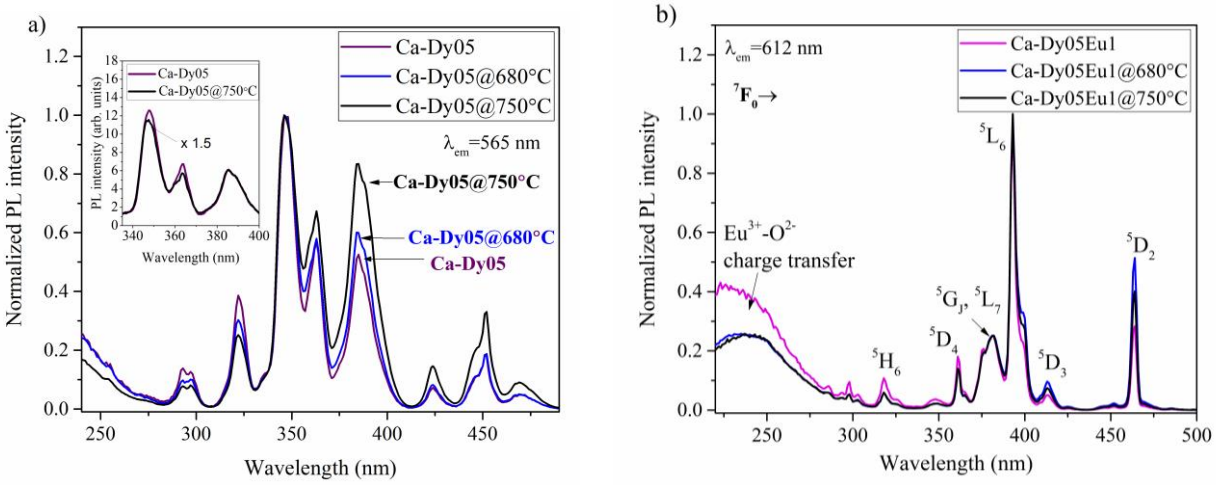

Figure 4.7(a-b). a) normalized luminescence excitation spectra of Dy^{3+} ions in glass and glass ceramics (λ_{em}=565 nm), b) normalized luminescence excitation spectra of Eu^{3+} ions inco-doped Ca-Dy05Eu1 series glass and glass ceramic samples (λ_{em}=612 nm).

In **Figure 4.8.(a-b).** luminescence spectra of Dy^{3+} and Dy^{3+}/Eu^{3+} doped samples are shown in comparative intensity (λ_{ex}=453 nm). In the glass-ceramic sample series with Dy^{3+} ions (**Figure 4.8.a**), a strong decrease in the luminescence intensity of Dy^{3+} ions can be observed, compared to glass. The decrease in intensity correlates with the increase in the size of CaF_2 nanocrystallites (see **Table 4.1.**) – the luminescence intensity of Dy^{3+} ions is lower in glass-ceramic samples with larger nanocrystallites. In co-doped samples (see **Figure 4.8b**), the luminescence intensity of Dy^{3+} ions in glass ceramics decreases slightly, as does the luminescence intensity of Eu^{3+} ions. A similar picture was observed with 350 nm excitation.

The difference in the luminescence intensity of Dy^{3+} ions in Dy^{3+}-doped and Dy^{3+}/Eu^{3+} co-doped samples could be explained by the fact that the presence of Eu^{3+} ions (in the general case – trivalent RE ions) inhibits the formation of Dy^{3+} ion clusters and thus reduces the efficiency of cross-relaxation processes between Dy^{3+} ions [18]. In co-doped glass-ceramic samples, Dy^{3+} and Eu^{3+} ions compete for incorporation into CaF_2 nanocrystallites, and when Eu^{3+} ions replace Ca^{2+} ions, the distance between neighboring Dy^{3+} ions of CaF_2 will be greater compared to the case if all replacing ions were Dy^{3+}.

Eu^{3+} ion luminescence (612 nm, $^5D_0 \rightarrow {}^7F_2$) is observed in co-doped samples with 393 nm excitation, but the luminescence intensity of Dy^{3+} ions is low. The shape of the luminescence spectrum of Eu^{3+} ions (i.e. the ratio of $^5D_0 \rightarrow {}^7F_2$ and $^5D_0 \rightarrow {}^7F_1$ bands) in glass ceramics does not change compared to glass.

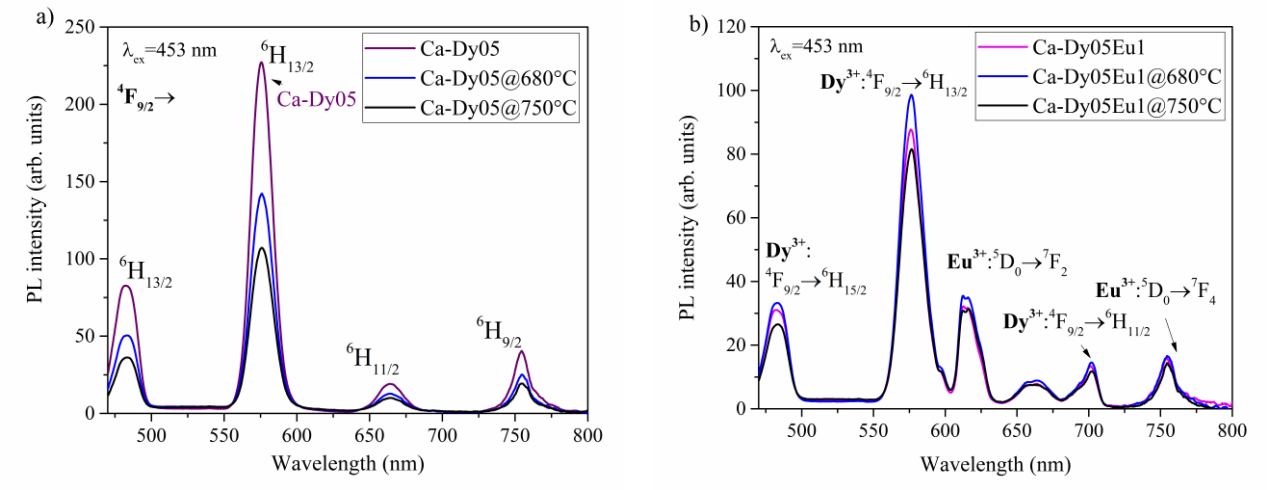

Figure 4.8(a-b). Luminescence spectra in comparative intensity with a) Dy^{3+} ions (0.5 mol%) and b) Dy^{3+} (0.5 mol%) and Eu^{3+} (1 mol%) doped glass ceramic samples; (λ_{ex}=453 nm).

Summary: In glass ceramics, the relative intensity of the Dy^{3+} and Eu^{3+} ion excitation bands has slightly changed compared to glasses, indicating a change in the RE ion environment as a result of heat treatment. Excitation bands of Dy^{3+} ions are also observed in the excitation spectra of Eu^{3+} ions in co-doped glasses and glass ceramics, which indicate energy transfer from Dy^{3+} to Eu^{3+} ions.

In glass ceramics containing CaF_2 nanocrystallites, the luminescence intensity of Dy^{3+} and Eu^{3+} ions is slightly decreased compared to the original glasses, but the relative intensity of the luminescence bands in glass and glass-ceramic is similar. In time-integrated measurements, the luminescence bands do not show crystal-field splitting, indicating that most of the RE ions are positioned in the amorphous glass environment rather than in a crystalline environment of CaF_2 nanocrystallites.

4.1.5. Time-resolved luminescence spectra

In order to distinguish between the luminescence signals associated with different environments of RE ions – amorphous or crystalline environment (entering fluoride nanocrystallites) – time-resolved luminescence spectra were measured using a tunable nanosecond laser with a pulse duration of about 4 ns for excitation. The luminescence decay of RE ions in amorphous glass and fluoride crystallites with lower phonon energy proceeds at different rates, which allows partial separation of the luminescence signal coming from the crystalline environment (when the luminescence in the glassy phase is already quenched). The following time intervals were examined: 1) shortly after the end of excitation pulse (50 ns – 100 μs); 2) a longer time after that (10-20 ms – 45 ms). In addition, site-selective spectroscopy is employed – by varying the excitation wavelength, it is possible to obtain the luminescence spectra of RE ions in different environments.

In **Figure 4.9.(a-b).** time-resolved and site-selective luminescence spectra of samples annealed at 750°C are shown: a) time-resolved luminescence spectra of Dy^{3+} ions in sample Ca-Dy05@750°C (λ_{ex}=453 nm), b) time-resolved site-selective luminescence spectra of Eu^{3+} ions in sample Ca-Dy05Eu1@ 750°C.

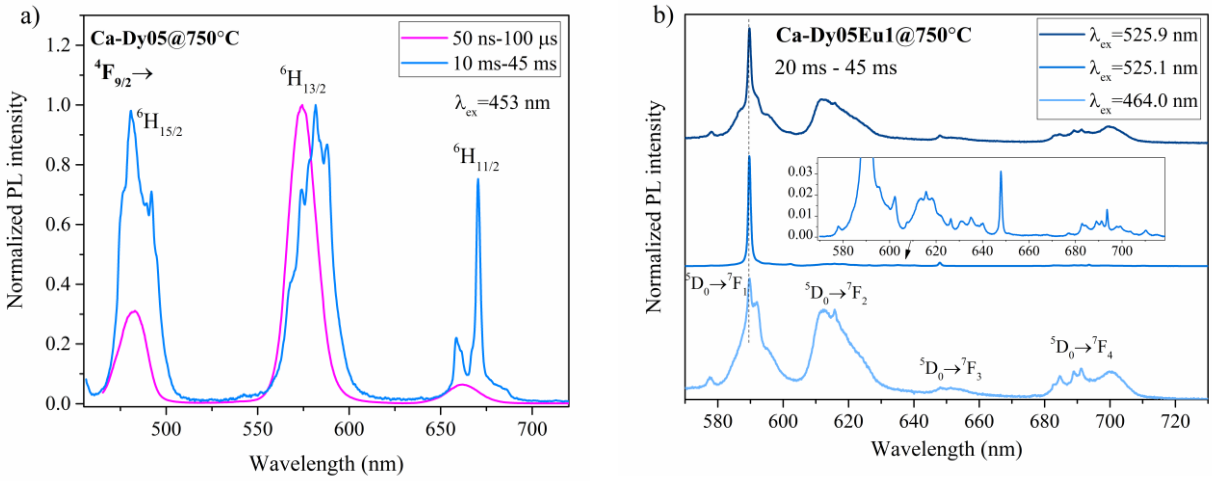

Figure 4.9.(a-b). Normalized a) time-resolved luminescence spectra of Dy^{3+} ions in sample Ca-Dy05@750°C (λ_{ex}= 453 nm), b) time-resolved site-selective luminescence spectra of Eu^{3+} ions in sample Ca-Dy05Eu1@750°C.

In **Figure 4.9.a.** it can be clearly seen that the luminescence spectra of Dy^{3+} ions are different in different time intervals. In the time interval of 50 ns – 100 µs after the laser pulse, the spectrum bands are smooth and correspond to the luminescence spectrum of Dy^{3+} ions in glass [50, 59, 64, 92], but in 10 ms – 45 ms – splitting of the bands is observed. The luminescence spectra of Dy^{3+} in the time interval 10 ms – 45 ms show the luminescence of Dy^{3+} ions in CaF_2 nanocrystallites, which is most clearly seen in the narrow group of luminescence bands in the 650 nm – 680 nm spectral range ($^4F_{9/2}\rightarrow{}^6H_{11/2}$), and it can be seen that the luminescence bands of Dy^{3+} in CaF_2 nanocrystallites are shifted to longer wavelengths by 2 – 10 nm compared to glass. The luminescence spectra of Dy^{3+} ions in the time interval of 10 – 45 ms correspond well to the Dy^{3+} spectra in CaF_2 single crystal described in the literature [18, 93], moreover [93] mentions that the spectra correspond to Dy^{3+} ions in cubic (O_h) symmetry. In Oh symmetry, the charge compensation, when the Dy^{3+} ion replaces the Ca^{2+} ion in the CaF_2 crystal (nanocrystallite), does not occur in the vicinity of the Dy^{3+} ion.

In the site-selective luminescence spectra (**Figure 4.9b**), the sharp $^5D_0\rightarrow{}^7F_2$ band at 590 nm (λ_{ex}=525.1 nm) is associated with the Eu^{3+} cubic center (O_h), a centrosymmetric position is also indicated by the low intensity of the other luminescence bands [24, 30, 45, 94]. The luminescence spectrum with excitation at 525.9 nm and a luminesence peak at 592 nm could be related to tetragonal centers (in CaF_2:Eu^{3+} crystals it is mentioned as one of the dominant Eu^{3+} centers) [24, 30] or Eu^{3+} ion clusters, which have also been studied in CaF_2 [30, 94].

The approximate concentration of Eu^{3+} ions in CaF_2 crystallites formed in oxyfluoride glass ceramics has been estimated in [30]. The composition of the glass matrix discussed in the publication [30] almost coincides with that discussed in the thesis. By combining XRD and EPR methods, it was determined that in glass ceramics with an added concentration of 1.0 mol% Eu^{3+}, the concentration of Eu^{3+} in the CaF_2 crystalline phase is around 2.4 ± 0.2 mol%, with added 10.0 mol% – 33.9 ± 3.4 mol% [30]. That is, by adding 10.0 mol% Eu^{3+} ions to the glass sample, about a third of them will have entered the CaF_2 nanocrystallites in the glass ceramic. However, the samples studied in the thesis are co-doped with Eu^{3+} and Dy^{3+} (or Tb^{3+}) ions, there is competition between rare earth ions to enter CaF_2 nanocrystallites and the concentration of both ions in CaF_2 nanocrystallites is difficult to estimate separately. Considering that integrated luminescence spectra are dominated by broad luminescence bands arising from the glassy phase, the concentration of RE ions in CaF_2 nanocrystallites could be small (below 10 mol %).

Summary: Time-resolved measurements, measured in the time interval from 10 or 20 ms to 45 ms after the laser pulse, confirm the partial incorporation of Dy^{3+} and Eu^{3+} ions into the CaF_2 crystallites, since the crystal-field splitting of the luminescence bands and the change of Eu^{3+} bands $^5D_0\rightarrow{}^7F_1$ and $^5D_0\rightarrow{}^7F_2$ relative intensity can be observed in the spectra measured in this time interval. The changes in spectra can be observed because in this time interval the luminescence of $Dy^{3+}$and Eu^{3+} ions in the glass environment is almost extinguished. The site-selective Eu^{3+} luminescence spectra in the mentioned time interval indicate at least 3 different environments of Eu^{3+} ions in the glass ceramic which is observed due to different charge compensation processes.

4.1.6. Eu^{2+} ion luminescence and electron paramagnetic resonance spectra

The previous chapters discussed the luminescence of Eu^{2+} ions in glass. Since Eu^{2+} ions have a short luminescence decay time ($\tau < 1$ μs) [10, 39, 85], time-resolved luminescence measurements were performed, at the time interval 30 ns – 1 μs, for comparison also measuring in a longer time interval (30 ns – 45 ms). Time-resolved luminescence spectra in Ca-Dy05Eu1 series glass and glass-ceramic samples with 330 nm excitation are shown in **Figure 4.9a**. It can be seen that in the time interval of 30 ns – 1 μs only a broad luminescence band of Eu^{2+} ions ($4f^65d^1 \rightarrow {}^8S_{7/2}$) can be observed in both glass and glass ceramics, while in a longer measurement interval it is relatively weaker compared to the luminescence bands of Eu^{3+} and Dy^{3+} ion.

In order to find out in which environment – in the glassy phase or in the nanocrystallites – the Eu^{2+} ions are located, electron paramagnetic resonance (EPR) measurements were also performed on the samples. The EPR spectra of the Ca-Dy05Eu1 series and the Ca-Eu1 sample are shown in **Figure 4.9b.** In the EPR spectra in the magnetic field interval ~95-150 mT, with the exciting microwave frequency 9.83 GHz, microwave absorption (its first derivative) can be observed. The signal corresponds to Eu^{2+} ions in the glass [95]. A signal related to Eu^{2+} ions in the crystalline environment was not detected. It can be concluded that the majority of Eu^{2+} ions are in an amorphous environment, although a small concentration of them in CaF_2 nanocrystallites cannot be ruled out. The EPR signal of Eu^{2+} ions is about an order of magnitude less intense than the signal of Gd^{3+} ions when 0.1 mol% of Gd^{3+} ions is added to the sample. It can be concluded that the concentration of Eu^{2+} ions in the samples studied in the thesis is very small.

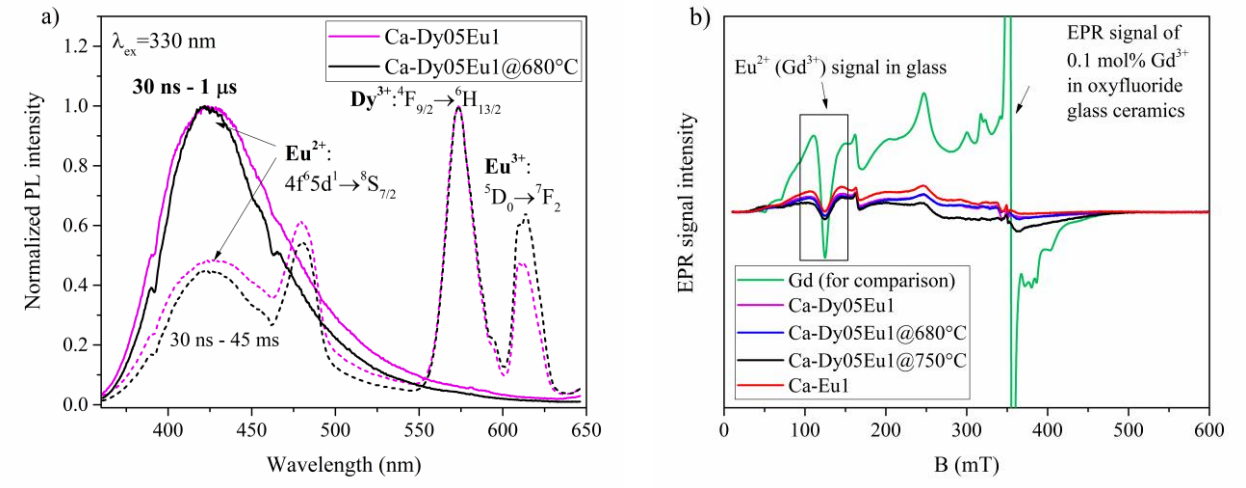

Figure 4.9.(a-b). a) normalized time-resolved luminescence spectra of the sample Ca-Dy05Eu1@680°C with 330 nm excitation, b) EPR spectra of the Ca-Dy05Eu1 series and the Ca-Eu1 sample compared to the Gd^{3+} ion signal in previously studied oxyfluoride glass ceramics.

Summary: The spectral shape of Eu^{2+} luminescence bands ($4f^65d^1 \rightarrow {}^8S_{7/2}$) in co-doped glass and glass-ceramic are similar, indicating no significant change of Eu^{2+} environment from glass to glass-ceramic. The EPR spectra of the Ca-Dy05Eu1 series confirm the presence of Eu^{2+} ions in the samples, with a concentration of Eu^{2+} ions < 0.1 mol%, and also indicate that the majority of Eu^{2+} ions in glass ceramics is situated in the amorphous glass phase and not in CaF_2 nanocrystallites.

4.1.7. Luminescence decay kinetics and energy transfer between Dy^{3+} and Eu^{3+} ions

In order to study the interaction between RE ions, luminescence decay measurements of Dy^{3+} ions in glass samples with 453 nm ns laser excitation were performed. Measurements of Dy^{3+} luminescence band ${}^4F_{9/2} \rightarrow {}^6H_{13/2}$ (575 nm) were performed. The obtained decay curves are shown on a semi-logarithmic scale in **Figure 4.11.** The effective decay times are shown in **Table 4.4.**

As can be seen in **Table 4.4**, the effective decay time of Dy^{3+} ions decreases with the addition of Eu^{3+} ions. For the samples doped with 0.5 mol% Dy^{3+} ions, the decay time decreases proportionally to the increasing concentration of Eu^{3+} ions, which corresponds to what has been observed in the literature [59, 82]. Using the effective decay times, the calculated energy transfer efficiency from Dy^{3+} to Eu^{3+} ions is around 11% for Ca-Dy05Eu05 glass and 23% for Ca-Dy05Eu1 (see **Table 4.4**). The energy transfer efficiency in the Ca-Dy1Eu1 sample is 8%. Comparing the Ca-Dy05 and Ca-Dy1 glass samples, a significant decrease in the effective decay time can be seen, which could be related to the cross-relaxation processes characteristic of Dy^{3+} ions [56, 57, 59, 82, 89].

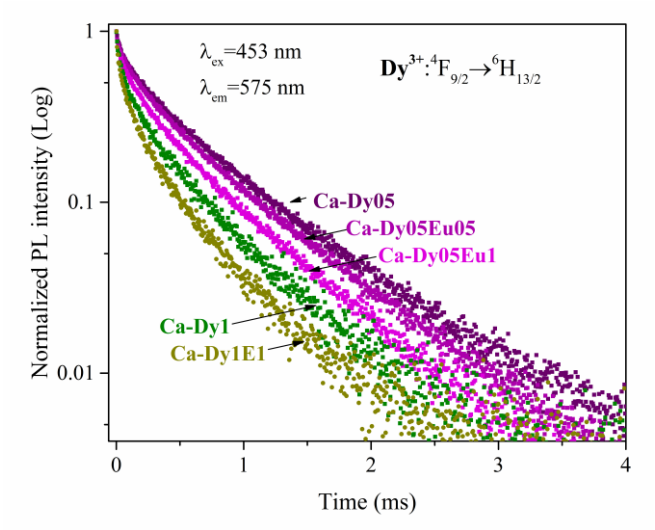

Figure 4.11. Dy^{3+} ion luminescence decay kinetics in glass samples (λ_{ex}=453 nm, λ_{em}=575 nm).

Table 4.4. Calculated Dy^{3+} ions effective decay times and energy transfer ($Dy^{3+}\rightarrow Eu^{3+}$) efficiency.

Sample (λ_{ex}=453 nm, λ_{em}=575 nm)	**τ (ms) ± 0.01 ms**	**η (%) ±1**
Ca-Dy05	0.74	-
Ca-Dy05Eu05	0.66	11
Ca-Dy05Eu1	0.57	23
Ca-Dy1	0.52	-
Ca-Dy1Eu1	0.48	8

Figure 4.12.(a-b). shows the luminescence decay kinetics in glass and glass ceramic samples of Ca-Dy05 and Ca-Dy05Eu1 series with 453 nm excitation. In **Table 4.5.** the calculated luminescence decay times of Dy^{3+} ions and energy transfer ($Dy^{3+}\rightarrow Eu^{3+}$) efficiency are shown.

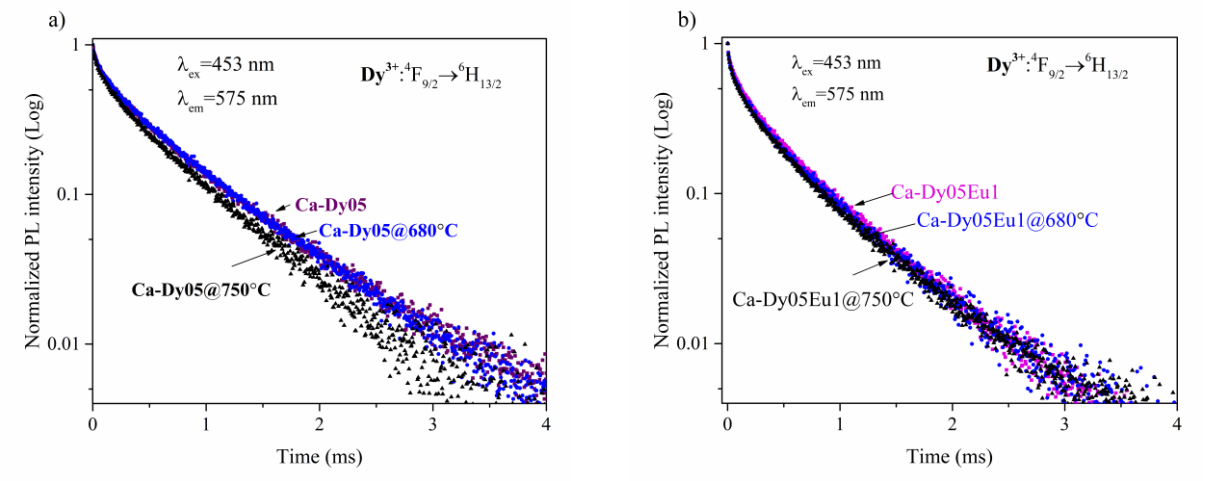

Figure 4.12(a-b). Luminescence decay kinetics of sample series Ca-Dy05 and Ca-Dy05Eu1.

Table 4.5. Luminescence decay times in Dy^{3+} (0.5 mol %) doped glass and glass ceramic samples.

Sample (λ_{ex}=453 nm, λ_{em}=575 nm)	**τ (ms) ± 0.01 ms**	**Sample (λ_{ex}=453 nm, λ_{em}=575 nm)**	**τ (ms) ± 0.01 ms**	**η (%) ±1**
Ca-Dy05	0.74	Ca-Dy05Eu1	0.57	23
Ca-Dy05@680°C	0.71	Ca-Dy05Eu1@680°C	0.60	16
Ca-Dy05@750°C	0.61	Ca-Dy05Eu1@750°C	0.62	-

Table 4.5. shows that in samples of the Ca-Dy05Eu1 series, the luminescence decay time in glass-ceramics increases slightly, however, overall, the decay curves are very similar (**Figure 4.12(a-b)**). On the other hand, the speeding up of luminescence decay can be observed in Ca-Dy05 series glass-ceramic samples. This could be related to the previously discussed cross-relaxation processes of Dy^{3+} ions. The energy transfer efficiency in glass ceramics Ca-Dy05Eu1@680°C slightly decreases compared to glasses, which could indicate that Dy^{3+} cross-relaxation processes are dominant, or that Dy^{3+} and Eu^{3+} ions are not close to each other in the crystallites, and also, it should be taken into account that the increase in the luminescence decay time can also be caused by the incorporation of RE ions into the environment with lower phonon energy (i.e. in fluoride nanocrystallites).

The luminescence decay kinetics of Eu^{2+} ions in a series of Ca-Dy05Eu1 samples were also recorded. The following decay times of Eu^{2+} ions were obtained: Ca-Dy05Eu1 – 409 ns, Ca-Dy05Eu1@680°C – 453 ns (measurement error ± 20 ns). The increase in the decay time of Eu^{2+} ions in glass ceramics could be explained by the partial incorporation of Eu^{2+} ions into fluoride nanocrystallites.

Summary: The slowest luminescence decay of Dy^{3+} ions (emission transition $^4F_{9/2}\rightarrow{}^6H_{13/2}$) and the longest effective decay time is observed in the glass sample with 0.5 mol% Dy^{3+} (Ca-Dy05, 0.74 ms). By adding Eu^{3+} ions, the decay time of Dy^{3+} ions decreases to 0.57 ms, due to non-radiative energy transfer to Eu^{3+} ions. The energy transfer efficiency in Ca-Dy05Eu1 glass reaches 23%.

The luminescence decay time of Dy^{3+} ions in glass ceramics containing only Dy^{3+} ions is shortened compared to the precursor glasses, but in co-doped glass ceramics it increases slightly. The shortening of the decay time in Dy^{3+} ion singly-doped glass ceramics is associated with more efficient cross-relaxation processes. The energy transfer efficiency in glass-ceramics decreases slightly compared to glass, which could be related to efficient cross-relaxation processes of Dy^{3+} ions as ell, which can interfere with energy transfer to Eu^{3+} ions. The decay time of Eu^{2+} in glass ceramics increases compared to glass, which could be explained by the partial entry of Eu^{2+} ions into fluoride nanocrystallites with lower phonon energy.

4.1.8. Color coordinates of samples

CIE color coordinates of samples doped with Dy^{3+}/Eu^{3+} ions are shown in **Figure 4.13.** and in **Table 4.6.**

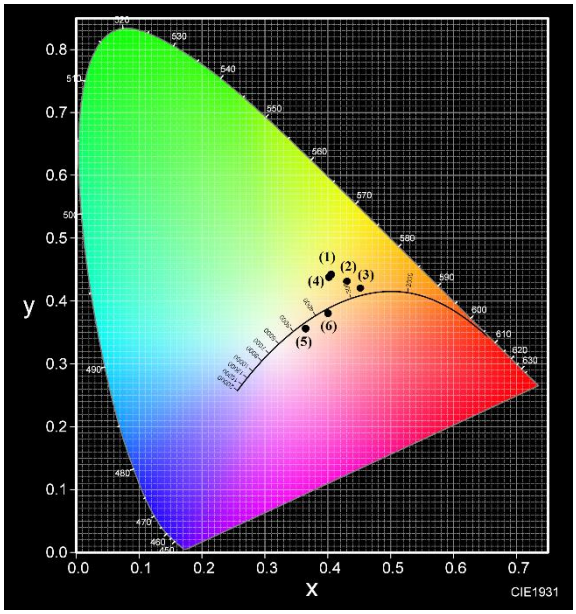

Figure 4.13. CIE 1931 color coordinates of samples doped with Dy^{3+}/Eu^{3+} ions.

Table 4.6. The CIE colour coordinates of the data points shown in **Figure 4.13**.

Sample number	Sample name	Excitation wavelength (nm)
1	Ca-Dy05	453
2	Ca-Dy05Eu05	453
3	Ca-Dy05Eu1	453
4	Ca-Dy05	350
5	Ca-Dy05Eu05	350
6	Ca-Dy05Eu1	350

Summary: By varying the concentration ratio of $Dy^{3+}$and Eu^{3+} ions in glasses, it is possible to vary the CIE color coordinates. With UV excitation, it is possible to obtain light close to white light in co-doped glass samples. Using the blue LED chip as an excitation source, white light would also be obtained with 453 nm excitation.

4.2. Dy^{3+}/Eu^{3+} co-doped glasses and glass ceramics containing SrF_2 nanocrystallites

4.2.1. Differential Thermal Analysis (DTA)

The DTA curve of the sample Sr-Dy05Eu1 is shown in **Figure 4.14.a.**

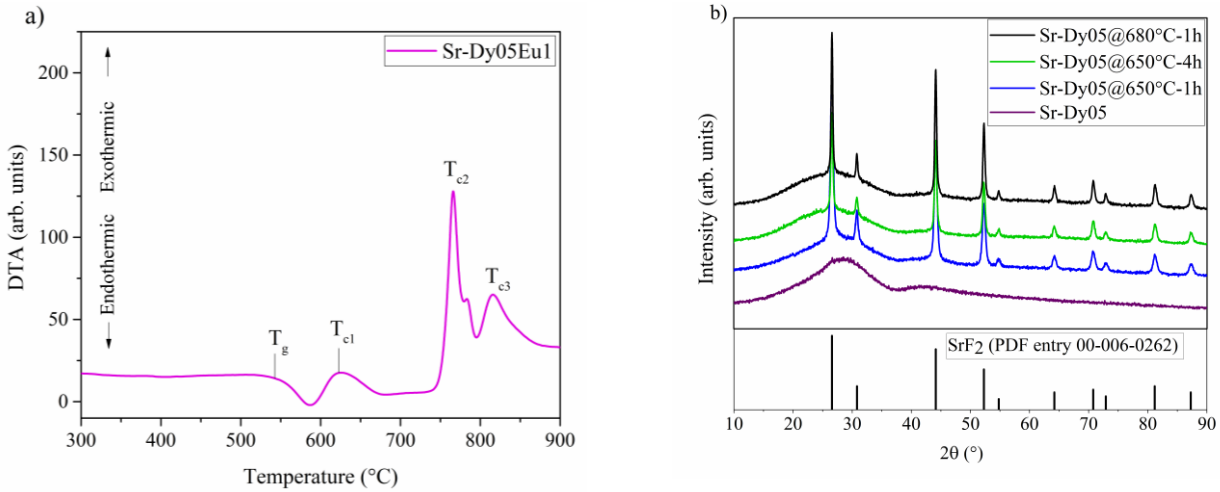

Figure 4.14.(a-b). a) DTA curve of sample Sr-Dy05Eu1, b) X-ray diffractograms of a series of Sr-Dy05 samples and diffraction peaks of the SrF_2 crystalline phase.

The glass transition temperature (T_g) is around 542 °C, but three exothermic peaks are located around 622 °C, 766 °C, 819 °C (T_{c1}, T_{c2}, T_{c3}). T_{c1} is related to the formation of the SrF_2 crystalline phase in the sample, while the sharp peaks T_{c2} and T_{c3} are due to the crystallization of the aluminosilicate phase, which is not desirable.

Summary: Based on DTA data, temperatures of 650 °C and 680 °C were chosen for the production of glass ceramic samples containing SrF_2 nanocrystallites.

4.2.2. X-ray diffraction (XRD)

The diffractograms of the sample series Sr-Dy05 and the diffraction peaks of the SrF_2 crystalline phase are shown in **Figure 4.14b.** Using Scherer's formula, the sizes of SrF_2 nanocrystallites were calculated for selected samples, which are summarized in **Table 4.7.**

Table 4.7. Calculated SrF_2 crystallite sizes (± 2 nm).

	650°C-1h	**650°C-4h**	**680°C-1h**
Sr-Dy05	21	28	37
Sr-Dy05Eu05	18		28
Sr-Dy1	18		
Sr-Dy1Eu1		22	

Summary: SrF_2 nanocrystallites with a diameter of 18-21 nm formed in the samples annealed at 650 °C for 1 hour, 22-28 nm in the one annealed at 650 °C for 4 hours, and 28-37 nm at 680 °C, hence, when heated at a higher temperature or for a longer time (4 hours), SrF_2 nanocrystallites of a slightly larger size were formed.

4.2.3. Luminescence in glass

The excitation spectra of Dy^{3+} ions in glass samples are shown in **Figure 4.15(a-b).** As in the Ca-Dy^{3+}/Eu^{3+} sample series, also in this case the Dy^{3+} ion excitation spectra were taken for 565 nm emission to avoid the influence of Eu^{3+} ions luminescence bands. **Figure 4.15b** shows the excitation spectra of Eu^{3+} ions.

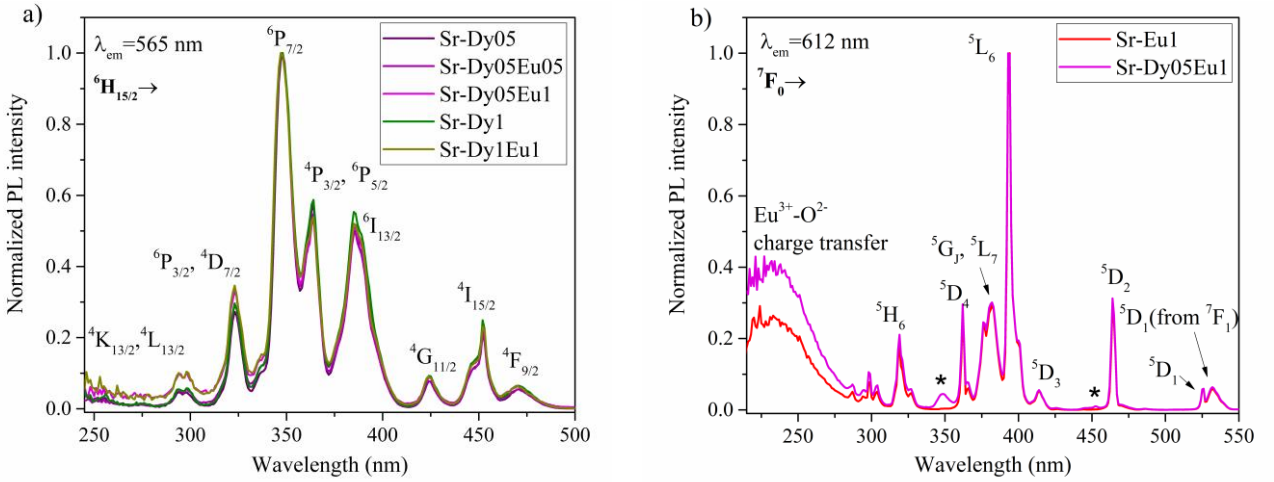

Figure 4.15(a-b). a) excitation spectra of Dy^{3+} ions in glass samples (λ_{em}=565 nm), b) excitation spectra of Eu^{3+} ions in Eu^{3+}-doped sample Sr-Eu1 and co-doped sample Sr-Dy05Eu1 (λ_{em}=612 nm).

The excitation spectra of Dy^{3+} ions in singly-doped and co-doped samples are almost the same – no excitation band of Eu^{2+} ions is observed, as it was in Ca-Dy^{3+}/Eu^{3+} series glasses (**Figure 4.3**). The excitation spectrum of Eu^{3+} ions (**Figure 4.15b**) is similar to the spectrum in the sample series Ca-Dy^{3+}/Eu^{3+}, the most intense excitation with 393 nm ($^7F_0 \rightarrow {}^5L_6$) and 464 nm ($^7F_0 \rightarrow {}^5D_2$). Also in this case additional excitation bands around 350 nm and 453 nm appear in co-doped samples, indicating energy transfer from Dy^{3+} to Eu^{3+} ions [59].

In **Figure 4.16.** luminescence spectra of glass samples in comparative intensity are shown. It can be seen that in singly-doped samples with 0.5 mol% and 1 mol% of Dy^{3+} ions, the luminescence intensity of Dy^{3+} ions is very similar.

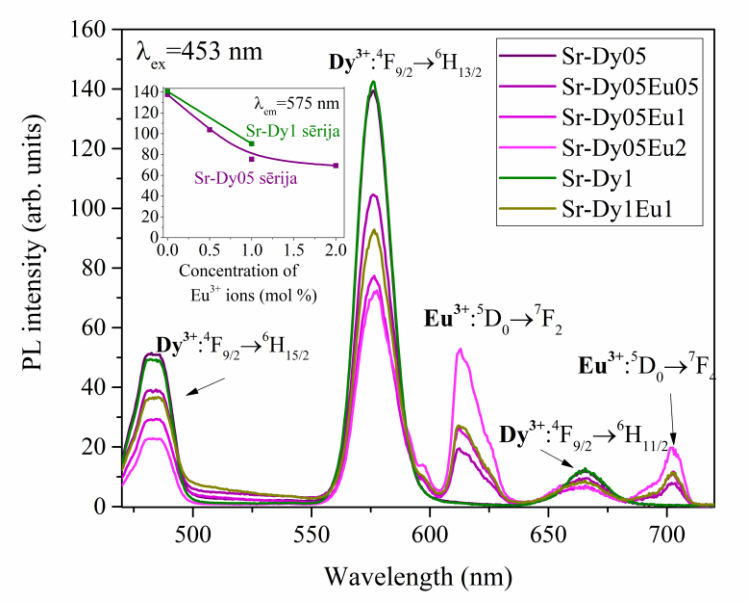

Figure 4.16. Luminescence spectra of glasses doped with Dy^{3+} and Eu^{3+} ions (λ_{ex}=453 nm). In the inset: the maximal intensity of Dy^{3+} ions (λ_{em}=575 nm) depending on the concentration of RE ions.

When Eu^{3+} ions are added, the luminescence intensity of Dy^{3+} ions decreases, which indicates energy transfer from Dy^{3+} to Eu^{3+} ions [59, 82]. A similar picture was observed with 350 nm excitation.

The luminescence spectra of Eu^{3+} ions with 393 nm and 464 nm excitation are similar to Eu^{3+} spectra in Ca-Dy^{3+}/Eu^{3+} series glasses (see **Figure 4.6a**) – the most intense is the hypersensitive ED transition of Eu^{3+} ions ($^5D_0 \rightarrow {}^7F_2$) at 612 nm, as it is expected in the environment without an inversion center [41, 90, 45, 75, 91].

With 330 nm excitation, a low-intensity Eu^{2+} luminescence band $4f^65d^1 \rightarrow {}^8S_{7/2}$ was observed, but its relative intensity compared to Eu^{3+} ions is much lower than in the Ca Dy^{3+}/Eu^{3+} series (**Figure 4.6b**), where the Eu^{2+} ions luminescence intensity with 330 nm excitation reached or even exceeded the luminescence intensity of Eu^{3+} ions at 612 nm ($^5D_0 \rightarrow {}^7F_2$).

Summary: In the investigated glass samples containing Dy^{3+}/Eu^{3+} ions, Dy^{3+} ions can be excited most efficiently with ~350 nm and 453 nm, Eu^{3+} ions – with 393 nm and 464 nm. Excitation transitions of Dy^{3+} ions are observed in the excitation spectrum of Eu^{3+} ions, which indicates energy transfer from Dy^{3+} to Eu^{3+} ions.

In glasses, depending on the excitation wavelength, the most intense is the Dy^{3+} emission band with a peak at 575 nm ($^4F_{9/2} \rightarrow {}^6H_{13/2}$) or the Eu^{3+} ion band at 612 nm ($^5D_0 \rightarrow {}^7F_2$, ED transition) as expected in positions with amorphous environment without an inversion center. In samples doped with 0.5 mol% and 1.0 mol% Dy^{3+} ions, with 453 nm excitation, the luminescence intensity of Dy^{3+} ions is similar, but in Dy^{3+}/Eu^{3+} co-doped samples, it decreases due to energy transfer from Dy^{3+} to Eu^{3+} ions. A broad luminescence band of Eu^{2+} ions ($4f^65d^1 \rightarrow {}^8S_{7/2}$) with a maximum around 435 nm was observed in the glasses.

4.2.4. Luminescence in glass ceramics

The normalized excitation spectra of Dy^{3+} ions in the original precursor glass and glass-ceramic are very similar and therefore not shown. Dy^{3+} ion excitation peaks around 350 nm and 453 nm are also visible in the excitation spectrum of Eu^{3+} ions in the co-doped glass ceramic samples, which indicates energy transfer from Dy^{3+} to Eu^{3+} ions [59, 82]. Also, it can be seen that the relative intensity of Eu^{3+} excitation bands at 393 nm ($^7F_0 \rightarrow {}^5L_6$) and 464 nm ($^7F_0 \rightarrow {}^5D_2$) in the samples is different, this indicates a different environment of Eu^{3+} ions in the studied samples. In all samples of the Sr-Dy05Eu1 series, an Eu-O charge transfer band is also observed in the UV spectral part, indicating Eu^{3+} and O^{2-} bonds.

Figure 4.17.(a-b) shows the luminescence spectra of glasses and glass ceramics with a) 0.5 Dy^{3+} ions and b) Dy^{3+}/Eu^{3+} ions with 453 nm excitation in comparative intensity.

In glass ceramic samples doped with 0.5 mol% Dy^{3+} ions (**Figure 4.17a**), the luminescence intensity of Dy^{3+} ions has significantly decreased. The inset of **Figure 4.17a** shows the dependence of Dy^{3+} ion intensity (575 nm, $^4F_{9/2}\rightarrow{}^6H_{13/2}$) on heat treatment temperature and duration with 453 nm and 350 nm excitation. The decrease in the luminescence intensity of Dy^{3+} ions in glass ceramics correlates with the diameter of SrF_2 nanocrystallites (see **Table 4.7)** – as it increases, the luminescence intensity decreases. With 350 nm excitation, the luminescence intensity in glass ceramics decreased slightly more than with 453 nm excitation. There is no crystal-field splitting of the luminescence bands observed in the spectra.

Also, in the sample Sr-Dy1@650°C-1h (**Figure 4.17.b**), the luminescence intensity of Dy^{3+} ions decreased compared to glass. In the co-doped sample Sr-Dy1Eu1@650°C-4h, the luminescence intensity of Dy^{3+} ions decreased only slightly compared to glass, this indicates that Eu^{3+} ions, entering SrF_2 nanocrystallites, inhibit the formation of Dy^{3+} clusters and increase the average distance between Dy^{3+} ions, preventing effective cross-relaxation processes between Dy^{3+} ions [18].

It was observed that in the sample series Sr-Dy05Eu1, the relative ratio of luminescence bands of Dy^{3+} and Eu^{3+} ions in glass and glass ceramics is different – in glass ceramics, the intensity of Eu^{3+} ion luminescence decreased more strongly than the luminescence of Dy^{3+} ions. This is partly explained by the reduction from Eu^{3+} to Eu^{2+} ions during the thermal treatment [35, 36, 40, 64], which can reduce the number of Eu^{3+} ions in the samples and, subsequently, also their contribution to luminescence.

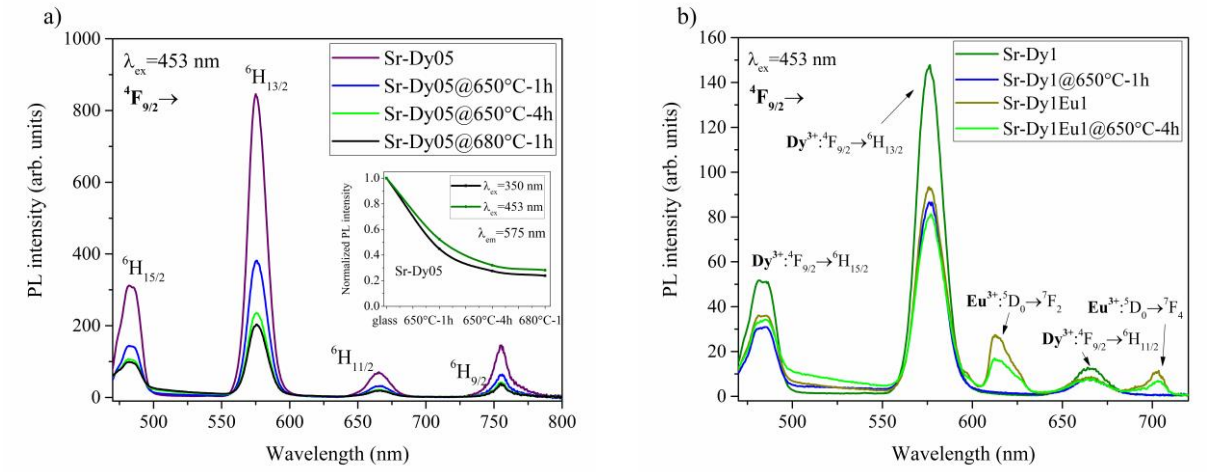

Figure 4.17. Luminescence spectra in comparative intensity in glass ceramic samples doped with a) Dy^{3+} ions (0.5 mol%) and b) Dy^{3+} (0.5 mol%) and Eu^{3+} (1 mol%); (λ_{ex}=453 nm).

In the luminescence spectra of Eu^{3+} ions in the sample series Sr-Dy05Eu1 with 393 nm excitation, there is no change in the $^5D_0\rightarrow{}^7F_1$ (592 nm) and $^5D_0\rightarrow{}^7F_2$ (612 nm) band ratio, so there was no effective incorporation of Eu^{3+} ions into the SrF_2 nanocrystallites in the centrosymmetric Sr^{2+} position (in that position the $^5D_0\rightarrow{}^7F_1$ luminescence transition would dominate) [41, 90, 45, 75, 91]. A shoulder around 690 nm can be observed in the $^5D_0\rightarrow{}^7F_4$ luminescence band, indicating a slight crystal-field splitting.

Summary: The excitation spectra of Dy^{3+} ions in glass and glass-ceramic samples are similar indicating a similar local environment of Dy^{3+} ions in these samples. The ratio of Eu^{3+} ion excitation bands $^7F_0\rightarrow{}^5L_6$ and $^7F_0\rightarrow{}^5D_2$ in the studied glass-ceramics of different compositions is different, which indicates different environments of Eu^{3+} ions in the samples. Excitation bands of Dy^{3+} ions are also observed in the excitation spectra of Eu^{3+} ions in co-doped glasses and glass ceramics indicating energy transfer from Dy^{3+} to Eu^{3+} ions.

In Dy^{3+}-doped glass ceramics containing SrF_2, Dy^{3+} ion luminescence intensity has decreased compared to the precursor glasses, indicating effective cross-relaxation processes between Dy^{3+} ions. In co-doped glass and glass-ceramic samples, the relative ratio of the luminescence bands of Dy^{3+} and Eu^{3+} ions is different from each other, this could be partly explained by the reduction of Eu^{3+} to Eu^{2+} ions under the influence of heat treatment of the initial

glasses. In time-integrated measurements, no crystal-field splitting of the luminescence bands was observed, therefore, most of the RE ions are located in the amorphous glass environment rather than in the SrF_2 nanocrystallites.

4.2.5. Time-resolved luminescence spectra

In the sample Sr-Dy05@680°C, in the time-resolved luminescence spectra (λ_{ex}=453 nm), measured in the time interval 10 ms - 45 ms after the exciting laser pulse, the crystal-field splitting of the luminescence bands of Dy^{3+} ions was observed, and the spectral positions are similar to those in Ca-Dy^{3+}/Eu^{3+} series (see **Figure 4.9a**), however, the splitting is less pronounced in the studied samples of Sr-Dy^{3+}/Eu^{3+} series. This could be related to a different size of fluoride crystallites - it was larger (68 nm) in Ca-Dy05@750°C than here (37 nm). A smaller proportion of Dy^{3+} ions can enter fluoride nanocrystallites of smaller size.

Figure 4.18.(a-b). shows the site-selective time-resolved luminescence spectra of Eu^{3+} ions with different excitation wavelengths, measured in the time interval 20 ms – 45 ms after the laser pulse. The co-doped glass ceramic sample Sr-Dy05Eu1@680°C-1h (**Figure 4.18.a**) shows a similar picture as in the previous series of samples (**Figure 4.9.b**) – there are several different luminescence spectra of Eu^{3+} ions, however, with 524.7 nm excitation (in the middle) the $^5D_0 \rightarrow {}^7F_1$ transition at 590 nm is not as intense as it was in Figure 4.9b, so the distribution of centres is slightly different.

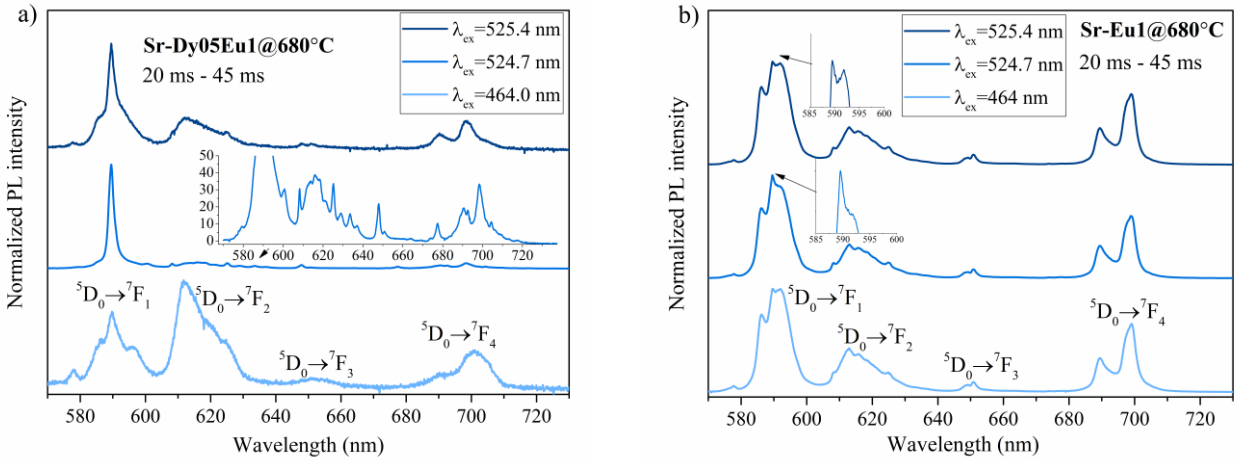

Figure 4.18.(a-b). Time-resolved luminescence spectra of Eu^{3+} ions in glass ceramic samples in the time interval 20 ms – 45 ms with several excitation wavelengths: a) Sr-Dy05Eu1@680°C, b) Sr-Eu1@680°C.

In the singly-doped glass-ceramic sample with Eu^{3+} ions (**Figure 4.18b**), Eu^{3+} center of one type dominates with all used excitation wavelengths, the most intense band of which is $^5D_0 \rightarrow {}^7F_2$, but the band is significantly wider than in the case of cubic centers. A pronounced splitting of the $^5D_0 \rightarrow {}^7F_4$ band into two components peaking at 689.5 nm and 699 nm is observed (in glass, the peak was at 702 nm, see **Figure 4.16**). Such Eu^{3+} spectra in SrF_2 have also been observed in other studies [75, 81, 96], but were not identified in these publications.

Summary: Time-resolved luminescence measurements, measured in the time interval from 10 or 20 ms to 45 ms after the laser pulse, confirm the partial incorporation of Dy^{3+} ions into SrF_2 nanocrystallites, as the crystal-field splitting of the Dy^{3+} luminescence bands is observed. The site-selective luminescence spectra of Eu^{3+} in the 20 ms to 45 ms time interval indicate at least 3 different positions of Eu^{3+} ions in Eu^{3+}-doped and Dy^{3+}/Eu^{3+} co-doped glass ceramics which is observed due to different charge compensation processes.

4.2.6. Luminescence of Eu^{2+} ions

In glass, the luminescence of Eu^{2+} ions with 330 nm excitation, when measuring time-integrated spectra with each data point accumulated for 0.5 s, was very weak. However, when performing time-resolved measurements in the time interval 50 ns – 1 μs, a broad Eu^{2+} ion luminescence band $4f^65d^1 \rightarrow {}^8S_{7/2}$ can be observed in both glass and glass ceramics (**Figure 4.19(a-b))**. In glass ceramics, the relative luminescence intensity of Eu^{2+} ions compared to Eu^{3+} luminescence has increased, this indicates the reduction of europium ions during the production of glass ceramics. **Figure 4.19(a-b)** also shows that in glass ceramics the luminescence band of Eu^{2+} ions is shifted to shorter wavelengths compared to glass, this is especially evident when looking at the Eu^{2+} band in one short time interval (530 ns – 580 ns; **Figure 4.19b**).

A similar picture was observed in samples activated only with europium ions: the peak of the luminescence band of Eu^{2+} ions in glass ceramics shifted by 20 nm to shorter wavelengths compared to glass (in glass - ~450 nm, in glass ceramics ~430 nm).

The shift of the Eu^{2+} bands, as well as the increase in their relative intensity, indicates changes in the valence and environment of the ions during the thermal treatment of glasses (i.e. glass-ceramic production). In the studies of glass and glass-ceramics of similar composition [41], using the EPR method, it was concluded that in glass-ceramics most of the Eu^{2+} ions have entered SrF_2 nanocrystallites, while the EPR signal of Eu^{2+} ions was not detected in glass samples. EPR measurements were also performed on selected samples of the studied series Sr-Dy^{3+}/Eu^{3+}, but no clearly distinguishable EPR signal of Eu^{2+} ions was detected in the glass or in the fluoride phase, most likely because the concentration of Eu^{2+} ions was too low.

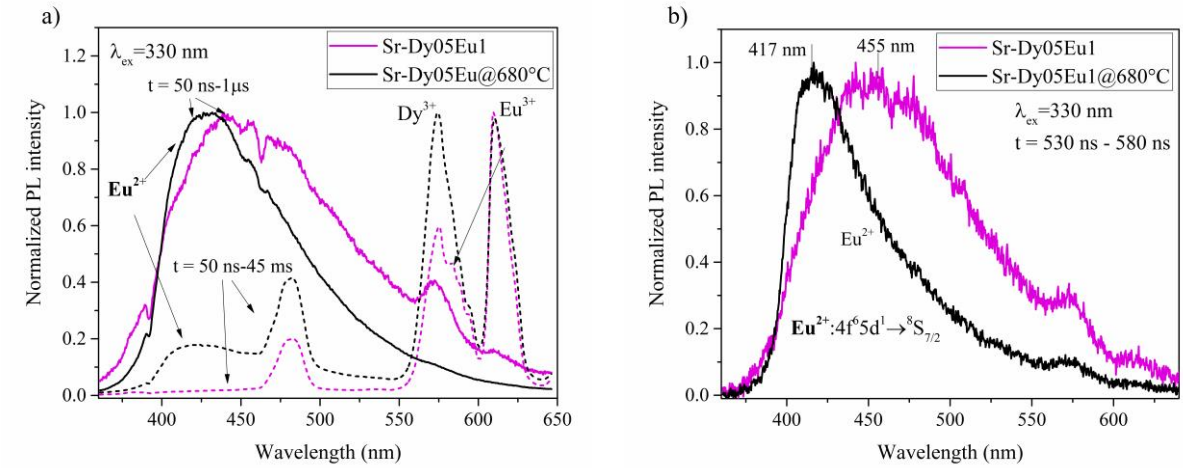

Figure 4.19.(a-b). Normalized time-resolved luminescence spectra of a Sr-Dy05Eu1 sample series with 330 nm excitation in the time intervals a) 50 ns – 1 μs and 50 ns – 45 ms, and b) 550 ns – 580 ns.

Summary: With 330 nm excitation, an increase in the relative intensity of Eu^{2+} ion luminescence ($4f^65d^1 \rightarrow {}^8S_{7/2}$) is observed in glass-ceramic samples, compared to the precursor glasses, and the band in glass-ceramics is shifted to shorter wavelengths. This indicates a partial reduction of Eu^{3+} ions to Eu^{2+} ions under the influence of heat treatment of the initial glasses and a change in the environment of Eu^{2+} ions in glass ceramics, when part of Eu^{2+} ions enter SrF_2 nanocrystallites.

4.2.7. Luminescence decay kinetics in glass and glass ceramic samples and energy transfer between Dy^{3+} and Eu^{3+} ions

The luminescence decay curves of glass samples doped with Dy^{3+} ions for the transition ${}^4F_{9/2} \rightarrow {}^6H_{13/2}$ (575 nm) are shown in **Figure 4.20.a.** The decay curves have a non-exponential character, especially in samples with a higher concentration of Dy^{3+} ions (1 mol% Dy^{3+}). The calculated effective

luminescence decay times are shown in **Table 4.8.** As in the Ca-Dy^{3+}/Eu^{3+} sample series, here as well, by adding Eu^{3+} ions, the decay times of Dy^{3+} ions decrease. The energy transfer efficiency is calculated to be 10.5-28.9%, in the sample with 1 mol% Dy^{3+} and Eu^{3+} ions – 9.6%.

The luminescence decay kinetics in glass and glass ceramic samples are shown in **Figure 4.20(a-b).** The calculated decay times and energy transfer efficiency are summarized in **Table 4.9.**

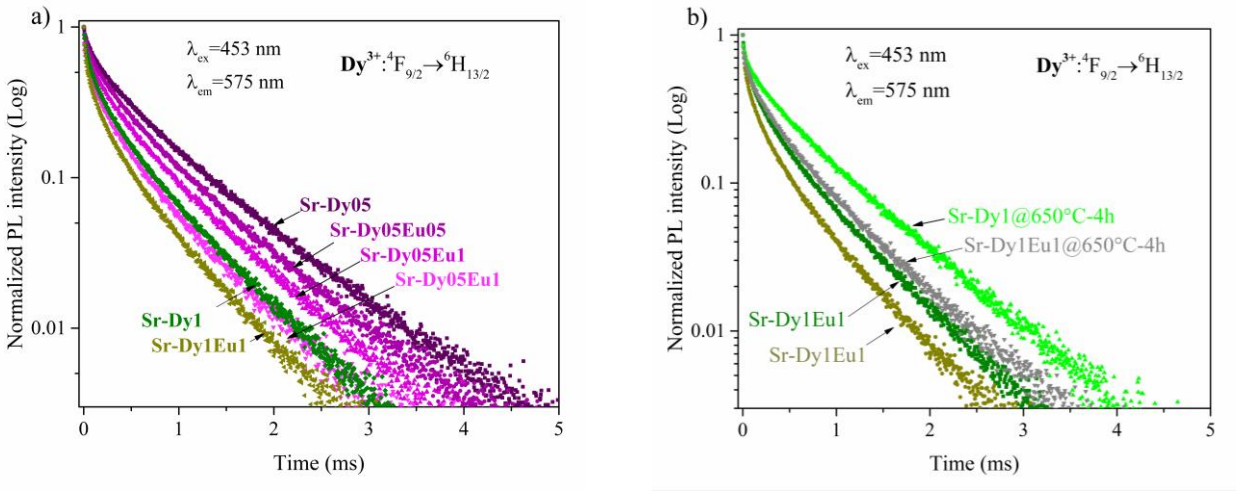

Figure 4.20.(a-b). Luminescence decay kinetics of Dy^{3+} ions (λ_{ex}=453 nm, λ_{em}=575 nm) in a) glass samples, b) glass and glass ceramics (Sr-D1 and Sr-Dy1Eu1 series samples).

Table 4.8. Calculated Dy^{3+} ion decay times and energy transfer (Dy^{3+}→Eu^{3+}) efficiency.

Sample (λ_{ex}=453 nm, λ_{em}=575 nm)	**τ (ms) ± 0.01 ms**	**η (%) ± 1**
Sr-Dy05	0.76	-
Sr-Dy05Eu05	0.68	11
Sr-Dy05Eu1	0.62	19
Sr-Dy05Eu2	0.54	29
Sr-Dy1	0.52	-
Sr-Dy1Eu1	0.47	10

Table 4.9. Calculated effective luminescence decay times (τ) and energy transfer efficiency (η) in glass and glass-ceramic samples.

Sample (λ_{ex}=453 nm, λ_{em}=575 nm)	**τ (ms) ± 0.01 ms**	**Sample (λ_{ex}=453 nm, λ_{em}=575 nm)**	**τ (ms) ± 0.01 ms**	**η (%) ± 1**
Sr-Dy05	0.76	Sr-Dy05Eu05	0.68	11
Sr-Dy05@650°C-1h	0.80	Sr-Dy05Eu05@650°C-1h	0.73	9
Sr-Dy05@650°C-4h	0.81	Sr-Dy05Eu05@650°C-4h	0.77	5
Sr-Dy05@680°C-1h	0.81	Sr-Dy05Eu05@680°C-1h	0.75	7
Sr-Dy1	0.52	Sr-Dy1Eu1	0.47	10
Sr-Dy1@650°C-4h	0.70	Sr-Dy1Eu1@650°C-4h	0.59	16

From **Table 4.9.** it can be seen that in the glass ceramic doped with 0.5 mol% Dy^{3+} ions, the luminescence decay is a little slower than in the precursor glasses. The heat treatment temperature did not affect the luminescence decay time of Dy^{3+} ions. More evident changes are observed in the sample with 1 mol% Dy1 – the luminescence decay has become significantly slower (from 0.53 to 0.70 ms) in the glass ceramic, annealed for 4 hours. In Sr-Dy05Eu05 glass ceramics, the energy transfer efficiency has slightly decreased compared to glass, while in Sr-Dy1Eu1@650°C-4h – has increased.

Eu^{2+} luminescence decay times in glass and glass-ceramics vary in the range of about 350-650 ns, in glass-ceramics they become longer, this could be related to the incorporation of Eu^{2+} ions into SrF_2 nanocrystallites – an environment with lower phonon energy. Since the concentration of Eu^{2+} ions in the samples is small, no pronounced concentration quenching processes between Eu^{2+} ions are expected.

The luminescence decay times of Eu^{2+} ions are shown in **Table 4.10.**

Table 4.10. Calculated effective decay times of Eu^{2+} ions.

Sample (λ_{ex}=330 nm, λ_{em}=425 nm)	**τ (ns) ± 40 ns**	**Sample (λ_{ex}=330 nm, λ_{em}=425 nm)**	**τ (ns) ± 20 ns**
Sr-Eu1	488	Sr-Dy05Eu1	367
Sr-Eu1@680°C	626	Sr-Dy05Eu1@680°C	418

Summary: The slowest luminescence decay of Dy^{3+} ions and the longest effective decay time is observed in the glass sample with 0.5 mol% Dy^{3+} (Sr-Dy05, 0.76 ms). When adding Eu^{3+} ions, the decay time of Dy^{3+} ions decreases to 0.54 ms (Sr-Dy05Eu2), due to energy transfer to Eu^{3+} ions. The energy transfer efficiency in Sr-Dy05Eu2 glass reaches 29%. Dy^{3+} ion singly-doped glass ceramics exhibit slower luminescence decay than the precursur glasses which could be due to the partial entry of Dy^{3+} ions into SrF_2 nanocrystallites while not forming clusters that would effectively quench the luminescence of Dy^{3+} ions. In Sr-Dy05Eu05 glass ceramics, the energy transfer efficiency has slightly decreased compared to glass, while in Sr-Dy1Eu1@650°C-4h has increased indicating a decrease in the average distances between Dy^{3+} and Eu^{3+} ions in this glass ceramic sample. Eu^{2+} luminescence decay times in glass and glass-ceramics vary in the range of about 350 -650 ns, they become greater in glass-ceramics which could be explained by the partial entry of Eu^{2+} ions into fluoride nanocrystallites possessing lower phonon energy.

4.2.8. Color coordinates of samples

CIE color coordinates of luminescence of samples doped with Dy^{3+}/Eu^{3+} ions are shown in **Figure 4.21.** and in **Table 4.11.** It can be seen that when a higher concentration of Eu^{3+} ions are added, with 484 nm excitation, the CIE color coordinates of the samples shift to the red part, but in co-doped glass ceramics with UV excitation, the blue spectral component also appears (primarily, due to the luminescence of Eu^{2+} ions, as well as the relative decrease of Eu^{3+} ions luminescence intensity in glass ceramics versus the intensity of Dy^{3+} ions), shifting the CIE color coordinates towards the white light (white light – coordinates (0.33, 0.33)).

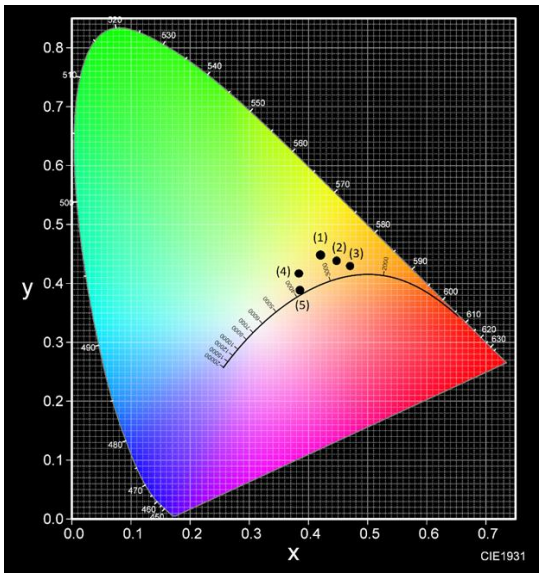

Figure 4.21. CIE 1931 color coordinates of samples doped with Dy^{3+}/Eu^{3+} ions.

Table 4.11. The CIE colour coordinates of the data points shown in **Figure 4.21.**

Sample number	Sample name	Excitation wavelength (nm)
1	Sr-Dy05	453
2	Sr-Dy05Eu05	453
3	Sr-Dy05Eu1	453
4	Sr-Dy05Eu05@650°C-4h	350
5	Sr-Dy05Eu1@650°C-4h	350

Summary: By varying the ratio of Dy^{3+} and Eu^{3+} ions in the glasses and the heat treatment conditions of the glasses, it is possible to change the CIE color coordinates of the luminescence of the samples, bringing them closer to white light. Color adjustment is achieved by the relative increase in the luminescence of Eu^{2+} ions and the decrease in the relative intensity of the luminescence of Eu^{3+} ions in the red part of the spectrum in glass-ceramics compared to the initial glasses.

4.3. Tb^{3+}/Eu^{3+} doped glasses and glass ceramics containing SrF_2 nanocrystallites

4.3.1. Differential Thermal Analysis (DTA)

Figure 4.22.a. shows the DTA curve for a glass sample with 1 mol% Eu^{3+} ions (Sr-Eu1).

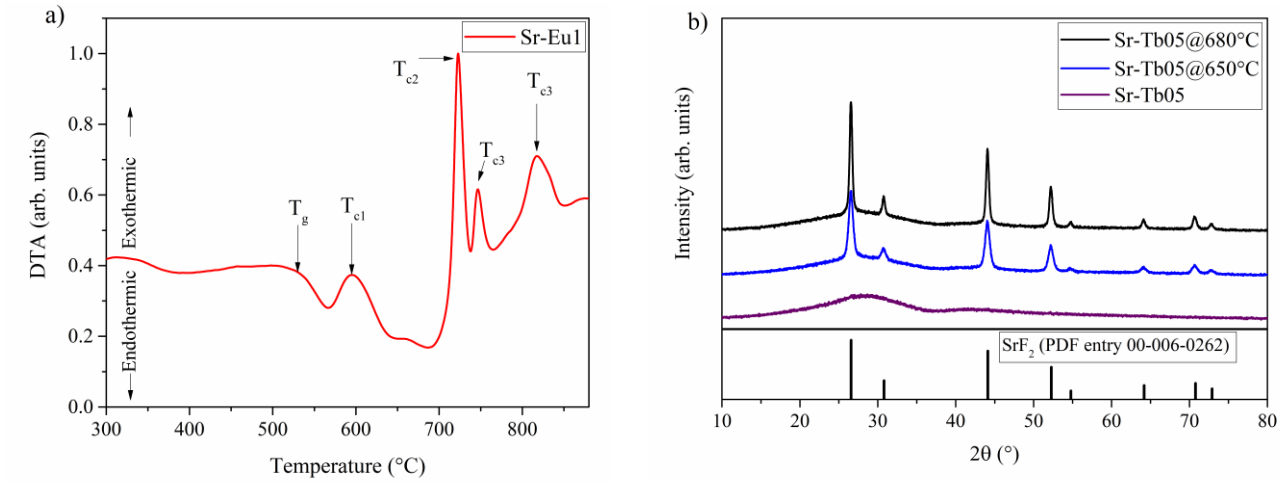

Figure 4.22.(a-b). a) DTA curve and characteristic temperatures of sample Sr-Eu1, b) diffractograms of samples doped with Tb^{3+} ions (0.5 mol%) and diffraction peaks of the SrF_2 crystalline phase.

The exothermic peak at 595 ± 5 °C is related to the formation of SrF_2 nanocrystallites in the material. At temperatures above 700 °C, the formation of crystalline structures of aluminosilicates is observed.
Summary: Based on DTA data, temperatures of 650 °C and 680 °C were chosen for the production of glass ceramic samples.

4.3.2. X-ray diffraction measurements (XRD)

XRD measurements were performed on all studied samples. The diffractograms of the Sr-Tb05 series of samples are shown in **Figure 4.22b.** Using Scherer's formula, the size (diameter) of fluoride crystallites in glass-ceramic samples was estimated. The calculated crystallite sizes (± 2 nm) are summarized in **Table 4.12.**

Table 4.12. Calculated SrF_2 crystallite sizes (± 2 nm).

	glass	650 °C	680 °C
Sr-Tb05		17	27
Sr-Tb05Eu05	*	29	36
Sr-Tb05Eu1	*	22	26
Sr-Tb1		24	36
Sr-Tb1Eu1		15	26

In some glass samples doped with Tb^{3+} and Eu^{3+} ions (Sr-Tb05Eu05 and Sr-Tb05Eu1, marked with *), the presence of small-sized SrF_2 nanocrystallites can already be observed. In the Sr-Tb05Eu1 sample, their presence is insignificant, because they are very small in size, but in the SrTb05Eu05 sample, slightly larger fluoride nanocrystallites have formed, however, their size is too small to make correct crystallite size calculations using Scherrer's formula. The formation of small-sized crystallites in the glass could be explained by the peculiarities of the composition and the sample preparation and pouring process.

Summary: SrF_2 nanocrystallites with a diameter of 15-29 nm were formed in the samples annealed at 650 °C, and 26-36 nm in diameter annealed at 680 °C. Small-sized SrF_2 nanocrystallites were observed in some glass samples.

4.3.3. Luminescence in glass

Excitation spectra of Tb^{3+} ions were measured for the luminescence band at 542 nm, which corresponds to the luminescence transition $^5D_4 \rightarrow {}^7F_5$. Normalized excitation spectra are shown in **Figure 4.23.** The corresponding excitation transitions are shown in **Table 4.13.**

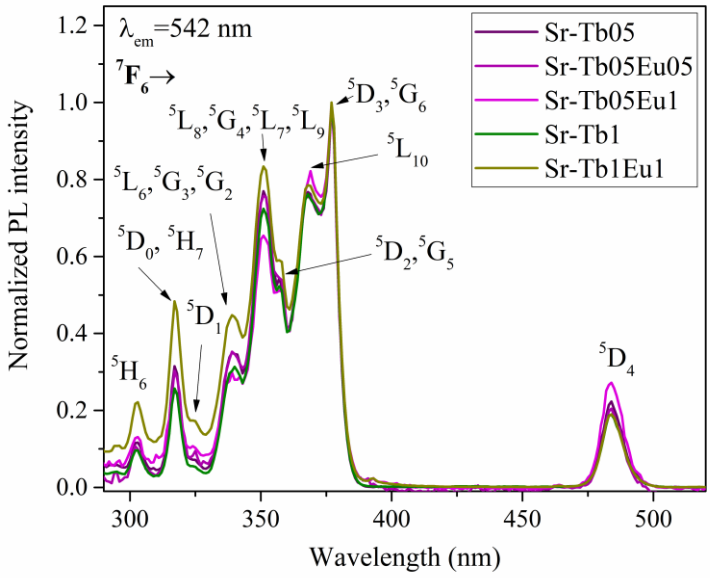

Figure 4.23. Normalized luminescence excitation spectra of Tb^{3+} ions in Tb^{3+} and Tb^{3+}/Eu^{3+} doped glass samples (λ_{em}=542 nm).

Table 4.13. Excitation transitions of Tb^{3+} ions in glass samples (from ground state $^7F_6$) [62]

Position (nm)	**Electronic transition**
302	$^5H_6$
317 nm	$^5D_0$, $^5H_7$
324 nm	$^5D_1$
339 nm	$^5L_6$, $^5G_3$, $^5G_2$
351 nm	$^5L_8$,$^5G_4$,$^5L_7$, $^5L_9$
358 nm	$^5D_2$, $^5G_5$
368 nm	$^5L_{10}$
377 nm	$^5D_3$, $^5G_6$
484 nm	$^5D_4$

From **Figure 4.23.** it can be seen that the relative intensity of the excitation bands changes slightly depending on the concentration of activators added to the sample, however, the changes are not significant and can partly be explained by the measurement background. The excitation spectrum of Tb^{3+} ions (**Figure 4.23**) shows several excitation transitions in the 300-380 nm range, as well as transitions in the blue spectral region at 484 nm ($^7F_6 \rightarrow {}^5D_4$). Although the most intense is the excitation transition $^7F_6 \rightarrow {}^5D_3$ at 377 nm, however, taking into account the arrangement of energy levels of Tb^{3+} and Eu^{3+} (will be discussed below) and the technical properties of the nanosecond laser used in the research, the excitation wavelengths 350 nm and 484 nm were chosen for the excitation of Tb^{3+} ions for further studies, respectively, from the ground state $^7F_6$ to the excited states $^5L_8$, $^5G_4$, $^5L_7$, $^5L_9$ and $^5D_4$ [62].

The excitation spectra of Eu^{3+} ions in glass are very similar to the previously discussed Eu^{3+} excitation spectra in **Figures 4.4, 4.7b, 4.15b**. – excitation transition $^7F_0 \rightarrow {}^5L_6$ (393 nm) dominates.

In glasses containing Tb^{3+} ions, with 350 nm excitation (**Figure 4.24**), in the 480 nm – 650 nm spectral range, the shape of the luminescence spectra of Tb^{3+} ions in samples with 0.5 mol% and 1 mol% Tb^{3+} ions is almost the same (the most intense transition $^5D_4 \rightarrow {}^7F_5$, 542 nm), but in the UV and blue spectral range (360 nm – 480 nm) in the sample with a higher Tb^{3+} ion concentration (1 mol%), the relative intensity of the luminescence bands $^5D_3 \rightarrow {}^7F_{3,4,5,6}$ is lower than in the sample with lower Tb^{3+}

ion concentration (0.5 mol%). The decrease in the intensity of the $^5D_3 \rightarrow {}^7F_J$ luminescence bands is due to the cross-relaxation processes between the energy levels $^5D_3 \rightarrow {}^5D_4$ and $^7F_6 \rightarrow {}^7F_{0,1}$, which occur already at a relatively low concentration of Tb^{3+} ions (see *Chapter 2.3.5. Luminescence properties of Tb^{3+} ions*) [6, 52].

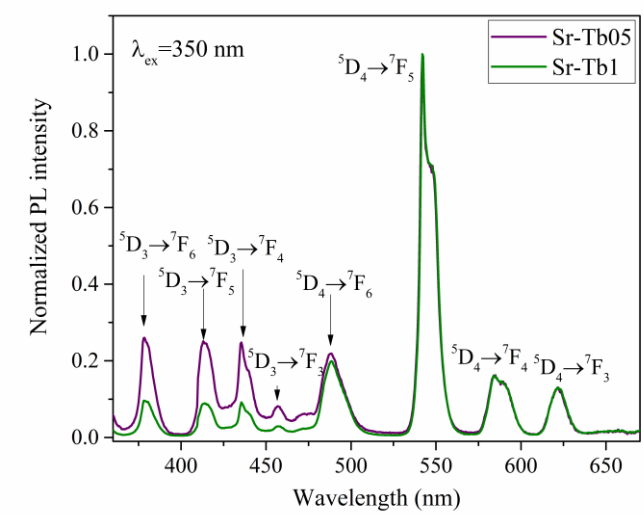

Figure 4.24. Normalized luminescence spectra of Tb^{3+} ions in glass samples singly-doped with Tb^{3+} ions (λ_{ex} = 350 nm).

In the **Figure 4.25.** the luminescence spectra of Tb^{3+} and Eu^{3+} ions are shown in comparative intensity (in the inset: the maximal intensity of Tb^{3+} ions (λ_{em}=542 nm) depending on the concentration of added Eu^{3+} ions). The maximal intensity of Tb^{3+} ions is observed in the sample with 1 mol% Tb^{3+}, the luminescence intensity in the sample with 0.5 mol% Tb^{3+} is about 50% lower. Upon addition of Eu^{3+} ions, the maximal intensity of Tb^{3+} ions decreases. The decrease in the luminescence intensity of Tb^{3+} ions by adding the Eu^{3+} ions is due to energy transfer from Tb^{3+} to Eu^{3+} ions [9, 10, 90].

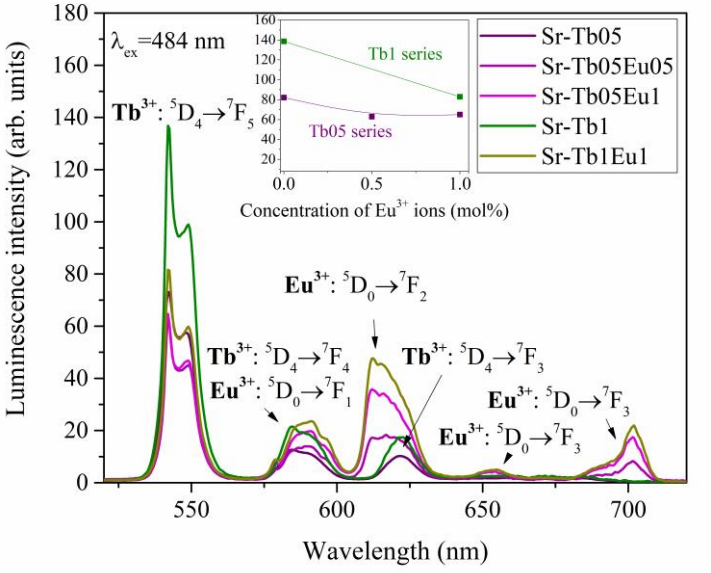

Figure 4.25. Luminescence spectra of glass samples (λ_{ex}=484 nm) in comparative intensity. In the inset: the maximal luminescence intensity of Tb^{3+} ions (λ_{em}=542 nm) depending on the added concentration of Eu^{3+} ions (0-1 mol%).

The luminescence spectra of Eu^{3+} ions with the characteristic Eu^{3+} excitation wavelengths of 394 nm and 464 nm were similar to the previous series of samples (see **Figure 4.6a**), but the relative ratio of the luminescence bands $^5D_0 \rightarrow {}^7F_1$ (592 nm) and $^5D_0 \rightarrow {}^7F_2$ (612 nm) slightly varies depending on

the excitation wavelength. The excitation transition $^7F_0 \rightarrow {}^5D_2$ (464 nm) and the emission transition $^5D_0 \rightarrow {}^7F_2$ (612 nm) are hypersensitive to the environment of the Eu^{3+} ion, so the observed differences in the spectra indirectly indicate different environments of the Eu^{3+} ions in the glass. The diffraction pattern in Sr-Eu1 glass (shown in [41], **Fig. 2(a)**, S1_PG) reveals that small-sized SrF_2 nanocrystallites have already formed in the glass. It is expected that different excitation wavelengths are expected to excite more efficiently Eu^{3+} ions in glassy or crystalline environment, leading to changes in the luminescence spectra [45].

Summary: In the studied samples containing Tb^{3+} and Tb^{3+}/Eu^{3+} ions, Tb^{3+} ions can be excited most efficiently with ~377 nm and 484 nm, Eu^{3+} ions with 393 nm and 464 nm excitation. In glasses, depending on the excitation wavelength, the most intense is the Tb^{3+} ion emission transition at 542 nm ($^5D_4 \rightarrow {}^7F_5$) or the Eu^{3+} ion transition ($^5D_0 \rightarrow {}^7F_2$). The luminescence spectra of Tb^{3+} ions in glass with 350 nm excitation show luminescence bands $^5D_3 \rightarrow {}^7F_{3,4,5,6}$ in the 360 nm – 480 nm range, the intensity of which strongly depends on the added concentration of Tb^{3+} ions – this band is due to cross relaxation in samples with 1.0 mol% Tb^{3+} ions the relative intensity is lower than in samples with 0.5 mol% Tb^{3+}.

4.3.4. Luminescence in glass ceramics

Figure 4.26.a. shows the excitation spectrum of Tb^{3+} ions in a series of Sr-Tb05 samples. It can be seen that the relative ratio of the excitation peaks (367 nm, 377 nm) has changed in glass ceramics, indicating a change in the environment of Tb^{3+} ions in the glass-ceramic. In co-doped glass-ceramic samples, the relative intensity ratio of peaks at 367 nm and 377 nm is similar to the precursor glass sample, which suggests that in co-doped glass-ceramic samples, incorporation of Tb^{3+} ions into fluoride nanocrystallites has been less effective.

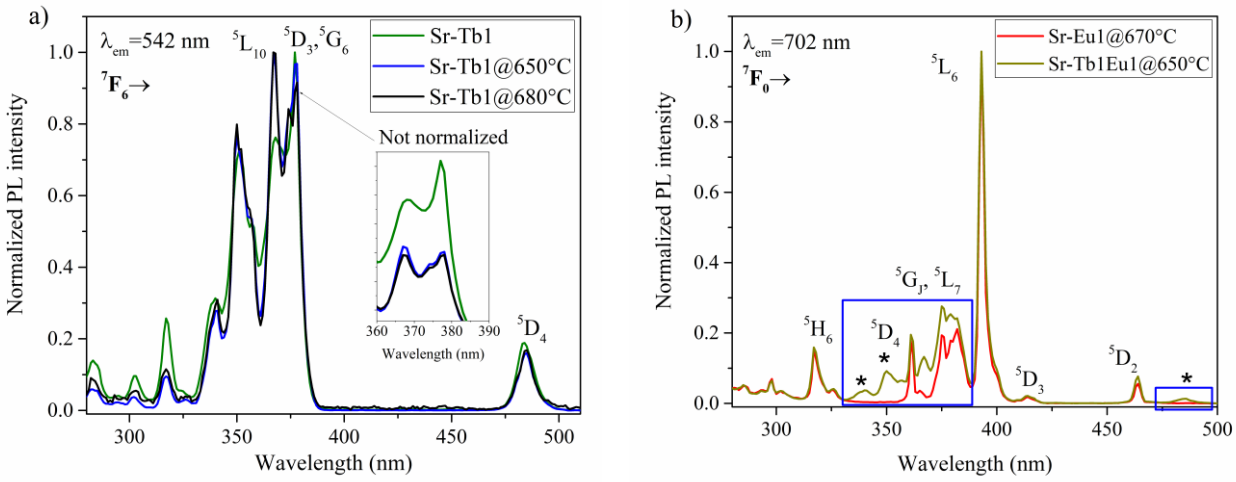

Figure 4.26.(a-b). a) normalized luminescence excitation spectra of Tb^{3+} ions in glass and glass ceramics with 1 mol% Tb^{3+} ions, b) normalized excitation spectra of Eu^{3+} ions in glass ceramic samples doped with Eu^{3+} and Eu^{3+}/Tb^{3+} ions (λ_{em}=702 nm).

In the excitation spectra of Eu^{3+} ions of co-doped samples, both the 612 nm and 702 nm emission bands (**Figure 4.26b**) show a rise in the range of 335 nm – 385 nm (highlighted, marked with *), which is not visible in samples singly-doped with Eu^{3+} ions. The excitation bands observed in these spectral regions coincide with the bands of the excitation spectrum of Tb^{3+} ions, which indicates energy transfer from Tb^{3+} to Eu^{3+} ions, both in co-doped glasses and glass ceramics (**Figure 4.26b**) [46, 63, 81, 83].

Luminescence spectra of glass and glass ceramic samples doped with Tb^{3+} ions (0.5 mol%) with 350 nm excitation are shown in **Figure 4.27a**. Relatively intense luminescence in the blue spectral range (electronic transitions $^5D_3 \rightarrow {}^7F_{3,4,5,6}$) can be observed in the glass sample, but their intensity is lower in the glass-ceramic samples. This is related to the previously described cross-relaxation – concentration quenching. It is expected that Tb^{3+} ions have partially entered SrF_2 nanocrystallites, and there are smaller

distances between them than in the amorphous glass – in other words, the concentration of Tb^{3+} ions (number of ions per unit volume) has locally increased in some areas. In **Figure 4.27.a.**, in the glass-ceramics, a more detailed structure appears in the spectrum compared to glass (see inset image), which is due to the crystal-field splitting of the luminescence bands of Tb^{3+} ions in SrF_2 nanocrystallites [74, 79, 81]. This also serves as evidence for the partial incorporation of Tb^{3+} ions into SrF_2 nanocrystallites.

Comparative luminescence spectra (**Figure 4.27b**) show that the luminescence intensity (λ_{ex}=484 nm) decreases in glass ceramics compared to glass. This could be mainly due to concentration quenching. In the sample with 1 mol% Tb^{3+}, the luminescence intensity of the glass ceramic annealed at 680 °C is slightly higher than at 650 °C. This could be explained by different incorporation efficiency in fluoride nanocrystallites, which leads to different concentration quenching and phonon effects on the probability of Tb^{3+} radiative transitions, and different size of nanocrystallites.

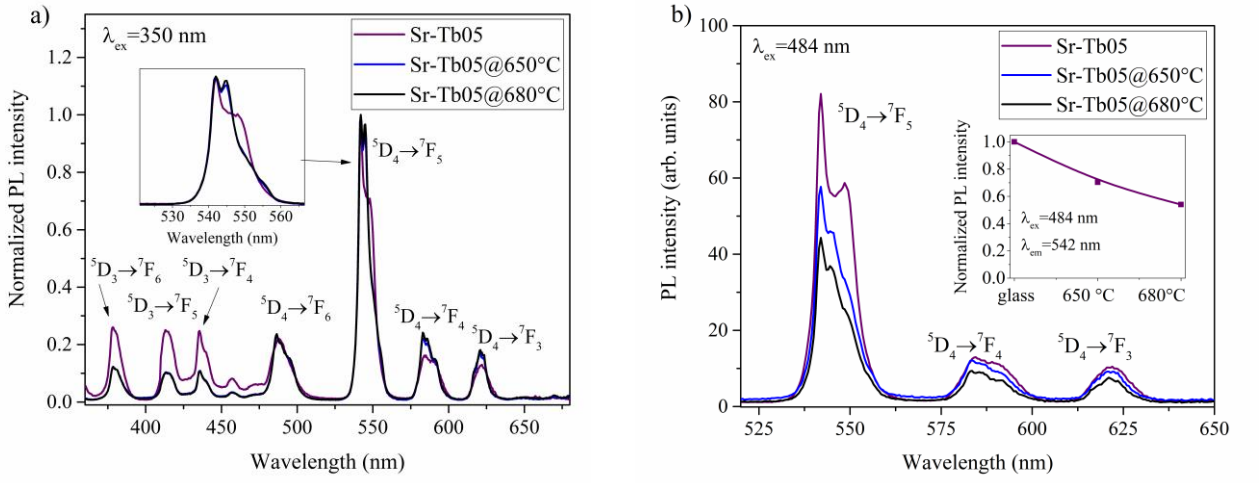

Figure 4.27.(a-b). a) normalized luminescence spectra of glass and glass-ceramic samples doped with 0.5 mol% Tb^{3+} ions (λ_{ex}=350 nm), b) luminescence spectra of glass and glass-ceramic samples doped with Tb^{3+} ions in comparative intensity (λ_{ex}=484 nm).

Luminescence spectra of Sr-Tb05Eu1 series samples with 484 nm excitation in comparative intensity are shown in **Figure 4.28a**. It can be seen that the luminescence of Tb^{3+} at 542 nm ($^5D_4 \rightarrow {}^7F_5$) dominates in the glass, while the luminescence of Eu^{3+} ions at 592 nm ($^5D_0 \rightarrow {}^7F_1$) dominates in the corresponding glass ceramic. The same picture was observed in the Sr-Tb1Eu1 sample series. The emission transition of Eu^{3+} ions ($^5D_0 \rightarrow {}^7F_2$) is hypersensitive and dominates in the environment without an inversion center, including in glass, but in a centrosymmetric environment, such as the position of Sr^{2+} in the crystalline phase of SrF_2, it is forbidden. On the other hand, the magnetic dipole transition at 592 nm ($^5D_0 \rightarrow {}^7F_1$) is relatively little dependent on the environment and this luminescence band is the most intense in centrosymmetric symmetry [41, 45, 84].

The dependence of the luminescence intensity of Tb^{3+} ions (λ_{em}=542 nm, λ_{ex}=484 nm) on the sample processing temperature is shown in **Figure 4.28.b.** (normalized by the maximal intensity of Tb^{3+} ions in the precursor glass samples). It can be seen that in the glass ceramic samples in which Eu^{3+} ions are added, the luminescence intensity in the glass ceramic evidently decreases more abruptly compared to the precursor glass samples. For example, in the sample Sr Tb05@680°C the luminescence intensity of Tb^{3+} ions is 54% of the intensity of Tb^{3+} in the glass, while in the sample Sr-Tb05Eu1@680°C – only 21% of the intensity in the glasses. This indicates that part of the excitation energy of Tb^{3+} ions is transferred to Eu^{3+}. It is expected that energy transfer from Tb^{3+} to Eu^{3+} ions in glass ceramics takes place more efficiently than in glass, because there are smaller distances between Tb^{3+} and Eu^{3+} ions embedded in SrF_2 nanocrystallites than in glass, where the ions are arranged in a disordered environment [63, 79, 85].

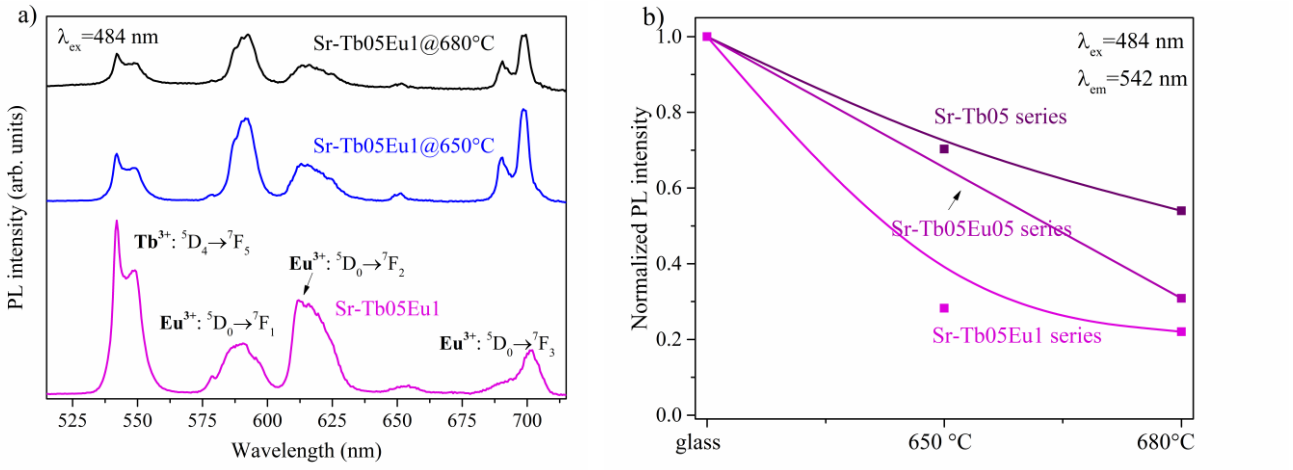

Figure 4.28.(a-b). a) Luminescence spectra of a series of Sr-Tb05Eu1 samples in comparative intensity (λ_{ex}=484 nm), b) dependence of the luminescence of Tb^{3+} ions on the heat treatment temperature in a series of samples with 0.5 mol% Tb^{3+}.

Also, the $^5D_0 \rightarrow {}^7F_1$ luminescence band was the most intense band in Eu^{3+}-doped and co-doped glass-ceramic samples with 393 nm excitation.

Summary: In glass ceramics containing SrF_2 nanocrystallites, the relative intensity of the Tb^{3+} and Eu^{3+} ions excitation bands has slightly changed compared to glasses which indicates a change in the environment of RE ions, when they partially enter the SrF_2 nanocrystallites in the glass ceramics. Excitation bands of Tb^{3+} ions are observed in the excitation spectrum of Eu^{3+} ions indicating energy transfer from Tb^{3+} to Eu^{3+} ions.

In glass-ceramics, with 350 nm excitation, the relative intensity of Tb^{3+} ion luminescence bands $^5D_3 \rightarrow {}^7F_{3,4,5,6}$ in the 360 nm – 480 nm range has decreased compared to the precursor glasses due to cross-relaxation processes, indicating a higher concentration of Tb^{3+} ions locally, with ions partially entering in SrF_2 nanocrystallites. In glass ceramics, with 484 nm excitation, the luminescence intensity of Tb^{3+} ions decreases compared to glass samples – a larger decrease in co-doped samples indicates energy transfer from Tb^{3+} to Eu^{3+} ions in glass ceramics. In the luminescence spectrum of Eu^{3+} ions in glass ceramics, the $^5D_0 \rightarrow {}^7F_1$ MD luminescence band dominates, indicating the effective incorporation of Eu^{3+} ions into SrF_2 nanocrystallites in centrosymmetric positions possessing inversion symmetry. Crystal-field splitting of Tb^{3+} and Eu^{3+} luminescence bands can be observed in glass ceramics.

4.3.5. Luminescence of Eu^{2+} ions

In addition to the luminescence of Tb^{3+} and Eu^{3+} ions, a low-intensity luminescence of Eu^{2+} ions was also observed in the samples with UV excitation. Time-resolved luminescence spectra in the time interval of 30 ns – 1 μs in co-doped glass and glass ceramic samples showed a broad luminescence band of Eu^{2+} ions in the range 370 nm – 650 nm with a maximal intensity around 440 nm. In glass-ceramics, the band is slightly shifted towards shorter wavelengths compared to glasses. It has been reported in the literature that the luminescence peak of Eu^{2+} ions in SrF_2:Eu^{2+} with UV excitation is around 418 nm – 420 nm [39, 41].

The EPR signal of Eu^{2+} ions was detected only in SrF_2-containing Sr-Eu1 series glass-ceramic samples doped with europium ions (the Sr-Eu1 EPR signal was not detected in the precursor glass) [41]. In [41] it was concluded that the EPR signal of Eu^{2+} in glass ceramics annealed at 650°C corresponds to the signal in the SrF_2 phase (and not in the amorphous glass phase), and that probably most of the Eu^{2+} ions are on the surface of the nanocrystallites [41]. The EPR signal was not detected in the co-doped samples studied in the thesis, presumably because the concentration of Eu^{2+} ions is too low.

Summary: Weak Eu^{2+} luminescence bands with a maximum around 440 nm were observed in the samples, their shape does not change in co-doped glass and glass ceramics. Electron paramagnetic resonance measurements of Sr-Eu1 series samples [41] confirm that in glass ceramics (650 °C) most of the Eu^{2+} ions entered SrF_2 nanocrystallites or are located on their surfaces.

4.3.6. Time-resolved luminescence spectra in glasses and glass ceramics

Figure 4.29a shows the time-resolved spectra in the glass ceramic sample Sr-Tb05@650°C (λ_{ex}=484 nm). It can be seen that shortly after the excitation the Tb^{3+} luminescence band is smooth in glass ceramics, but in the time interval 20 ms – 45 ms after excitation, when the signal from Tb^{3+} ions incorporated in SrF_2 nanocrystallites is detected, the band is split into several components. A similar picture is also seen in the Sr-Tb1@650°C sample and in co-doped glass-ceramic samples (however, in co-doped samples the splitting is less pronounced).

Figure 4.29b shows the time-resolved site-selective spectra of Eu^{3+} ions with several excitation wavelengths. Unlike in the Ca-Dy^{3+}/Eu^{3+} series of samples, where several very different Eu^{3+} centers were observed, in the studied series there is one dominant center, which is also observed in the literature [75, 81, 96] in the SrF_2 phase. Excitation wavelengths were selected from the excitation spectra – splitting of the $^7F_0 \rightarrow {}^5D_1$ excitation band (peak at 525.6 nm in glass) into 2 components – 524.7 nm and 525.4 nm – was observed in glass ceramic sample.

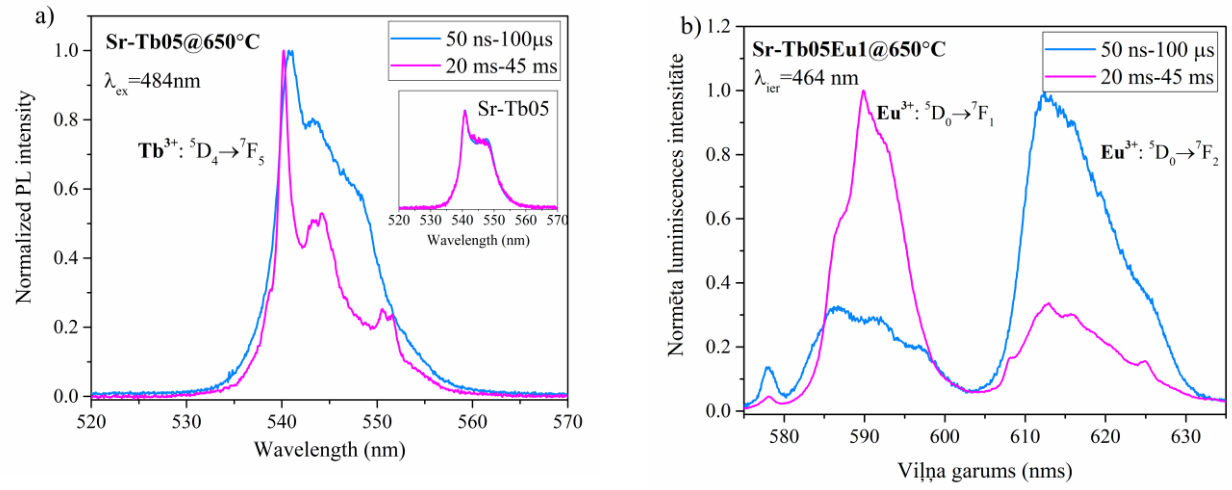

Figure 4.29(a-b). a) time-resolved luminescence spectra of Tb^{3+} ions in glass ceramic sample Sr-Tb05@650°C (λ_{ex}= 484 nm). In the inset, time-resolved spectra in the precursor glass. b) time-resolved luminescence spectra of Eu^{3+} ions in glass ceramic Sr-Tb05Eu1@680°C in the time interval 20 ms – 45 ms with several excitation wavelengths.

Summary: The time-resolved measurements, measured in the time interval from 20 ms to 45 ms after the laser pulse, confirm the partial incorporation of Tb^{3+} and Eu^{3+} ions into the SrF_2 nanocrystallites in glass-ceramic samples, since the crystal-field splitting of the luminescence bands of Tb^{3+} ions (with 484 nm excitation) can be observed in the luminescence spectra measured in this time interval as well as changes in the relative ratio of Eu^{3+} luminescence bands $^5D_0 \rightarrow {}^7F_1$ (MD transition) and $^5D_0 \rightarrow {}^7F_2$ (hypersensitive ED transition) with 464 nm excitation. The site-selective luminescence spectra of Eu^{3+} ions in the 20 ms to 45 ms time interval indicate at least 3 different environments of Eu^{3+} ions in Eu^{3+}-singly doped and Tb^{3+}/Eu^{3+} co-doped glass ceramics due to different charge compensation processes.

4.3.7 Luminescence decay kinetics in glasses and glass ceramics and energy transfer between Tb^{3+} and Eu^{3+} ions

In order to study the interaction of rare earth ions, luminescence decay kinetics measurements of Tb^{3+}, Eu^{3+}, Eu^{2+} ions in glass and glass ceramic samples were also performed.

The luminescence decay kinetics of Tb^{3+} ions in glass samples with and without the presence of Eu^{3+} ions (with 484 nm excitation) are shown in **Figure 4.30.** Decay kinetics were measured for the luminescence transition $^5D_4 \rightarrow {}^7F_5$ (λ_{em}=542 nm). The calculated effective luminescence decay times of Tb^{3+} ions are shown in **Table 4.14.**

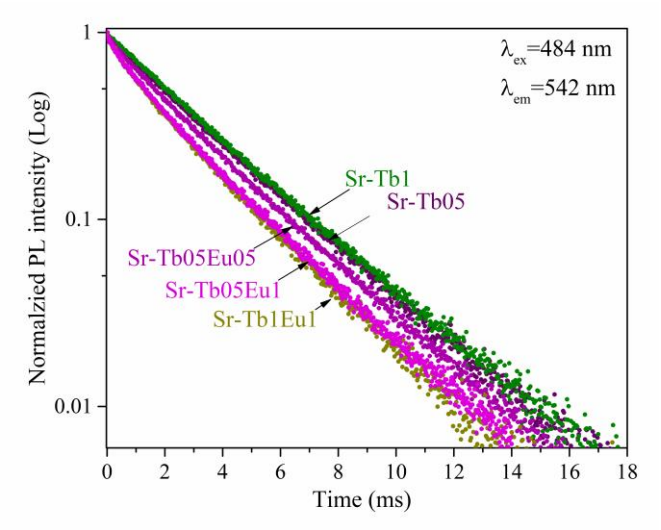

Figure 4.30. Normalized luminescence decay kinetics of Tb^{3+} ions in glasses doped with Tb^{3+} and Tb^{3+}/Eu^{3+} ions (λ_{ex}=484 nm, λ_{em}=542 nm).

Table 4.14. Calculated decay times (τ) of Tb^{3+} ions and energy transfer ($Tb^{3+} \rightarrow Eu^{3+}$) efficiency (η).

Sample (λ_{ex}=484 nm, λ_{em}=542 nm)	**τ (ms) ± 0.02 ms**	**η (%)**
Sr-Tb05	3.13	-
Sr-Tb05Eu05	2.96	5.4 ± 1.3
Sr-Tb05Eu1	2.63	15.8 ± 0.6
Sr-Tb1	3.19	-
Sr-Tb1Eu1	2.61	18.2 ± 1.1

In **Table 4.14.** it can be seen that the decay time of Tb^{3+} ions, when Eu^{3+} ions are added, decreases from 3.13 ms (Sr-Tb05) to 2.63 ms (Sr-Tb05Eu1), due to the energy transfer from Tb^{3+} to Eu^{3+} ions [63, 74, 83, 90]. The energy transfer efficiency increases with increasing Eu^{3+} concentration. In the Sr-Tb1Eu1 sample, the energy transfer efficiency is higher than in the samples with 0.5 mol% Tb^{3+}. It is mentioned in literature that the energy transfer from Tb^{3+} to Eu^{3+} ions in polycrystalline SrF_2 [11] occurs due to the electric quadrupole-quadrupole interaction (see *Chapter 2.1.3*).

The luminescence decay kinetics of glass and glass ceramic samples doped with 0.5 mol% Tb^{3+} ions are shown in **Figure 4.31a**.

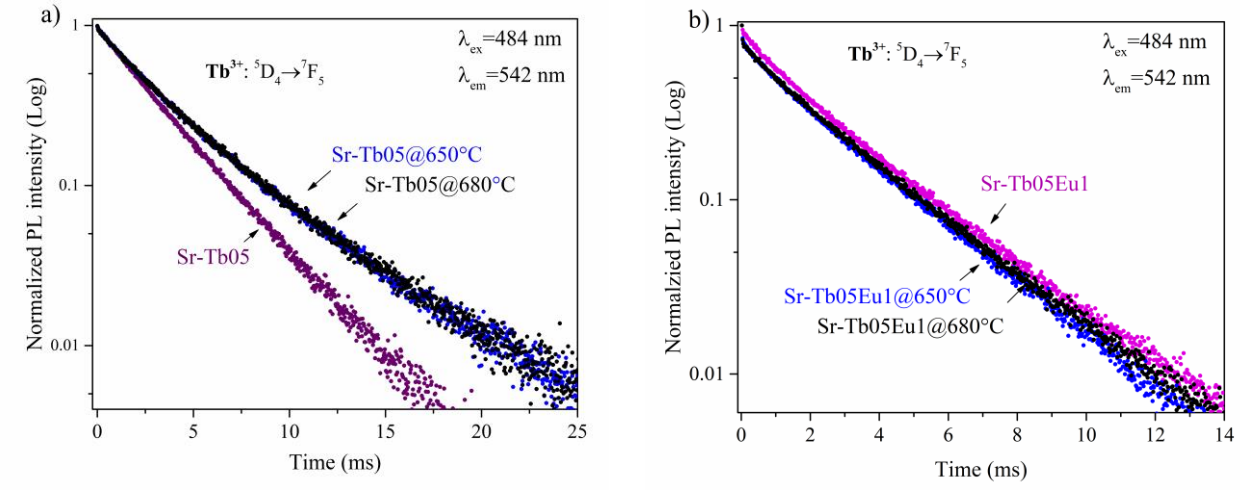

Figure 4.31.(a-b). a) normalized luminescence decay kinetics curves of the Sr-Tb05 sample series (λ_{ex}=484 nm, λ_{em}=542 nm), b) normalized luminescence decay kinetics curves of the Sr-Tb05Eu1 sample series (λ_{ex}=484 nm, λ_{em}=542 nm).

In the glass ceramic samples, the luminescence decay occurs slower than in the glass sample: the initial part of the kinetics is similar to the Tb^{3+} decay in glass, but after that a slower part of the decay kinetics appears, which is associated with Tb^{3+} ions in a environment with lower phonon energy [63, 84].

Figure 4.31.b. shows the luminescence decay of Tb^{3+} ions in co-doped samples of the Sr-Tb05Eu1 series. It can be seen that in co-doped glass ceramics, the luminescence decay of Tb^{3+} ions occurs faster than in glasses. The differences are mainly observed in the initial part of the kinetics. This can be explained by energy transfer from Tb^{3+} to Eu^{3+} ions. After the initial fast kinetics part, further decay in glass and glass-ceramic samples occurs similarly. The calculated luminescence decay times in glass ceramics with 0.5 mol% Tb^{3+} are summarized in **Table 4.15.**

Table 4.15. Calculated decay times (τ) of Tb^{3+} ions and energy transfer ($Tb^{3+}\rightarrow Eu^{3+}$) efficiency (η) in 0.5 % Tb^{3+} doped samples.

Sample (λ_{ex}=484 nm, λ_{em}=542 nm)	**τ (ms) ± 0.02 ms**	**Sample (λ_{ex}=484 nm, λ_{em}=542 nm)**	**τ (ms) ± 0.02 ms**	**η (%)**
Sr-Tb05	3.13	Sr-Tb05Eu05	2.96	5.4 ± 1.3
Sr-Tb05@650°C	4.28	Sr-Tb05Eu05@650°C	2.81	34.4 ± 0.8
Sr-Tb05@680°C	4.31	Sr-Tb05Eu05@680°C	2.93	32.0 ± 0.8
		Sr-Tb05Eu1	2.63	15.8 ± 0.6
		Sr-Tb05Eu1@650°C	2.53	40.7 ± 0.5
		Sr-Tb05Eu1@680°C	2.62	39.2 ± 0.5

In **Table 4.15.** it can be seen that in glass ceramic samples (Sr-Tb05 series) singly-doped with 0.5 mol% Tb^{3+}, the effective decay time increases to ~4.3 ms (in the precursor glass – 3.13 ms). In co-doped glass-ceramic samples, the luminescence decay times are similar to those in glass samples.

The energy transfer efficiency calculated in the glass sample Sr-Tb05Eu05 is 5.4 ms, and in the sample Sr-Tb05Eu1 – 15.8 ms. In co-doped glass-ceramic samples, its efficiency has increased compared to glasses, up to 32%-34% in SrTb05Eu05@650°C and Sr-Tb05Eu05@680°C, and 39%-40% in Sr-Tb05Eu1@650°C and Sr-Tb05Eu1@680°C, respectively.

In the sample series Sr-Tb1 and Sr-Tb1Eu1 similar observations were made.

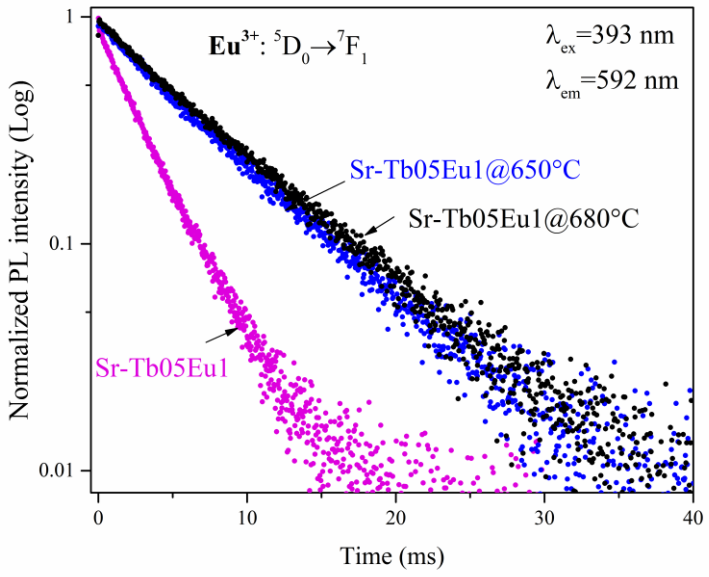

Figure 4.32. Luminescence decay kinetics curves of Eu^{3+} ions in a series of Sr-Tb05Eu1 samples (λ_{ex}=393 nm, λ_{em}=592 nm).

Luminescence decay measurements of the Eu^{3+} ion transition $^5D_0\rightarrow{}^7F_1$ (**Figure 4.32**) revealed that in glass-ceramic samples, with 393 nm excitation, Eu^{3+} ion luminescence decay occurs significantly

slower than in the glass sample – the luminescence decay time in glass is 5.52 ms, in glass-ceramic samples – 7.40 ms and 7.68 ms. In all samples, the decay fits well to an exponential function (i.e., a straight line on a semi-logarithmic scale). The increase of luminescence decay time indicates a change in the environment of Eu^{3+} ions in the glass ceramic, i.e. partial incorporation in a crystalline environment with a lower phonon energy. The luminescence decay time of Eu^{2+} ions in the sample Sr-Tb05Eu1@680°C (λ_{ex}=330 nm) is 670 ns, it is about 4 orders of magnitude shorter than the luminescence decay time of Eu^{3+} ions in the corresponding sample.

Summary: In co-doped glass samples, with increasing concentration of Eu^{3+} ions, the effective decay time of Tb^{3+} luminescence band $^5D_4 \rightarrow ^7F_5$ with 484 nm excitation decreases due to energy transfer to Eu^{3+} ions. In glass-ceramic samples containing only Tb^{3+} ions, the $^5D_4 \rightarrow ^7F_5$ (Tb^{3+}) decay time with 484 nm excitation increases significantly compared to the precursor glasses indicating the efficient incorporation of Tb^{3+} ions into SrF_2 nanocrystallites. In co-doped glass ceramics, the decay times of Tb^{3+} ions in glass and glass ceramics are similar, which indicates energy transfer from Tb^{3+} to Eu^{3+} ions thus shortening the decay time of Tb^{3+} ions luminescence, compared to glass ceramics containing only Tb^{3+} ions, as well as indicates less effective incorporation of Tb^{3+} ions into SrF_2 nanocrystallites. In glass ceramics, the energy transfer efficiency from Tb^{3+} to Eu^{3+} ions with 484 nm excitation increases compared to glasses (Sr-Tb05Eu1 – 15.8 %, Sr Tb05Eu1@680°C – 39.2 %). The luminescence decay time of Eu^{3+} ions in Sr-Tb05Eu1 series glass ceramics with 393 nm excitation has significantly increased compared to the initial glass, which indicates the effective incorporation of Eu^{3+} ions into SrF_2 nanocrystallites – an environment possessing lower phonon energy.

4.3.8. Color coordinates of samples

The CIE 1931 color coordinates of Tb^{3+}/Eu^{3+} doped glass and glass ceramic samples are shown in the CIE color diagram in **Figure 4.33**, in **Table 4.16**. the corresponding samples and excitation wavelengths are indicated.

From **Figure 4.33.** it can be seen that the luminescence of Tb^{3+} ions with 484 nm excitation appears green to the observer. Adding of Eu^{3+} ions adds the red component. On the other hand, in co-doped glass ceramics with 350 nm excitation (samples with numbers 2 and 3) there is also a blue light component, which is due to the luminescence of Eu^{2+} ions, as well as due to Tb^{3+} bands in the blue spectral range.

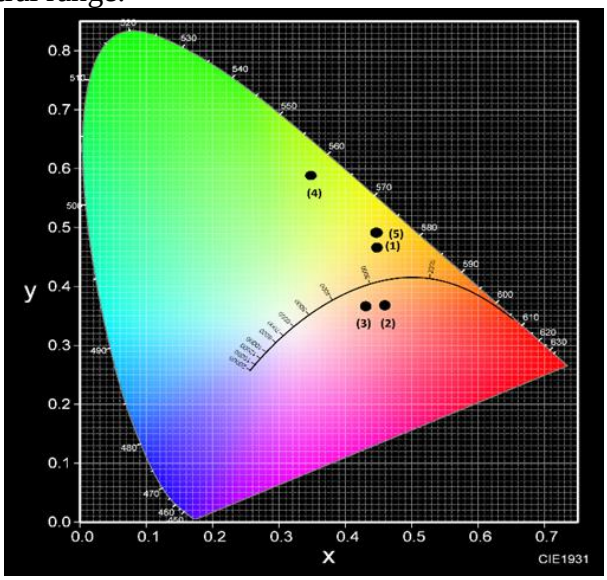

Figure 4.33. CIE 1931 color coordinates of samples doped with Tb^{3+}/Eu^{3+} ions.

Table 4.16. The CIE colour coordinates of the data points shown in **Figure 4.32.**

Sample number	**Sample name**	**Excitation wavelength (nm)**
1	Sr-Tb1Eu1	350
2	Sr-Tb1Eu1@650°C	350
3	Sr-Tb1Eu1@680°C	350
4	Sr-Tb1	484
5	Sr-Tb1Eu1	484

Summary: Addition of Eu^{3+} ions in Tb^{3+}-containing glass samples and heat treatment of the glasses allows to adjust the color of the luminescent light in a wide range and bring it closer to white light due to changes in the relative ratio of Tb^{3+} and Eu^{3+} ions luminescence in glass ceramics, compared to initial glass, and due to the luminescence band of Eu^{2+} ions.

CONCLUSIONS

Energy transfer from Dy^{3+} to Eu^{3+} ions was observed in oxyfluoride glass co-doped with Dy^{3+} and Eu^{3+} ions and glass ceramics containing CaF_2 nanocrystallites, as indicated by the appearance of Dy^{3+} excitation bands in the excitation spectrum of Eu^{3+} ions and the shortening of the luminescence decay time of Dy^{3+} ions upon addition of Eu^{3+} ions. Energy transfer in glass and glass ceramics occurs with similar efficiency. The most intense luminescence of Dy^{3+} ions is observed in the glass sample with 0.5 mol% Dy^{3+} ions, and it decreases at a higher concentration of Dy^{3+} ions or, when Eu^{3+} ions are added. A broad luminescence band of Eu^{2+} ions in the blue-green spectral range, which is excited by UV radiation, was also observed in both glass and glass-ceramic samples. Luminescence and EPR measurements suggest that in glass ceramics, the most of Eu^{2+} ions are located in the glass environment. Time-resolved luminescence spectra measured 10 or 20 ms – 45 ms after excitation show that some portion of the trivalent RE ions (Dy^{3+}, Eu^{3+}) reside in the CaF_2 nanocrystallites because their bands are split. However, the share of RE ions in nanocrystallites is small, because in time-integrated spectra (measured without time resolving), the luminescence spectra in glass and glass-ceramics have the same shape, i.e. glass environment dominate. Site-selective spectroscopy measurements show that CaF_2 nanocrystallites contain multiple types of Eu^{3+} centers, when Eu^{3+} ions occupy the Ca^{2+} position, one of the centers is identified as cubic (O_h).

Energy transfer from Dy^{3+} to Eu^{3+} ions has also been observed in Dy^{3+}/Eu^{3+} co-doped glass and glass ceramics containing SrF_2 nanocrystallites, its efficiency in glass ceramics tends to decrease slightly compared to glasses. In glass samples with 0.5 mol% and 1.0 mol% Dy^{3+} ions, the luminescence intensity is similar. In glass-ceramic samples containing only Dy^{3+} ions, a greater drop in intensity is observed in glass-ceramics compared to co-doped glasses, this indicates more efficient cross-relaxation processes between Dy^{3+} ions, as the distances between them decrease in glass-ceramics. Band splitting in the time-integrated spectra was not observed, but in co-doped glass and glass-ceramic samples the relative ratio of the luminescence bands of Dy^{3+} and Eu^{3+} ions is different, this could be partly explained by the reduction of Eu^{3+} to Eu^{2+} ions. It was observed that the relative luminescence intensity of Eu^{2+} ions compared to Eu^{3+} ions increases in glass ceramics, and also, the Eu^{2+} luminescence band shifts to shorter wavelengths. Similar to the series contaning CaF_2 nanocrystallites, time-resolved and site-selective spectra show splitting of RE ion bands and multiple types of Eu^{3+} ion centers in SrF_2 nanocrystallites.

In glass Tb^{3+}/Eu^{3+} ions co-doped glasses and in glass ceramics containing SrF_2 nanocrystallites, the most efficient incorporation of RE ions into fluoride crystallites was observed, as evidenced by a more evident crystal-field splitting of the luminescence bands (in glass ceramics) and the change in the 5D0→7F1 and $^5D_0 \rightarrow {}^7F_2$ luminescence bands ratio (Eu^{3+}). The quenching of the $^5D_3 \rightarrow {}^7F_{3,4,5,6}$ luminescence bands in glass ceramics also indicates a local increase in the concentration of Tb^{3+} ions. The luminescence decay kinetics of Tb^{3+}, Eu^{3+} and Eu^{2+} ions in glass-ceramics is slower than in glasses. Weak Eu^{2+} luminescence bands with a maximum around 440 nm were observed in the samples, the shape of which does not change in co-doped glass and glass ceramics. Time-resolved and site-selective spectra show RE ion band splitting and multiple types of Eu^{3+} ion centers in SrF_2, however, a greater dominance of a single type of Eu^{3+} center is observed than in the other series. In glass ceramics, the efficiency of energy transfer from Tb^{3+} to Eu^{3+} ions increases, compared to glasses.

The CIE colour (photometric) coordinates of the luminescence of co-doped oxyfluoride glass and glass ceramics is well adaptable to the desired application in white LEDs or other devices – the luminescence spectrum can be controlled by the added RE ion concentration, excitation wavelength and thermal treatment properties, which can change both the ratio of the trivalent RE ion luminescence bands and increase the luminescence intensity of Eu^{2+} ions in the blue-green spectral range.

THESES

1. In the Dy^{3+} and Eu^{3+} co-doped glass ceramics in comparison with the precursor amorphous glasses, changes in the relative luminescence intensities of the activator ions are seen, but the energy transfer efficiency between Dy^{3+} and Eu^{3+} ions in the glass ceramics does not change significantly compared to initial glasses.
2. In Tb^{3+} and Eu^{3+} doped glass ceramics containing SrF_2 nanocrystallites, an increase in energy transfer efficiency is observed, compared to glasses, which is explained by the partial incorporation of Tb^{3+} and Eu^{3+} ions into SrF_2 nanocrystallites and the decrease of mutual distances between Tb^{3+} and Eu^{3+} ions.
3. The energy transfer between rare-earth ions, enhanced by the heat treatment induced crystallization, and changes in the environment of Eu^{3+} ions in Tb^{3+} and Eu^{3+} co-doped oxyfluoride glass ceramics serve as a means of tuning the luminescence spectrum, approaching the application in white light sources.

LITERATURE

[1] Dramicanin, M., Luminescence Thermometry. Methods, Materials, and Applications, Woodhead Publishing, 2018

[2] Vij, D. R., Handbook of Applied Solid State Spectroscopy, Springer, 2006

[3] Blasse, G, Grabmaier, B. C., Luminescent Materials, Springer, 1994. https://doi.org/10.1007/978-3-642-79017-1

[4] Noomnarm, U., Clegg, R. M, Photosynthesis research, 101 (2009)181-194. https://doi.org/10.1007/s11120-009-9457-8

[5] Huang, L., Qin, G., Arai, Y., Jose, R., Suzuki, T., Ohishi, Y., Yamashita, T. Akimoto, Y., Journal of Applied Physics, 102(9) (2007) 093506. https://doi.org/10.1063/1.2802289

[6] Ronda, C. R., Luminescence: from theory to applications, John Wiley & Sons, 2007

[7] Hänninen, P., Härmä, H., Lanthanide Luminescence. Photophysical, Analytical and Biological Aspects, Springer, 2013. https://doi.org/10.1007/978-3-642-21023-5

[8] Kitai, A.H., Solid State Luminescence. Theory, materials and devices, Springer, 1993. https://doi.org/10.1007/978-94-011-1522-3

[9] Pawlik, N., Szpikowska-Sroka, B., Goryczka, T., Pisarska, J., Pisarski,W. A., Materials, 14(4) (2021) 754. https://doi.org/10.3390/ma14040754

[10] Ma, Y., Fei, M., Zhang, W., Teng, L., Hu, F., Wei, R., Guo, H, Journal of Luminescence, 219 (2020) 116966. https://doi.org/10.1016/j.jlumin.2019.116966

[11] Shelby, J. E., Introduction to glass science and technology, Royal Society of Chemistry, 2005. https://doi.org/10.1039/9781847551160-FP005

[12] Rao, K. J., Structural chemistry of glasses, Elsevier, 2002. https://doi.org/10.1016/B978-0-08-043958-7.X5017-1

[13] Fedorov, P.P., Luginina, A. A., Popov, A. I., Journal of Fluorine Chemistry 172 (2015) 22-50. https://doi.org/10.1016/j.jfluchem.2015.01.009

[14] Li, P., Xu, X., Zhao, J., Awasthi, P., Qiao, X., Du, J., X, Fan, Qian, G.,. Journal of Rare Earths, 40(2), (2022) 169-192. https://doi.org/10.1016/j.jre.2021.09.014

[15] Bocker, C., Wiemert, J., Rüssel, C., Journal of the European Ceramic Society, 33(10) (2013) 1737-1745. https://doi.org/10.1016/j.jeurceramsoc.2013.02.008

[16] Liu, X., Zhou, J., Zhou, S., Yue, Y., Qiu, J., Progress in Materials Science, 97 (2018) 38-96. https://doi.org/10.1016/j.pmatsci.2018.02.006

[17] Chen, D., Xiang, W., Liang, X., Zhong, J., Yu, H., Ding, M.,Lu, H, Ji, Z., Journal of the European Ceramic Society, 35(3) (2015) 859-869. https://doi.org/10.1016/j.jeurceramsoc.2014.10.002

[18] Gao, X., Fang, G., Wang, Y., Zhu, Z., You, Z., Li, J., Sun, J.,Tu, C., Journal of Alloys and Compounds, 856 (2021) 158083. https://doi.org/10.1016/j.jallcom.2020.158083

[19] Khenata, R., Daoudi, B., Sahnoun, M., Baltache, H., Rérat, M., Reshak, A. H., Bouhafs B., Abid H., Driz, M., The European Physical Journal B-Condensed Matter and Complex Systems, 47 (2005) 63-70. https://doi.org/10.1140/epjb/e2005-00301-6

[20] Chuklina, N., Mysovsky, A., Radiation Measurements, 128 (2019) 106135.

https://doi.org/10.1016/j.radmeas.2019.106135

[21] Bougradja, F., Diaf, M., Fartas, R., Boubekri, H., Khiari, S., Optical Materials, 108 (2020) 110143. https://doi.org/10.1016/j.optmat.2020.110143

[22] Gao, X., Zou, Y., Zheng, L., Wang, Y., Zhu, Z., You, Z.,Li, J., Sun, J., Lakshminarayana, G., Tu, C., Journal of Alloys and Compounds, 907 (2022) 164513. https://doi.org/10.1016/j.jallcom.2022.164513

[23] Antuzevics, A., Kemere, M., Krieke, G., Journal of Alloys and Compounds, 762 (2018) 500-507. https://doi.org/10.1016/j.jallcom.2018.05.283

[24] Wells, J. P. R., Reeves, R. J., Physical Review B, 64(3) (2001) 035102. https://doi.org/10.1103/PhysRevB.64.035102

[25] Hamers, R. J., Wietfeldt, J. R., & Wright, J. C., The Journal of Chemical Physics, 77(2) (1982) 683-692 https://doi.org/10.1063/1.443882

[26] de Mesquita, B. R., Rezende, M. V. D. S., dos Santos, M. A. C., Journal of Luminescence, 238 (2021) 118297. https://doi.org/10.1016/j.jlumin.2021.118297

[27] Rabbiner, N.,. Physical Review, 132(1) (1963) 224 https://doi.org/10.1103/PhysRev.132.224

[28] Jouart, J. P., Bouffard, M., Klein, G., Mary, G., Journal of luminescence, 50(5) (1991) 273-277. https://doi.org/10.1016/0022-2313(91)90032-Q

[29] Antuzevics, A., Kemere, M., Ignatans, R., Journal of Non-Crystalline Solids, 449 (2016) 29-33. https://doi.org/10.1016/j.jnoncrysol.2016.07.015

[30] Antuzevics, A., Krieke, G., Pavlovska, E., Rogulis, U., Journal of Non-Crystalline Solids, 522 (2019) 119548. https://doi.org/10.1016/j.jnoncrysol.2019.119548

[31] Jamison, S. P., Reeves, R. J., Physical Review B, 67(11) (2003) 115110.

https://doi.org/10.1103/PhysRevB.67.115110

[32] Leśniak, K., The Journal of Chemical Physics, 94(5) (1991) 3919-3927. https://doi.org/10.1063/1.460668

[33] Wen-Chen, Z., Hui-Ning, D., Shao-Yi, W., Sheng, T., Physica B: Condensed Matter, 344(1-4) (2004) 103-107. https://doi.org/10.1016/j.physb.2003.09.246

[34] Van Der Voort, D., Dirksen, G. J., Blasse, G., Journal of Physics and Chemistry of Solids, 53(2) (1992) 219-225. https://doi.org/10.1016/0022-3697(92)90048-I

[35] Lin, Z., Zeng, H., Yang, Y., Liang, X., Chen, G., Sun, L., Journal of the American Ceramic Society, 93(10) (2010) 3095-3098. https://doi.org/10.1111/j.1551-2916.2010.04067.x

[36] Zhu, C., Wu, D., Zhang, Y., Zhang, M., Yue, Y., Journal of Alloys and Compounds, 632 (2015) 291-295. https://doi.org/10.1016/j.jallcom.2015.01.207

[37] Itoh, M., Sakurai, T., Yamakami, T., Fu, J., Journal of luminescence, 112(1-4) (2005) 161-165. https://doi.org/10.1016/j.jlumin.2004.09.017

[38] Fu, J., Parker, J. M., Flower, P. S., Brown, R. M., Materials Research Bulletin, 37(11) (2002) 1843-1849. https://doi.org/10.1016/S0025-5408(02)00862-0

[39] Wang, C., Chen, X., Luo, X., Zhao, J., Qiao, X., Liu, Y., Fan, X.,Qian, G., Zhang, X, Han, G., RSC advances, 8(60) (2018) 34536-34542. https://doi.org/10.1039/C8RA06843G

[40] Malchukova, E., Boizot, B., Materials Research Bulletin, 45(9) (2010) 1299-1303. https://doi.org/10.1016/j.materresbull.2010.04.027

[41] Antuzevics, A., Kemere, M., Krieke, G., Ignatans, R., Optical Materials, 72, (2017). 749-755. https://doi.org/10.1016/j.optmat.2017.07.024

[42] Dhoble, S., Pawade, V., Swart, H., Chopra, V., Spectroscopy of Lanthanide Doped Oxide Materials, Woodhead Publishing, 2019. https://doi.org/10.1016/C2018-0-02471-8

[43] Kim, P., Anderko, A., Navrotsky, A., Riman, R. E., Minerals, 8(3) (2018) 106. https://doi.org/10.3390/min8030106

[44] Huang, C., Rare Earth Coordination Chemistry: Fundamentals and Applications, Wiley, 2010. https://doi.org/10.1002/9780470824870

[45] Binnemans, K., Coordination Chemistry Reviews, 295 (2015) 1-45. https://doi.org/10.1016/j.ccr.2015.02.015

[46] Fangfang, H. U., Zhangmei, Z. H. A. O., Fengfeng, C. H. I., Xiantao, W., Min, Y. I. N.,Journal of Rare Earths, 35(6) (2017) 536-541. https://doi.org/10.1016/S1002-0721(17)60945-1

[47] Wang, Q., Liao, M., Lin, Q., Xiong, M., Mu, Z., Wu, F., Journal of Alloys and Compounds, 850 (2021) 156744. https://doi.org/10.1016/j.jallcom.2020.156744

[48] Pawlik, N., Szpikowska-Sroka, B., Sołtys, M., Pisarski, W. A., Journal of Rare Earths, 34(8) (2016) 786-795. https://doi.org/10.1016/S1002-0721(16)60095-9

[49] Gupta, I., Singh, S., Bhagwan, S., Singh, D., Ceramics international, 47(14) (2021) 19282-19303. https://doi.org/10.1016/j.ceramint.2021.03.308

[50] Rajesh, D., Brahmachary, K., Ratnakaram, Y. C., Kiran, N., Baker, A. P., Wang, G. G., Journal of alloys and compounds, 646 (2015) 1096-1103. https://doi.org/10.1016/j.jallcom.2015.05.138

[51] Yu, C., Yang, Z., Huang, A., Chai, Z., Qiu, J., Song, Z., Zhou, D., Journal of Non-Crystalline Solids, 457 (2017) 1-8. https://doi.org/10.1016/j.jnoncrysol.2016.11.025

[52] Kalusniak, S., Castellano-Hernández, E., Yalçinoğlu, H., Tanaka, H., Kränkel, C., Applied Physics B, 128(2) (2022) 33. https://doi.org/10.1007/s00340-022-07759-1

[53] Martín-Ramos, P., Silva, M. R., Lanthanide-Baseed Multifunctional Materials: From OLEDs to SIMs, Elsevier, 2018 https://doi.org/10.1016/C2017-0-00381-6

[54] Tanner, P. A., Duan, C. K., Coordination Chemistry Reviews, 254(23-24) (2010) 3026-3029. https://doi.org/10.1016/j.ccr.2010.05.009

[55] Babu, P., Jang, K. H., Rao, C. S., Shi, L., Jayasankar, C. K., Lavín, V., Seo, H. J., Optics express, 19(3) (2011) 1836-1841. https://doi.org/10.1364/OE.19.001836

[56] Cavalli, E., Optical Materials: X, 1 (2019) 100014. https://doi.org/10.1016/j.omx.2019.100014

[57] Meza-Rocha, A. N., Camarillo, I., Lozada-Morales, R., Caldiño, U. Journal of Luminescence, 183 (2017) 341-347. https://doi.org/10.1016/j.jlumin.2016.11.068

[58] Tian, Y., Chen, B., Tian, B., Hua, R., Sun, J., Cheng, L., Zhong, H., Li, X., Zhang, J., Zheng, Y., Huang, L., Meng, Q., Journal of alloys and compounds, 509(20) (2011) 6096-6101. https://doi.org/10.1016/j.jallcom.2011.03.034

[59] Kemere, M., Rogulis, U., Sperga, J., Journal of Alloys and Compounds, 735 (2018) 1253-1261. https://doi.org/10.1016/j.jallcom.2017.11.077

[60] Kesavulu, C. R., Kim, H. J., Lee, S. W., Kaewkhao, J., Chanthima, N., Tariwong, Y., Journal of Alloys and Compounds, 726 (2017) 1062-1071. https://doi.org/10.1016/j.jallcom.2017.08.091

[61] Ma, Y., Peng, X., Fei, M., Zhang, W., Teng, L., Hu, F.,Wei, R, Guo, H., Journal of Alloys and Compounds, 846 (2020) 156435 https://doi.org/10.1016/j.jallcom.2020.156435

[62] Terra, I. A., Borrero-González, L. J., Almeida, J. M., Hernandes, A. C., Nunes, L. A. Química Nova, 43 (2020) 188-193. https://doi.org/10.21577/0100-4042.20170465

[63] Li, X., Peng, Y., Wei, X., Yuan, S., Zhu, Y., Chen, D., Journal of Luminescence, 210 (2019) 182-188. https://doi.org/10.1016/j.jlumin.2019.01.061

[64] Kemere, M., Sperga, J., Rogulis, U., Krieke, G., Grube, J., Journal of Luminescence, 181 (2017) 25-30. https://doi.org/10.1016/j.jlumin.2016.08.062

[65] Galca, A. C., Preda, N., Secu, C. E., Luculescu, C. R., Secu, M., Optical Materials, 34(8) (2012) 1493-1496. https://doi.org/10.1016/j.optmat.2012.03.015

[66] Xusheng, Q., Qun, L., Xianping, F., Minquan, W., Journal of Rare Earths, 26(6) (2008) 883-888. https://doi.org/10.1016/S1002-0721(09)60026-0

[67] Secu, M., Secu, C. E., Polosan, S., Aldica, G., Ghica, C., Journal of Non-Crystalline Solids, 355(37-42) (2009) 1869-1872. https://doi.org/10.1016/j.jnoncrysol.2009.04.062

[68] Ye, R., Cui, Z., Hua, Y., Deng, D., Zhao, S., Li, C., Xu, S., Journal of non-crystalline solids, 357(11-13) (2011) 2282-2285. https://doi.org/10.1016/j.jnoncrysol.2010.11.071

[69] Bu, Y. Y., Wang, Y. M., Yan, X. H., Applied Physics A, 123 (2017) 1-8. https://doi.org/10.1007/s00339-017-0949-7

[70] Lakshminarayana, G., Yang, R., Mao, M., Qiu, J., Kityk, I. V.,. Journal of Non-Crystalline Solids, 355(52-54) (2009) 2668-2673. https://doi.org/10.1016/j.jnoncrysol.2009.08.029

[71] Yang, Y., Zhou, Z., Mei, B., Li, W., Zhang, Y., Liu, X., Journal of the European Ceramic Society, 41(15) (2021) 7835-7844. https://doi.org/10.1016/j.jeurceramsoc.2021.08.042

[72] Sun, X. Y., Gu, M., Huang, S. M., Jin, X. J., Liu, X. L., Liu, B., Ni, C. Journal of Luminescence, 129(8) (2009) 773-777. https://doi.org/10.1016/j.jlumin.2009.02.017

[73] Sun, X. Y., Huang, S. M., Nuclear Instruments and Methods in Physics Research Section A: Accelerators, Spectrometers, Detectors and Associated Equipment, 621(1-3) (2010) 322-325. https://doi.org/10.1016/j.nima.2010.04.032

[74] Ritter, B., Haida, P., Fink, F., Krahl, T., Gawlitza, K., Rurack, K., Scholz, G., Kemnitz, E., Dalton Transactions, 46(9) (2017) 2925-2936. https://doi.org/10.1039/C6DT04711D

[75] Wang, X., Chen, J., Li, J., Guo, H., Journal of non-crystalline solids, 357(11-13) (2011) 2290-2293. https://doi.org/10.1016/j.jnoncrysol.2010.11.068

[76] Dharmaiah, P., Viswanath, C. D., Basavapoornima, C., Krishnaiah, K. V., Jayasankar, C. K., Hong, S. J., Materials Research Bulletin, 83 (2016) 507-514. https://doi.org/10.1016/j.materresbull.2016.06.044

[77] Walas, M., Lisowska, M., Lewandowski, T., Becerro, A. I., Łapiński, M., Synak, A.,Sadowski, W., Kościelska, B., *Journal of Alloys and Compounds*, *806* (2019) 1410-1418. 10.1016/j.jallcom.2019.07.017

[78] Zheng, C., Sun, Z., Li, W., Yang, Y., Mei, B., Materials Chemistry and Physics, 273 (2021) 125141. https://doi.org/10.1016/j.matchemphys.2021.125141

[79] Luo, Q., Qiao, X., Fan, X., Zhang, X, Journal of non-crystalline solids, 356(50-51) (2010) 2875-2879. https://doi.org/10.1016/j.jlumin.2019.03.040

[80] Qiao, X., Fan, X., Xue, Z., Xu, X., Luo, Q., Journal of luminescence, 131(10) (2011) 2036-2041. https://doi.org/10.1016/j.jlumin.2011.05.012

[81] Kłonkowski, A. M., Wiczk, W., Ryl, J., Szczodrowski, K., Wileńska, D., Journal of Alloys and Compounds, 724 (2017) 649-658. https://doi.org/10.1016/j.jallcom.2017.07.055

[82] An, J., Zhang, S., Liu, R., Hu, G., Zhang, Z., Qiu, Y., Zhou, Y., Zeng, F., Su, Z., Journal of Rare Earths, 39(1) (2021) 26-32. https://doi.org/10.1016/j.jre.2020.01.013

[83] Yan, Y., Tan, Y., Li, D., Luan, F., Guo, D., Journal of Luminescence, 211 (2019) 209-217. https://doi.org/10.1016/j.jlumin.2019.03.040

[84] Szpikowska-Sroka, B., Pawlik, N., Goryczka, T., Pietrasik, E., Bańczyk, M., Pisarski, W. A. Ceramics International, 43(11) (2017) 8424-8432. https://doi.org/10.1016/j.ceramint.2017.03.192

[85] Fu, H., Qiao, X., Cui, S., Luo, Q., Qian, J., Fan, X., Zhang, X. Materials Letters 71 (2012) 15-17. 10.1016/j.matlet.2011.12.004

[86] Stoll, S., Schweiger, A., Journal of magnetic resonance, 178(1) (2006) 42-55. https://doi.org/10.1016/j.jmr.2005.08.013

[87] Antuzevičs, A., S-stāvokļa retzemju jonu lokālā struktūra fluorīdos un oksifluorīdu stikla keramikās, promocijas darbs (PhD Thesis), Latvijas Universitāte, 2017. Available: https://dspace.lu.lv/dspace/handle/7/37284

[88] Fairchild, M. D., Color appearance models, Wiley, 2005

[89] Babu, P., Jang, K. H., Kim, E. S., Shi, L., Vijaya, R., Lavin, V., Jayasankar, C. K., Seo, H. J., Journal of non-crystalline solids, 356(4-5) (2010) 236-243. https://doi.org/10.1016/j.jnoncrysol.2009.11.010

[90] Wang, R., Zhou, D., Qiu, J., Yang, Y., Wang, C., Journal of Alloys and Compounds, 629 (2015) 310-314. https://doi.org/10.1016/j.jallcom.2014.12.233

[91] Heise, M., Scholz, G., Krahl, T., Kemnitz, E., Solid State Sciences, 91 (2019) 113-118. https://doi.org/10.1016/j.solidstatesciences.2019.03.014

[92] Cai, J. L., Li, R. Y., Zhao, C. J., Tie, S. L., Wan, X., Shen, J. Y., Optical Materials, 34(7) (2012) 1112-1115. https://doi.org/10.1016/j.optmat.2012.01.013

[93] Nara, H., Schlesinger, M.,. Solid State Communications, 9(14) (1971) 1247-1250. https://doi.org/10.1016/0038-1098(71)90021-4

[94] Olsen, L. R., Wright, A. O., Wright, J. C., Physical Review B, 53(21) (1996) 14135. https://doi.org/10.1103/PhysRevB.53.14135

[95] Antuzevics, A., EPR in glass ceramics. In Experimental Methods in the Physical Sciences (Vol. 50, pp. 161-190), Academic Press, 2019. https://doi.org/10.1016/B978-0-12-814024-6.00008-X

[96] Yagoub, M. Y. A., Swart, H. C., Coetsee, E., *Journal of Alloys and Compounds*, *858* (2021) 157741. https://doi.org/10.1016/j.jallcom.2020.157741

PUBLICITY OF THE AUTHOR

Publications on the topic of this work

1. Kemere, M., Rogulis, U., Sperga, J., "Luminescence and energy transfer in Dy^{3+}/Eu^{3+} co-doped aluminosilicate oxyfluoride glasses and glass-ceramics" *Journal of Alloys and Compounds 735* (2018): 1253-1261. (SNIP: 1.386, cited 34 times) https://doi.org/10.1016/j.jallcom.2017.11.077
2. Kemere, M., Sperga, J., Rogulis, U., Krieke, G., Grube, J. "Luminescence properties of Eu, RE^{3+} (RE= Dy, Sm, Tb) co-doped oxyfluoride glasses and glass–ceramics" *Journal of Luminescence* 181 (2017): 25-30. (SNIP: 1.048, cited 49 times) http://dx.doi.org/10.1016/j.jlumin.2016.08.062
3. Antuzevics, A., Kemere M., Krieke G., Ignatans R., „Electron paramagnetic resonance and photoluminescence investigation of europium local structure in oxyfluoride glass ceramics containing SrF_2 nanocrystals", *Optical Materials 72* (2017): 749-755 (SNIP: 1.009, cited 19 times) https://doi.org/10.1016/j.optmat.2017.07.024

Other publications related to RE activators in fluoride nanoparticles

1. Fedotovs, A., Antuzevics, A., Rogulis, U., Kemere, M., & Ignatans, R., Electron paramagnetic resonance and magnetic circular dichroism of Gd^{3+} ions in oxyfluoride glass–ceramics containing CaF_2 nanocrystals. *Journal of Non-Crystalline Solids*, *429* (2015) 118-121. (SNIP: 1.177, cited 15 times) https://doi.org/10.1016/j.jnoncrysol.2015.08.036
2. Antuzevics, A., Kemere, M., Ignatans, R, Local structure of gadolinium in oxyfluoride glass matrices containing SrF_2 and BaF_2 crystallites. *Journal of Non-Crystalline Solids*, *449* (2016) 29-33. (SNIP: 1.177, cited 11 times) http://dx.doi.org/10.1016/j.jnoncrysol.2016.07.015
3. Antuzevics, A., Kemere, M., Krieke, G., Multisite formation in gadolinium doped SrF_2 nanoparticles. *Journal of Alloys and Compounds*, *762* (2018) 500-507. (SNIP: 1.414, cited 3 times) https://doi.org/10.1016/j.jallcom.2018.05.283

Other publications

1. Di Marzio, A., Avotins, A., Ķemere, M., Šķērstiņa, R., Di Marzio, G. (2023, January). Fluorescence in European Owls. In *Annales Zoologici Fennici* (Vol. 60, No. 1, pp. 31-51). Finnish Zoological and Botanical Publishing Board. https://doi.org/10.5735/086.060.0106
2. Antuzevics, A., Elsts, E., Kemere, M., Lushchik, A., Moskina, A., Scherer, T. A., Popov, A. I. Thermal annealing of neutron irradiation generated paramagnetic defects in transparent Al_2O_3 ceramics. *Optical Materials*, *135* (2023) 113250. (SNIP: 1.009, cited 1 time) https://doi.org/10.1016/j.optmat.2022.113250
3. Milićević, B., Periša, J., Ristić, Z., Milenković, K., Antić, Ž., Smits, K., Kemere, M., Vitols, K., Sarakovskis, A., Dramićanin, M. D. Hydrothermal Synthesis and Properties of Yb^{3+}/Tm^{3+} Doped Sr_2LaF_7 Upconversion Nanoparticles. *Nanomaterials*, *13*(1) (2022) 30. (SNIP: https://doi.org/10.3390/nano13010030
4. Skruodiene, M., Juodvalkyte, R., Kemere, M., Ramanauskas, R., Sarakovskis, A., Skaudzius, R. Enhanced optical properties of yttrium aluminum garnet with the yttrium vanadate impurity phase. *Heliyon*, *8*(11) (2022) e11386. (SNIP: 1.27) https://doi.org/10.1016/j.heliyon.2022.e11386
5. Mironova–Ulmane, N., Brik, M. G., Grube, J., Krieke, G., Kemere, M., Antuzevics, A., Gabrusenoks, E., Skvortsova, V., Elsts, E., Sarakovskis, A., Piasecki, M., Popov, A. I. EPR, optical and

thermometric studies of Cr^{3+} ions in the α-Al_2O_3 synthetic single crystal. Optical Materials, 132 (2022) 112859. (SNIP: 1.009, cited 1 time) https://doi.org/10.1016/j.optmat.2022.112859

6. Saršūns, K., Kemere, M., Karziņins, A., Klimenkovs, I., Berzins, A., Sarakovskis, A., Rekis, T., Fine-Tuning Solid State Luminescence Properties of Organic Crystals via Solid Solution Formation: The Example of 4-Iodothioxanthone–4-Chlorothioxanthone System. Crystal Growth & Design, 22(8) (2022) 4838-4844. (SNIP:1.111, cited 3 times) https://doi.org/10.1021/acs.cgd.2c00313
7. Kemere, M., Antuzevics, A., Rodionovs, P., Rogulis, U., Sarakovskis, A., Photoluminescence and electron paramagnetic resonance studies of Mn^{2+} doped $CaAl_4O_7$. Optical Materials, 127 (2022) 112352. (SNIP:1.009, cited 1 time) https://doi.org/10.1016/j.optmat.2022.112352
8. Mironova-Ulmane, N., Brik, M. G., Grube, J., Krieke, G., Antuzevics, A., Skvortsova, V., Kemere, M., Elsts, E., Sarakovskis, A., Piasecki, M., Popov, A. I. Spectroscopic studies of Cr^{3+} ions in natural single crystal of magnesium aluminate spinel $MgAl_2O_4$. Optical Materials, 121 (2021) 111496. (SNIP: 0.955, cited 3 times) https://doi.org/10.1016/j.optmat.2021.111496
9. Inkrataite, G., Kemere, M., Sarakovskis, A., & Skaudzius, R., Influence of boron on the essential properties for new generation scintillators. Journal of Alloys and Compounds, 875 (2021) 160002. (SNIP: 1.038, cited 4 times) https://doi.org/10.1016/j.jallcom.2021.160002
10. Karipbayev, Z.T., Lisitsyn, V.M., Mussakhanov, D.A., Alpyssova, G.K., Popov, A.I., Polisadova, E.F., Elsts, E., Akilbekov, A.T., Kukenova, A.B., Kemere, M., Sarakovskis, A., Lushchik, A, "Time-resolved luminescence of YAG:Ce and YAGG:Ce ceramics prepared by electron beam assisted synthesis." *Nuclear Instruments and Methods in Physics Research, Section B: Beam Interactions with Materials and Atoms*, 479 (2020): 222-228. (SNIP: 0.927, cited 13 times) https://doi.org/10.1016/j.nimb.2020.06.046
11. Lisitsyn, V.M., Vaganov, V.A., Lisitsyna, L.A., Karipbayev, Z.T., Kemere, M., Tulegenova, A.T., Ju, Y., Panchenko, Y.N, "Luminescence of YAG:Ce Phosphors Excited by UV Laser Radiation." *Russian Physics Journal, 63 (6)* (2020): 1003-1009. (SNIP: 0.754, cited 2 times) https://doi.org/10.1007/s11182-020-02130-3
12. Лисицын Виктор, Ваганов Виталий, Лисицына Людмила, Карипбаев Жакып, Кемере Мелдра, Тулегенова Аида Тулегенкызы, Цзюй Янян. "Люминесценция ИАГ:Се-люминофоров при возбуждении лазерным УФ-излучением." *Изв. вузов. Физика.* № 6 (2020): 94-99. https://doi.org/10.17223/00213411/63/6/94

Awards

The authors' collective* study "New materials for use in infrared radiation converters and white light sources" was awarded the LZA award for the most significant achievements in applied science in 2017.

**Research authors: LZA academicianDr.habil.phys. Uldis Rogulis, Dr.habil.phys. Maris Springis, Dr.phys. Anatolijs Sarakovskis, Dr.phys. Jurģis Grube, Dr.phys. Andris Fedotovs, Dr.phys. Edgars Elsts, Dr. phys. Guna Krieke, Dr.phys. Andris Antuzevics, Mg.phys. Meldra Kemere (Institute of Solid State Physics, University of Latvia)*

PARTICIPATION IN CONFERENCES

Local conferences (on the topic of the thesis)

1. Sperga, J., Ķemere, M., Rogulis, U., Grūbe, J.,***"Ar eiropiju un disproziju koaktivētu oksifluorīdu stiklu luminescence",*** ISSP UL 32nd Scientific Conference, 17th February 2016, LU CFI, Riga (poster)

2. Ķemere, M., Rogulis, U., Sperga, J., ***"Fotoluminiscence un enerģijas pārnese ar Dy^{3+} un Eu^{3+} koaktivētos stiklos un stikla keramikās",*** ISSP UL 33rd Scientific Conference, 22nd February 2017, LU CFI, Riga (oral)

3. Ķemere, M., Rogulis, U., ***"Enerģijas pārneses pētījumi ar retzemju joniem ko-aktivētos CaF_2 un SrF_2 nanokristalītus saturošos stiklos un stikla keramikās"***, ISSP UL 34th Scientific Conference, 20th February 2018, LU CFI, Riga (oral)

4. Ķemere, M., Rogulis, U., ***"Enerģijas pārneses pētījumi ar Dy^{3+} un Eu^{3+} joniem aktivētos oksifluorīdu stiklos un stikla keramikās"***, 76th UL Scientific Conference, session of UL Fund stipendiates, 13th April 2018, UL Nature house, Riga (oral)

5. Ķemere, M., Rogulis, U., ***"Retzemju jonu luminiscences un enerģijas pārneses pētījumi oksifluorīdu stiklos un stikla keramikās"***, 77th UL Scientific Conference, session of UL Fund stipendiates, 29th March 2019, UL Nature house, Riga (oral)

6. Ķemere, M.,Rogulis, U., ***"Tb^{3+} un Eu^{3+} luminiscence un enerģijas pārnese SrF_2 nanokristalītus saturošā oksifluorīdu stikla keramikā*** ISSP UL 36th Scientific Conference, 11th February 2020, LU CFI, Riga (oral)

International conferences (on the subject of the thesis)

1. Kemere, M., Sperga, J., Rogulis, U., Grube, J., ***„Luminescence properties of europium and dysprosium co-doped oxyfluoride glasses"***, "Open Readings 2016", 17th March 2017, Vilnius University, Vilnius, Lithuania (poster)

2. Kemere, M., Rogulis, U., Schweizer, S., Steudel, F., Loos, S., Rimbach, A. Ch., Ignatans, R. ***„Luminescence and quantum efficiency of europium doped oxyfluoride glasses and glass-ceramics"***, 12th International Young Scientist conference "Developments in Optics and Communications" (DOC Riga 2016), 22th March 2016, UL Nature house, Riga (poster)

3. Kemere, M., Rogulis, U., Sperga, J., ***"Photoluminescence properties of dysprosium and europium co-doped oxyfluoride glasses and glass ceramics",*** DOC 2017, 6th April 2017, UL Nature house, Riga (oral)

4. Kemere, M., Rogulis, U., Sperga, J., ***"Studies of photoluminescence and energy transfer in europium and dysprosium co-doped oxyfluoride glasses and glass ceramics"*,** 15th Conference and Exhibition of Europen Ceramic Society (ECerS 2017), 12th July 2017, Budapest, Hungary (poster)

5. Kemere, M., Rogulis, U.,***"Energy transfer in Dy^{3+}/Eu^{3+}co-doped glasses and glass-ceramics containing fluoride nanocrystallites"***, DOC 2018, 12th April 2018, UL Nature house, Riga (oral)

6. Kemere, M., Rogulis, U., ***"Photoluminescence of Eu^{3+}/Tb^{3+} doped glass-ceramics containing SrF_2 nanocrystallites",*** DOC 2019, 11th April 2019, UL Science house, Riga (poster)

7. Kemere, M., Rogulis, U., "***Luminescence properties and energy transfer in Dy^{3+}/Eu^{3+} and Tb^{3+}/Eu^{3+} doped oxyfluoride glasses and glass-ceramics",*** "Functional Materials & Nanotechonologies" un "Nanotechnology and Innovation in the Baltic Sea region" joint conference (FM&NT-NIBS 2022), 4th July 2022, LU Science house, Riga (poster)

ACKNOWLEDGMENTS

I express my gratitude to the supervisor Dr. habil. phys. Uldis Rogulis for scientific consultations, recommendations, encouragements both in the elaboration of the doctoral thesis and in orienteering activities, searching for the most advantageous route. I am also thankful for the trust in me and the opportunity to participate in various scientific projects.
I am very grateful for the support of Dr. phys. Guna Krieke, who taught me the first steps in synthesis of glass and glass ceramics and was always ready to answer my questions about the topic of the work and the properties of rare earth ions. Thanks also to Dr. phys. Jurgis Grube for his help in the first steps of spectroscopy measurements, Dr. phys. Edgars Elsts for informative and friendly support.
Thanks to close colleagues Dr. phys. Andris Antuzevics for discussions and suggestions and Mg. phys. Guna Doke for mood-enhancing conversations.
Thanks to my parents and everyone else who encouraged and supported me.

Funding for the development of the doctoral thesis was received from the grant project "**Strengthening of the capacity of doctoral studies at the University of Latvia within the framework of the new doctoral model**", identification No. 8.2.2.0/20/I/006

The research was carried out thanks to the donation of SIA "Mikrotik". The donation is administered by the The University of Latvia Foundation.

Thanks for the financial support to the Latvian Science Council project "**Novel transparent nanocomposite oxyfluoride materials for optical applications**" (Nr. LZP-2018/1-0335)
I am grateful for the financial support from the European Regional Development Fund project "**Novel materials for development of all-optical temperature sensor**" (No. 1.1.1.1/19/A/020).

The Institute of Solid State Physics of University of Latvia as a Center of Excellence has received support from the H2020-WIDESPREAD-01-2016-2017-TeamingPhase2 project CAMART2 of the European Union framework program "Horizon 2020", contract no. 739508.